STUDY OF PLASMA IN A MULTI-POLE LINE CUSP MAGNETIC FIELD

By

AMITKUMAR PATEL

PHYS06201204003

Institute for Plasma Research, Gandhinagar

A thesis submitted to the

Board of Studies in Physical Sciences

In partial fulfillment of requirements

for the Degree of

DOCTOR OF PHILOSOPHY

of

HOMI BHABHA NATIONAL INSTITUTE

February, 2019

Homi Bhabha National Institute[1]

Recommendations of the Viva Voce Committee

As members of the Viva Voce Committee, we certify that we have read the dissertation prepared by AMITKUMAR PATEL entitled "STUDY OF PLASMA IN A VERSATILE MULTI-POLE CUSP MAGNETIC FIELD" and recommend that it may be accepted as fulfilling the thesis requirement for the award of Degree of Doctor of Philosophy.

Chairman – Prof. P. K. Chattopadhyay	21.06.19
Guide – Dr. N. Ramasubramanian	21/June/19
Examiner - Prof. H. Bailung	21.06.19
Member 1- Prof. R. Ganesh	21/06/2019
Member 2- Dr. Joydeep Gosh	21/6/19
Member 3- Dr. L. M. Awashti	21.06.19

Final approval and acceptance of this thesis is contingent upon the candidate's submission of the final copies of the thesis to HBNI.

I hereby certify that I have read this thesis prepared under my/our direction and recommend that it may be accepted as fulfilling the thesis requirement.

Date: 21-06-2019 **Signature:**

Place: IPR, Gandhinagar **Dr. N. Ramasubramanian**

[1] This page is to be included only for final submission after successful completion of viva voce.

STATEMENT BY AUTHOR

This dissertation has been submitted in partial fulfillment of requirements for an advanced degree at Homi Bhabha National Institute (HBNI) and is deposited in the Library to be made available to borrowers under rules of the HBNI.

Brief quotations from this dissertation are allowable without special permission, provided that accurate acknowledgement of source is made. Requests for permission for extended quotation from or reproduction of this manuscript in whole or in part may be granted by the Competent Authority of HBNI when in his or her judgment the proposed use of the material is in the interests of scholarship. In all other instances, however, permission must be obtained from the author.

Amitkumar Patel

DECLARATION

I, hereby declare that the investigation presented in the thesis has been carried out by me. The work is original and has not been submitted earlier as a whole or in part for a degree / diploma at this or any other Institution / University.

Amitkumar Patel

List of Publications arising from the thesis

Journal

1. A. D. Patel, M. Sharma, N. Ramasubramanian, R. Ganesh, and P. K. Chattopadhyay, *Rev. Sci. Instrum.* **89**, 043510 (2018).
2. A. D. Patel, M. Sharma, R. Ganesh, N. Ramasubramanian, and P. K. Chattopadhyay, *Phys. Plasmas* **25**, 112114 (2018).
3. A. D. Patel, M. Sharma, N. Ramasubramanian, J. Ghosh and P. K. Chattopadhyay, "Characterization of Argon plasma in a variable multi pole line cusp magnetic field configuration" (under review in *Phys. Scripta* (**2019**)).
4. A. D. Patel, M. Sharma, N. Ramasubramanian, R. Ganesh, and P. K. Chattopadhyay, "Temperature gradient driven turbulence in an inhomogeneous variable multi-pole line cusp magnetic field (VMMF) configuration" (Manuscript under preparation).

Conferences

1. A. D. Patel, Meenakshee Sharma, N. Ramasubramanian, and P. K. Chattopadhyay, "On the Characteristics of Argon Plasma in a Multi-Pole line Cusp Variable Magnetic Field" 9th International Conference on the Frontiers of Plasma Physics and Technology (FPPT-9), Negombo, Sri-lanka, 8-12 April 2019 (Awarded by best poster presentation).
2. A. D. Patel, M. Sharma, N. Ramasubramanian, R. Ganesh, and P. K. Chattopadhyay, "Characterization of Argon Plasma in a Multi-Pole Line Cusp Magnetic Field: Towards a Favorable Source for NBI System", 27th IAEA Fusion Energy Conference (FEC 2018), Institute for Plasma Research, Gandhinagar, India 22-27 Oct 2018.

3. A. D. Patel, M. Sharma, N. Ramasubramanian, and P. K. Chattopadhyay, "Electro-Magnet for Cesium Plasma Confined in a Multi-Pole Line Cusp Magnetic Field", 44th European Physical Society Conference on Plasma Physics, Queen's University, Belfast, Northern Ireland, UK, 26-30 Jun 2017.
4. A. D. Patel, Meenakshee Sharma, N. Ramasubramanian, and P. K. Chattopadhyay "Hot Tungsten Plate based ionizer for Cesium Plasma in a Multi-Cusp field Experiment", 10th Asia Plasma and Fusion Association Conference (APFA-2015), Institute for Plasma Research, Gandhinagar, India, 14-18, Dec 2015.

Amitkumar Patel

Dedicated to

My son

(Gunj)

ACKNOWLEDGEMENTS

First, I would like to express my sincere gratitude to my thesis supervisor Dr N. Ramasubramanian for his continuous support during my PhD work and for his patience, motivation, enthusiasm, and immense knowledge. His guidance helped me in all the time of research and writing of this thesis. I am deeply grateful to him for the discussions that helped me short out the technical details of my work. I could not have imagined having a better advisor and mentor for my PhD study, his encouragement made it possible to achieve the goal.

I am also thankful to Prof. P. K. Chattopadhyay and Prof. R. Ganesh for their help and discussion. Their Patience and support helped me overcome many crisis situations and finish this thesis. They have been always there to listen and give advice. Their insightful comments and constructive criticisms at different stages of my research were thought provoking and they helped me focus my ideas. I humbly appreciate their motivating ideas and fruitful discussions we had.

I want to acknowledge my Doctoral committee members, Dr Joydeep Ghosh and Dr Lalit Mohan Awasthi, whose help and sympathetic attitude at every point during my research helped me to work in time. I would like to express my warm thank to Prof. Y. C. Saxena and late Prof. P. K. Kaw who supported me at every bit, especially during the making of presentations. Their critical review and valuable comments on my presentations always helped me to convey the main message easily to the audiences during the oral talks.

I would like to thank Prof. Sudeep Sen Gupta, Dr Mainak Bandopadhayay, Dr Asim Chattopadhyay, Dr M. Kundu, Dr D. Sharma, and Dr G. Ravi for teaching me during my 1st year course work. I would like to thank Prof. S. Mukherjee for his guidance and quick response on things related to HBNI.

I am grateful to my colleagues in Beta Lab Meenakshi, Amulya, Lavekesh, Manu sir, Umesh, Zubin, Sayak Bose, Sonu Yadav for various fruitful discussions on

different occasions regarding the experimental results in the laboratory. This enabled me to develop a better understanding of experimental plasma physics.

I am also grateful to a staff member from the workshop, stores, electronics lab, computer centre, library, purchase section, administration, drafting section canteen and IPR security at Institute for Plasma Research for their co-operation and help during the entire duration of my PhD. A special thanks to Vijay Patel, Sunil Chudashmaji, and Kaila Bhai for their immense support for conducting the experiments. I would like to thank Mr. K. Satyanarayana sir, Mr Prakash Patel, Mrs Minsha Shah, Mr Pankaj Shrivatava for her invaluable help in designing and developing the necessary electronic circuits for my experiments. I would like to thank Jaydeep Khatri, Sushant Sahu, Rajni and Mukesh for working with me to make and install Multi-pole line cusp plasma Device.

Time spent at IPR was made enjoyable due to the presence of many friends, juniors and seniors that became a part of my life specially Sonu, Debraj, Anup, Ratan, Rane, Umesh, Rajnarayan Bhumika, Surabhi. A big hug goes to Arghya and Narayan (he was a true friend since we started to share our office and also help me to write a thesis and research article). A big thank to Jiva bhai and his wife for preparing delicious foods at IPR hostel. I would also like to thank my seniors Jugal, Satya, Kshitish, Ujjwal, Rameshwar, Shekar, Gurdatt, Vikram, Vikram Dharodi, Ashwin, Sharad, Pravesh, Shekar, Sanat, Sushil, Aditya, Veda, Neeraj, Roopender, Vara, Chandrashekar, Bhibhu, Mangilal, Deepa, Akanksha, Vidhi, Harish, Meghraj, Sameer for their support, valuable inputs during PhD and providing friendly the environment in scholar hall and hostel. I would also like to thank my juniors, Sagar, Atul, Jervis, Deepak, Prabhakar, Meenakshi, Pallavi, Alamgir, Sandeep, Harshita, Chetan, Arun, Shivam, Satya, Chinmay, Vivek, Gaurav, Jeet, Piyush, Prince, Jaganath, Mayank, and others for their humour without which our hostel would have been a very dull place.

I would like to thank my parent (though they are beyond my thank), whose love, guidance and blessings were always with me. Whatever I have achieved to date is due to their sacrifice in their life to fulfil my demands. A big thank to my sister (Anita) & my brother (Prakash) to take care of my parent in my absence.

I have no words left with me to thank my beloved wife Priyanka. She was always there to listen to my problems and frustrations. From the date we got married, she took the responsibilities of my home and parents so that I can focus on my research. I deeply acknowledge her for her patients that she has shown in the last few months during my PhD. Without her support, it would not have been possible. I would also like to especially thank my son (Gunj) for giving me his childhood time. I never realize when he becomes a sixth year old during the tenure of my PhD. I am really grateful to God for sending both in my life.

Contents

SYNOPSIS

In the multi-pole cusp configuration the field in the center is the nearly ($B \sim 0$) null, while a finite value of field being there in the edge regions confining the plasma. In this configuration, the center of curvature of the confining magnetic field will not be there in the region of the confined plasma itself. This helps to avoid instabilities which are usually observed in the laboratory devices. Hence it is prudent to have a high density, uniform and quiescent plasma confined in multi-cusp configuration. Due to these properties, it has found wide applications in the development of ion sources, plasma-etching reactors etc. There has been many instances in which these multi-pole cusp configurations have been studied before and well documented. But it has been generally observed that in most of the earlier studied cusp plasma devices permanent magnets were used, while which were arranged in a checkerboard or in line cusp configuration. Many results have been published for measurement of the width of plasma leakage at the cusp (near the pole magnet) and still an exact scaling for the amount of plasma being leaked in a given cusp configuration is yet to be ascertained. Though many scaling exists, ranging from electron gyro-radius to ion gyro-radius apart and also the so-called 'hybrid gyro-radius'. The systems with permanent magnets have a fixed magnetic field value and hence it was not possible to study plasma behavior with different magnetic field values. Also, most of the devices reported before with multi-pole cusp configurations had a very small volume of the low beta (edge) region) so as to maximize the usage of the central high beta region. Hence the various fluctuations present in the low beta (edge regions) and their effects on the central high beta region have not been studied before.

In this thesis work a filamentary quiescent plasma was produced in a multi-pole cusp magnetic field and their characteristics have been studied in detail. The device mainly consists of a vacuum chambers, plasma sources (hot cathode), pumping system, magnet system and plasma diagnostics. A multi-pole cusp magnetic field system has been designed such that a cylindrical high beta region is formed surrounded by a comparable volume of low beta region. This has been achieved by placing six electromagnets (with embedded profiled vacoflux-50 core and double pancake winding) over a large cylindrical chamber having dimension 103cm axial length and 40cm diameter. This multi-pole cusp magnetic field (VMMF) system has been made to be versatile such that many different configurations and field values can be made to confine the plasma. The 2-D simulation of the VVMF has been performed using the Finite Element Method Magnetic software and has been validated by experimentally measured values.

The whole chamber is pumped down to a pressure 10^{-6} mbar using a Turbo Molecular Pump (TMP) backed by a rotary pump, while a combination of the Ionization and Pirani gauges are used for pressure measurement. The argon gas is filled to a pressure of the order 10^{-4}mbar for plasma production. The plasma discharge has been struck between hot filament based cathode source and grounded chamber wall. The cathode source is fitted well inside the main chamber to avoid the edge effects of the magnets. These filaments are powered by a 500 A, 15 V floating power supply (V_f) while it is normally operated at around 16 - 19 A per filament. The source is biased with a voltage of - 76 V with respect to the grounded chamber walls using discharge power supply (V_d). The primary electrons emitted from the filaments travel in the electrical field directions, while they are confined by the cusp magnetic field lines. Because of

mirror effects due to cusp configuration, electrons move back and forth between the poles and they ionize the background gas atoms and thus an argon plasma is produced. The various plasma diagnostics (viz. simple Langmuir probe for plasma parameters (electron temperature, plasma density, and floating potential) measurement, emissive probe for plasma potential measurement, and rack probe for fluctuation measurement) have been constructed.

The argon plasma thus produced and confined by multi-pole line cusp magnetic field is found to be have different characteristics at different regions. The central high beta plasma volume is found to be quiescent and uniform and also it is found that to be controllable by changing the magnet current. This volume would be beneficial for basic plasma studies (viz. ion acoustic wave, soliton wave interaction, electron plasma wave, Landau damping, nonlinear coherent structure, wave-particle trapping and un-trapping etc.). While the edge regions surrounding the central high beta region is found to have many interesting phenomena, which is studied in detail here. The plasma characteristics, radially along the non-cusp region, were recorded for different magnetic field values at the poles using Langmuir probes. The profiles of electron density, temperature, floating potentials with different magnetic field values at the poles helped to complete the plasma characterization. One of the key parameters involving plasma confined in the cusp magnetic field is the effective leak width of plasma (the width of the profile of plasma escaping through the cusp). The estimated leak width has been compared with the calculations using previously published different scaling and found to be matching well.

The bulk plasma at the central region is uniform and dense (null region), this plasma diffused across the magnetic field and stream out along the magnetic field lines toward the cusp, as a result, the gradients in plasma parameters (plasma density, electron temperature, and floating potential) are formed. Using the scale length of plasma parameters, whole plasma has divided into three regions. The central plasma region is uniform and quiescent where density and electron temperature scale length are very high. In mid region of plasma, the temperature gradient is dominated compared to density gradient and in edge region density gradient is dominated compared to density gradient. These gradients are also controllable with changing magnetic field values. The fluctuations and hence instabilities due to the gradients in the density and temperature have been further studied to identify the sources of free energy and the role of magnetic field in these fluctuations have also studied for some cases. The presence of drift wave turbulence has been identified using the scale length of plasma parameters, frequency spectrum, cross-correlation function, and fluctuation level of plasma densities. The cross-field drift velocity due to fluctuation in plasma parameters have been measured from the wave number- frequency $S\ (k_z, \omega)$ spectrum and verified with the theoretical values obtained from density scale length formula. Further, from the $S\ (k_z, \omega)$ spectrum, it has been found that the drift velocity alternates the sign in the consecutive non-cusp regions.

A thesis comparing of following chapters have been completed.

Chapter 1: Introduction

In this chapter, a brief introduction about the multi-cusp confined plasma has been given which is mostly from previously published literature. The unexplored physics areas and motivation of this thesis has also been included in this chapter.

Chapter 2: ***A versatile multi-pole cusp magnetic field system***

In this chapter, the detailed design and construction of the magnet system is given along with the versatility of the field configuration and its utility for many physics experiments. The simulation of the field configuration done using Finite Element Magnetics Method has been added to this chapter for ready comparison.

Chapter 3: ***Plasma production and plasma diagnostics***

In chapter 3, detail of various systems of the devices followed by procedure of plasma production has been described.

Chapter 4: C*haracteristics of plasma confined in a VMMF*

Before embarking of proposed experiments it is desired to characterize the plasma in a multi-pole cusp magnetic field. In this chapter 4, the results of the characteristics with different magnetic field values have been described along with analysis of leak width. Moreover in this chapter the profile of the plasma parameters (plasma density, floating potential, electron temperature and particle confinement time etc.) have been given, estimated from the Langmuir probe measurements. The variations of these profiles with different magnetic field values have been also given.

Chapter 5: ***Plasma fluctuation at the different region of the device***

The profiles thus recorded and the fluctuations recorded at various locations have helped to identify some of the instabilities present in the plasma. This chapter contains the detailed analysis of instabilities identified due to gradients in the profiles along with the effect of magnetic field vales on those identified instabilities.

Chapter 6: ***Conclusion and future scope***

Finally, in chapter 6, the consolidation of the work has been done and also enumeration of some of the major tasks identified that can be undertaken for further research has been given.

List of figures

Chapter 1

Introduction

This Thesis discusses a detailed study on the characterization of Argon plasma confined in a versatile multi-pole line cusp magnetic field (VMMF). It also presents the development of a versatile multi-pole line cusp magnetic field (using six electromagnets and profiled with a core material) system, vacuum chamber, plasma source and the diagnostics. In this Chapter, a brief overview of this subject is presented along with the motivation for these studies in which several open problems are pointed out. Finally, this Chapter concludes with an outline of the remaining Chapters of this Thesis.

1.1 Overview and motivation

Plasma, is an ionized medium which contains sufficient number of charged particles and gas atoms for the overall behaviour of the system to be different from an ordinary gas and which exhibits collective behaviour. Plasma is considered the fourth state of matter. The 99% of the regular matter in the universe is in the plasma state and in the universe naturally occurring plasmas are: Aurorae, Ionospheres and magnetospheres of planets, Solar atmosphere, Coronal mass ejections, Interstellar medium, Intergalactic medium, Lightning and ball lightning, Solar and Stellar winds etc. In nature plasma is mainly confined by three ways viz. Gravitational confinement, Inertia confinement and Magnetic field confinement [1].

In a stars, confinement comes about because of the gravitational pressure of an enormous mass. High density and temperature thereby result toward the stellar centre inward directed momentum of the outer layers of the pellet, thereby yielding a high dense material, the inertia of which confines the fusion fuel against the fusion reaction volatile effect of disassembly for a sufficient time to allow sufficient fusion reactions to occur [1].

In the inertial confinement, principle is to apply a fast pulse of high energy to a large surface area of a pellet, causing it to simultaneously "implode" and heat to very high pressure and temperature. If the fusion fuel is sufficiently dense and hot, the fusion reaction rate will be rapid to burn a significant fraction of the fuel before it has dissipated. To attain these uttermost conditions, at first cold fusion fuel must be explosively compressed. This inertial confinement scheme is used in the hydrogen bomb, in which the driver is X-rays generated by a fission bomb itself. This scheme is also studied in the laboratory for controlled nuclear fusion, in which the driver is a high power laser or high energy collimated charged particle (ion, or electron) beam [1].

In magnetic confinement strong magnetic fields are used to confine the charged particles (plasma). The charged particles will follow the magnetic field lines and move parallel to magnetic field in helix path thus the charged particles are tied to the field lines. As a result in suitable shape of magnetic field cage it is possible to confine a plasma and keep it away from material walls. There exist several magnetic field configurations (magnetic cage) exist viz. the toroidal geometries of Tokamaks and Stellarators, an open-ended mirror confinement systems, and a multi-pole cusp magnetic field confinement, combination of cusp-mirror confinement etc [1-2].

In the experimental laboratory only inertial and magnetic field confinement is can be possibly be used to confine the plasma. The plasma confined by magnetic field found large application viz. commercial fusion, propulsion in space, plasma etching reactors plasma coating unit, plasma torch, plasma sources in different industrial applications etc. The plasma confinement by magnetic fields with different configurations have been extensively used to confine plasma at laboratory scale. Some of the magnetic field configurations studied are toroidal devices (viz. stellarators, tokamaks), linear devices (viz. mirror geometries, cusp geometries, solenoid geometries) etc. [2, 3]. The multi-pole cusp configuration as (shown in figure 1.1) has nearly zero magnetic field (null field) in the centre of the confining region and the maximum magnetic field at the poles. In this configuration the centre of curvature of the confining magnetic field does not exist in the region of confined plasma or in better words the plasma confined is in the good curvature region of magnetic field [4]. It helps to avoid many instabilities which are usually observed in the other laboratory plasma devices thus it enhances the plasma density at the confining region (null region) [4].

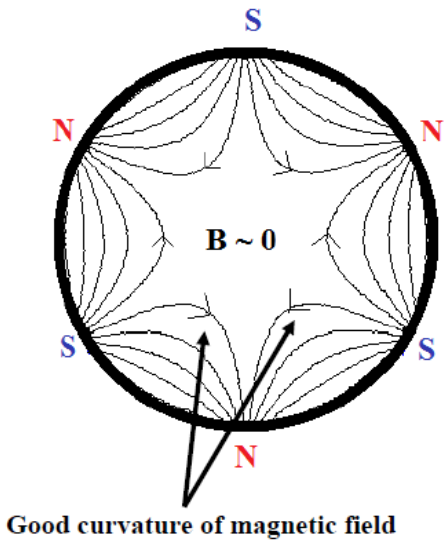

Figure 1.1. A multi-pole cusp magnetic field configuration.

Due to their ability to confine the large uniform volume and quiescent plasmas the magnetic field geometries containing cusp are widely used in the laboratory devices for basic plasma physics studies, plasma ion sources, neutral beam injection (NBI) system of tokamak etc. [5, 6]. These low temperature discharge devices employing multi pole cusps have been studied since 1973, when R. Limpaecher and K. R. MacKenzie [6] first showed that they could be used to confine large volume, uniform, and quiescent plasmas with densities much higher than other linear plasma devices. These authors showed that the increase in plasma density in a multi-pole device is primarily due to the confinement of the "primary" ionisation electrons. Leung *et al.* [7], studied different geometry of cusp magnetic field such as checker board, broken line cusp and full line cusp (as shown in figure 1.2) for confinement of plasma, and they have reported that full line cusps were found to give optimum plasma density. M. Sadowski [8], studied plasma containment in spherical multi-pole (SM) magnetic field. He showed that the high-order SM systems avoid line cusp loss-regions, occurring in the other minimum-B geometries.

Figure 1.2. (a) Checker board multi-pole cusp configuration and (b) full line multi-pole cusp configuration [7].

The following description highlight the importance of plasma confined by cusp geometry, followed by the drawback and unresolved problems of this geometry.

1.1.1Plasma ion sources

The multi cusp magnetic field can confine the uniform high density and quiescent plasma which is the essential requirement of high current collimated ion beam, thus it is widely used in plasma ion sources. Leung *et al.* [9], have investigated the properties of a steady state, dc discharge multi cusp ion source. The authors have reported that the magnetic multi-pole cusp plasma devices should be good candidates for the production of intense uniform ion beams. Kuriyama *et al.* [10], developed a NBI system having the specification; a beam energy of 500keV, an injection power of 10MW, a beam duration time of 10s, beam species of deuterium or hydrogen for JT-60U tokamak. Vainionpaa *et al.* [11], developed a RF driven multi cusp ion source. They designed the system to have a 90% proton fraction and small divergence with beam current at 5–6 A and a pulse length of 1 second occurring once every 1–2 min. Bhattacharjee *et al.* [12], studied Micro wave plasma source in Laboratory plasma using multi cusp magnetic field generated by permanent magnets, and further continue used this source to make focused ion beam system. Pathak *et al.* [13] studied a computer simulation for multi cusp RF based H^- ion sources. The authors also showed the compact RF ion source exhibit nearly 6 times better efficiency compared to large diameter ion source. Hosseinzadeh *et al.* [14], have performed numerical simulation for optimization of multi pole permanent magnets of multi cusp ion source. The authors showed that field free region of cusp magnetic field increase with increasing number of poles in cusp magnetic field. J. H. Kim [15], performed numerical simulation of multi cusp ion source. In his work a numerical simulation is performed to understand the effect of multi-cusp magnetic fields when the number of magnetic pole varied from 6 to 14. The author also found that the magnetic field free region

(null region) is increased with increasing magnetic pole and also provides stronger ion confinement.

The ion sources are also operating with wide range of neutral background pressure, and produce uniform, stable low temperature plasma. The energy, direction and density of the resultant ions are also controllable in these sources. Above said properties of these sources are also applicable in material processing application such as ion implantation [16] at low pressure, plasma etching, sputtering, and deposition for materials processing purpose at high pressure [11, 12, 14, 17]. Plasma etching is used to selectively remove the material from surfaces, and therefore it is used in a critical manufacturing of integrated circuit. In ion implantation techniques, ions from plasma deposited within the substrate, it improves surface properties such as wear and corrosion resistance. The plasma processes like nitriding, ion implantation, plasma etching reactors etc. used the surface cusp magnetic field to confine large volume quiescent and high dense plasma. S. Mukherjee and P. I. John [18], have studied the sheath assisted nitrogen ion implantation and diffusion hardening processes for surface treatment of metals. The plasma is produced by electron impact ionization of nitrogen based gas mixtures, and its density was enhanced by confining it in a cusp magnetic field at typical operating pressures of 0.5 mtorr. The sample was placed in the centre of the cusp (null region of cusp magnetic field) where the plasma density is sufficiently high and the magnetic field is low. They have reported that the processes can be made more efficient if the produced plasma density is high and also by creating a large volume plasma device for accommodating large samples. Recently it has been found that to heat the core plasma for future commercial nuclear fusion Tokamak to ignition temperatures, high power neutral beams having the energy of hundreds of keV (up to1MeV D^0 or up to 870 keV H^0) are required [19]. For this application, the

plasma source should be capable of producing quiescent, uniform and dense plasma in order to produce a well-collimated high current density beam; for example, the noise level and spatial density should be less than 10% over a several hundreds of square centimetres at a plasma density of a few times $10^{12}cm^{-3}$. The multi cusp magnetic field confined large volume quiescent plasma have density in the ordered of 10^{12} cm^{-3}. Another most crucial application of multi-pole cusp magnetic field based plasma ion sources is the ion thrusters. Nowadays ion thruster is ideally suited for deep space missions and orbit station-keeping for satellites owning to their high efficiency and long life time [20]. Because of above mentioned two recent applications, study of plasma confined in different geometries of multi-pole cusp magnetic field pay a great attention in plasma physics.

1.1.2 Leak width

James. S. Sovey [21] has optimized the efficiency of these magnetic cusp confinement devices (for various applications) which depends directly on plasma losses through cusps. The associated property of plasma losses is Leak width of cusp magnetic field i.e. the width of the profile of plasma escaping through the cusp. Many studies of plasma containment through magnetic cusp have focused on quantifying the Leak width at the magnet pole. The plasma leak is crucial in cusp magnetic field since it governs the efficiency of the confined plasma. In pulsed high-β experiments, the leak width was of the order of an ion Larmor radius ($2r_i$) [4, 22], and authors suggested that cross field Bohm diffusion was responsible for the large leak width. In dissimilarity to early experiments, Kitsunezaki *et al*. [23], Hershkowitz *et al.* [24], Leung *et al.* [25], Kozima *et al.* [26] and R. Jones [27] have experimentally measured the leak width at the magnet surface via a scanning Langmuir probe. Authors have reported leak widths is of the order of hybrid gyro diameter $2(r_i r_e)^{1/2}$ (where r_i, r_e are

the ion and electron Larmor radius respectively) in a low-β plasma at sufficiently low neutral pressures, although under different plasma conditions the leak widths of the order (r_i) also have been observed [28].

Plasma leak widths of the line and point-cusp magnetic fields formed by an array of permanent magnets were measured using Langmuir probe by H. Kozima [26]. The author has reported that in quiescent Argon and Helium plasmas confined by point and line cusp, the leak width of the point-cusp magnetic field was qualitatively different and large compared with that of the line cusp magnetic field. The leak width of line cusp was nearly equal to the hybrid gyrodiameter $2\rho_h = 2\,(m_e m_i T_e T_i)^{1/2}/eB$, where m_e, m_i, T_e, and T_i are mass of an electron, mass of the ion, electron temperature, ion temperature, and magnetic field respectively consistent with Hershkowitz's finding. Many aspects of the experimental results are not yet fully understood, and numerous explanations for the cusp leak widths have been given. M. G. Haines [29] and I. Spalding [4] have considered electrostatic effects, collisions, and turbulence to explain the observed leak widths. I. S. Landman and F. R. Ulinich [30] have also considered electrostatic effects and collisions for the cusp leak width. The physics basis of leak width scaling with the hybrid radius was put forth by G. Knorr and R. L. Merlino [31]. In this work the self-consistent electric field generated in the cusp region due to the relative difference of Larmour radius between the ions and electrons, which gives rise to charge separation within the cusp. As a result, ions are drawn in towards the cusp centreline and electrons are pulled out. C. Koch and G. Matthieussent [32] have considered collisions, as the possible explanation for the cusp leak width. They developed a collisional diffusion model of the low-β plasma under the assumptions of quasi-neutrality and ambipolar diffusion of plasma in the plane of the cusp magnetic field. The authors reported that the leak width is proportional to the

hybrid gyroradius. Horiike *et al.* [33], have evaluated leak width in a ring cusp magnetic field plasma source using a traversable thermocouple. The leak width was measured from the spatial temperature profile as the thermocouple travels through the cusp. Many of the experimental results are not yet fully understood and numerous explanations for the cusp leak widths have been proposed till date.

A detail experimental study on the confinement properties of low beta plasma discharge confined in a spindle cusp magnetic field has been performed by R. A. Bosch and R. L. Merlino [34]. The authors measured leak width of escaping plasma over a large range of magnetic field and neutral pressure and reported that leak width varies between hybrid gyroradius to ion gyroradius. The authors also proposed a simple model for leak width in which they accounted that plasma diffuses across the magnetic field as a result of neutral particle collision while streaming out of the cusp along the magnetic field line. They also found that for the ratio $\frac{\omega_{pe}}{\omega_c} < 0.1$ (where is ω_{pe} plasma frequency and ω_c is electron cyclotron frequency) the ion leak width approaches the ion gyroradius, but for $\frac{\omega_{pe}}{\omega_c} > 0.5$ the ion leak width approach hybrid gyroradius. They also studied the multi-dipole cusp confinement of Argon discharge plasma and Potassium plasma produced by contact ionization. A comparison of the non-discharge potassium plasma produced with and without multi-dipole confinement indicates that the ion confinement time was improved by a factor of approximately 15 by the multi-dipole magnetic field [35]. A theoretical approach to leak width was presented by R. A. Bosch and R. M. Gilgenbach [36] and scaled the leak width with the magnetic field (*B*) and neutral background pressure (*P*) of plasma and gives the different formula for leak widths. Cooper *et al.* [37] measured the leak width of magnetic multi-dipole ring cusp plasma. The authors suggested that the cusp leak

width is much larger than Debye length and electron gyroradius and comparable to collision length. Hubble *et al.* [38] measured the spatial variation of leak widths for magnetic cusp plasma device. The spatial density profiles were used to infer the leak width. The leak widths were found to scale with the hybrid gyroradius.

A number of experiment have been performed in order to measure the leak width. The exact scaling for the amount of plasma leaking is not well known, though many scaling exists ranging from ion gyro-radius to electron gyro-radius apart and also the so-called 'hybrid gyroradius' [7, 23, 24, 27, 34, 38].

Most of the devices developed before with multi cusp configurations had very small volume of low beta region so as to maximize the useful high beta region. Hence the various fluctuations present in the low beta regions (edge regions and in-between two magnets) and their effects on the central high beta region have not been studied before. Also, most of the earlier studies in the multi-cusp field configuration was created by using either permanent magnets or electromagnets without any core material. The former case with permanent magnets had fixed magnetic field values and it was not possible to perform experiments for a wide range of magnetic field values. Simple electromagnets could have variable field values but they might also give unwanted edge effects. The bulk plasma confined in cusp magnetic field diffuse across the magnetic field and stream out along the magnetic field. Since cusp magnetic field containing good curvature and bad curvature of magnetic field. Hence we have built a new device in a multi-pole line cusp magnetic field configuration using electromagnets with a profiled core material with the following characteristics viz. variable field values and uniformly profiled magnetic field without any edge effects, controllable quiescent plasma volume and finite beta volume.

1.2 Scope and outline of the thesis

The rest of the thesis describes the construction of a versatile multi-pole line cusp magnetic field (VMMF) and the characterization of Argon plasma confined in this magnetic field. In-house constructed six-pole line cusp magnetic field using electromagnets over a 40 cm diameter and 1 m axial length has full control over the field free region as well as scale length of magnetic field. The confined filamentary plasma in this configuration is uniform and quiescent radially as well as axially, where ions are unmagnetized in this region. Also this region is controllable radially as well as axially. Studying fundamental plasma phenomena such as Landau damping, nonlinear coherent structure, wave-particle trapping and un-trapping, Soliton wave interaction, plasma waves etc., require reasonably quiescent plasma while the field free region in which ions are unmagnetized is an added advantage. Also, in this this system electromagnet has been used so that it can control over the position as well as size of the null region and capable to produces different magnetic field configuration. These characteristics of the device may create a new path in plasma applications as well as in plasma studies.

The remaining Chapters of this thesis are organized as follows. In Chapter 2, a detailed description on the simulation and experimental effort behind making a versatile variable Multi-pole line cusp magnetic field (VMMF). The 2-D simulation of variable multi-pole cusp magnetic field (VVMF) is performed using Finite Element Method Magnetic [39]. The VMMF has been produced by placing six electromagnets (with embedded profiled vacoflux-50 core, (Soft Magnetic Alloy with low coercive field strength)) over a large cylindrical volume (1 m axial length and 40 cm diameter). The magnetic field have been measured by hall probe method and compared with simulated magnetic field by performing simulation using FEMM tools. Moreover, in

this Chapter we have also demonstrated the control over the size of the null region and control over positing over the null region within vacuum chamber by changing the desire magnets current.

In Chapter 3, we have described the experimental setup and plasma diagnostic. Experimental setup consisted mainly of the vacuum chambers, plasma sources (hot cathode), pumping system, magnet system, and plasma diagnostics. This Chapter also contains details of the design and construction of the vacuum chamber, the design and construction of co-axial (filament arrangement in circular) circular as well as rectangular (filament arrangement in array) plasma source (hot cathode) for plasma production and plasma diagnostics. The whole chamber is pumped down to a pressure 10^{-6} mbar using a combination of TMP and rotary pump and combination of the Ionization and Pirani gauges are used for vacuum measurement. This Chapter, also contains detailed discussion on the construction of plasma diagnostics (viz. simple Langmuir probe for plasma parameters (electron temperature, plasma density, and floating potential) measurement, emissive probe for plasma potential measurement, and rack probe for fluctuation measurement) as well as MATLAB scripts for analysis of data obtained from the probes. These probes are necessary for characterization of plasma as well as plasma fluctuations.

In Chapter 4, the results of plasma characteristics with changing magnetic field values of multi-pole line cusp magnetic field have been presented. The crucial problem of plasma confined in cusp magnetic field that directly affect the plasma characteristics is the effective leak width of plasma (the width of the profile of plasma escaping through the cusp). The leak width of plasma governs the efficiency of the multi-pole cusp magnetic field plasma devices and thus affects the mean plasma

parameters. The effect of leak width of plasma on the plasma parameters viz. floating potential, plasma density, particle confinement time, radial variation of plasma parameters, plasma fluctuation with changing magnetic field values of multi-pole line cusp magnetic field have also been discussed in this Chapter.

The confined bulk plasma at the null region (confined region) of multi-pole line cusp magnetic field is diffusing across the magnetic field. It streams out along the magnetic field line toward the cusps, and as a result gradients in plasma parameters (plasma density, electron temperature, and floating potential) are formed. These gradients are also controllable by changing the magnetic field values of the multi-pole cusp magnetic field. In Chapter 5, we have described the results of plasma diffusion in a variable multi-pole cusp magnetic field in detailed. The instabilities due to these plasma gradients have also been identified in this Chapter. The fluctuations in plasma parameters as well as the scale length, frequency spectrum, wave-number-frequency spectrum, cross-correlation etc. are measured to identify the plasma instabilities (due to gradient in plasma parameters) that are responsible for the diffusion of plasma across the magnetic field. It is also necessary to understand the different modes (instabilities) that are present in the plasma confined by a multi-pole line cusp magnetic field before embarking on the proposed active experiments.

Finally, in Chapter 6, we consolidated our work and enumerated the major task that can be undertaken for further research in this field geometry.

References

1. F. F. Chen, "*Introduction to Plasma Physics and Controlled Fusion*", Plenum Press, New York and London.
2. Michael A. Lieberman and Allan J. Litchtenberg, *"Principle of Plasma Discharges and Materials Processing"*, John Wiley and Sons, 2005.
3. J. Wesson, *Tokamaks*, 4th ed. (Oxford University Press, Oxford, 2011).
4. I. Spalding, *Advances in Plasma Physics*, edited by S. A. Simon and W. B. Thomson (Interscience, New York, 1971), **Vol. 4**, p. 79.
5. R. J. Taylor, K. R. Mackenzie and H. Ikezi, Rev. Sci. Instrum. **43** (1972) 1675.
6. R. Limpaecher and K. R. Mackenzie, Rev. Sci. Instrum. **4** (1973) 726.
7. K. N. Leung, T. K. Samec and A. Lamm, Phys. Lett. A. **51** (1975) 490.
8. M. Sadowski, J. plasma Phys. **4** (1970) 1.
9. K. N. Leung, R. D. Collier, L. B. Marshall, T. N. Gallaher, W. H. Ingham, R. E. Kribel and G. R. Taylor, Rev. Sci. Instrum. **49(3)** (1978) 321.
10. Kuriyama *et al.*, Fusion Engineering and Design **26** (1995) 445.
11. Jaakko Hannes Vainionpaa, Ka Ngo Leung, Richard A. Gough, and Joe W. Kwan, Rev. Sci. Instrum.**79** (2008) 02C102.
12. Sudeep Bhattacharjee and Hiroshi Amemiya, Rev. Sci. Instrum. **70**, 3332 (1999).
13. Manish Pathak, V.K. Senecha, Rajnish Kumar and Dharmraj. V. Ghodke, Nuclear Instrum. and Meth. **A 838** (2016) 96.
14. M. Hosseinzadeh and H. Afarideh, Nucl. Instrum. And Meth. **A 735** (2014) 416
15. J. H. Kim, Phys. Procedia **66**, 498 (2015).
16. N. R. White, Nucl. Instrum. and Meth. **B37/38**, (1989) 78.

17. M. Rhodes, J. M. Dawson, J. N. Boeuf and N. C. Luhmann, J. Phys. Rev. Lett. **48 (26)** (1982) 1821.
18. S. Mukherjee and P. I. John, Sur. and Coatings Technol. **93** (1997) 188.
19. L. R. Grishma *et. al.*, Fusion Engineering and Design **87** (2012) 1805.
20. D. Goebel, and I. Katz, Fundamental of electric Propulsion; Ion and Hall Thrusters, JPL Space Science and Technology Series, 2008.
21. James. S. Sovey, J. Spacecraft **19(3)** (1982) 257.
22. T. K. Allen, A. J. Cox and I. J. Spalding, Phenomena of Ionised gases Proc. 7th Int. Conf. Belgrade, 2 1976.
23. A. Kitsunezaki, M. Tanimoto and T. Sekiguchi, Phys. Fluids **17** (1974) 1895.
24. N. Hershkowitz, K. N. Leung and T. Romasser, Phys. Rev. Lett. **35** (1975) 277.
25. K. N. Leung, N. Hershkowitz and K. R. Mackenzie, Phys. Fluids **19(7)** (1976) 1045.
26. H. Kozima, S. Kawamoto and K. Yamagiwa, Phy. Lett. **86** (1981) 373.
27. R. Jones, Nuovo Cimento **34** (1982) 157.
28. R. Jones, Plasma Phys. **21** (1979) 505.
29. M. G. Haines, Nuclear Fusion **17** (1977) 811.
30. I. S. Landman and F. R. Ulinich, Sov. J. Phys. **8** (1982) 371.
31. G. Knorr and R. L. Merlino, Plasma Phys. and Control. Fusion **26** (1984) 433.
32. C. Koch and G. Matthieussent, Phys. Fluids **26** (1983) 545.
33. H. Horiike, M. Akiba, Y. Ohara, Y. Okumura, and S. Tanaka, Phys. Fluids **30(10)** (1987) 3268.
34. R. A. Bosch and R. L. Merlino, Phys. Fluids **29(6)** (1986) 1998.
35. R. A. Bosch and R. L. Merlino, Rev. Sci. Instrum. **57**(1986) 2940.
36. R. A. Bosch and R. M. Gilgenbach, Phys. Lett. A 128 **(8)** (1988) 437.

37. C. M. Cooper, D. B. Weisberg, I. Khalzov, J. Milhone, K. Flanagan, E. Peterson, C. Wahl, and C. B. Forest, Plasma Phys. **23** (2016) 102505.

38. A. A. Hubble, E. V. Barnat, B. R. Weatherford and J. E. Foster, Plasma Sources Sci. Technol. **23**(2014) 022001.

39. D. Meeker, *"Finite element method magnet"*, Version 4.2, User's Manual (2015), http://www.femm.info.

Chapter 2

Versatile **M**ulti-pole cusp **M**agnetic **F**ield (VMMF) system

Multi pole cusp **M**agnetic **F**ield (MMF) is usually created by placing rows of magnets along the length of cylindrical plasma chamber with alternating polarity. In 1973, Limpaecher *et al*. first observed that MMF generated by permanent magnets can increase the density of a DC discharge plasma [1]. Later confinement of plasma in different cusp geometries was investigated by Leung *et al.* and was observed that a full-line cusp geometry gives the highest density by confining primary electrons [2].

It is desirable to achieve a multi-pole line cusp configuration such that it has the following properties,

I. A field free region of cylindrical volume with 1m length and 10 cm radius.
II. The low plasma beat (β-ratio of plasma pressure to magnetic field pressure) cusp regions far from this field free region, so as to avoid the travelling of any disturbance in the low beta region towards the field free region.
III. To have the magnetic field values variable, so as to control the gradients in the low beta region and hence to minimize any possible instabilities due to the gradients. The gradients are avoidable due to the finite boundary of the plasma volume. Thus electromagnets are necessary.

Thus in the present chapter, we have demonstrated a detailed characteristics of a Versatile Multi-pole line cusp Magnetic Field (VMMF). The VMMF has been produced by placing six electromagnets (with embedded profiled vacoflux-50 core) over a large volume (1 m axial length and 40 cm diameter). The edge of vacoflux-50 core material is profiled in curvature shape to avoid edge effect on magnetic field lines. Similar field lines have been observed by performing simulation using Finite Element Method Magnetics tools (FEMM) [3]. The unique feature of this VMMF is that it is profiled using a core material of the electromagnets which will allow changing of field values with the effect of using different permanent magnets. Moreover, the VMMF also can be control the size of the null region without changing the number of the poles.

Based on these requirements, a simulation using the FEMM [3] was done with permanent magnets to finalize the size and axial length of the chamber to satisfy the basic experimental requirement (I and II) as shown in figure 2.1. After some iterations, it was found that the cusp magnetic field using six permanent magnets having the length of 1 m kept in the multi-pole cusp configuration at 60^{o} each along the circumference of 40 cm diameter cylinder meets the requirements. After finalizing this configuration, the desire for having electromagnets was looked upon so as to have the comfort of varying magnetic field values.

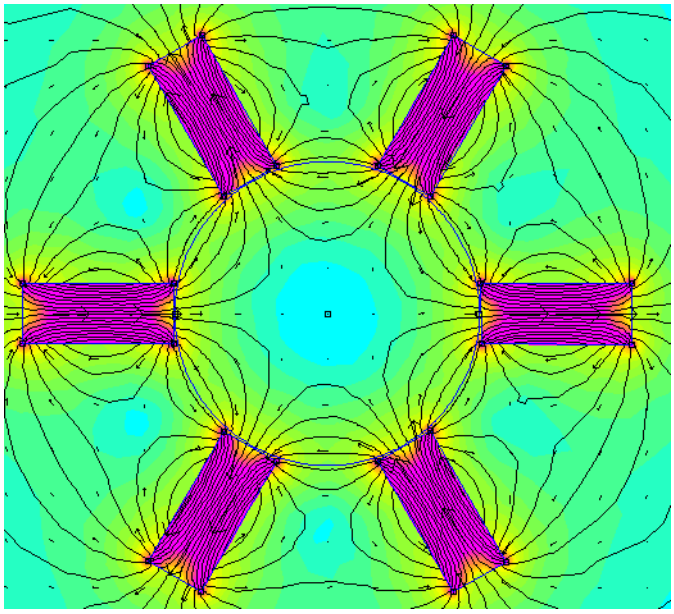

Figure 2.1. Constructed model of multi-pole cusp magnetic field in FEMM software using permanent magnets.

2.1 Electromagnet

Then having decided to have electromagnets the design of single unit was started to a magnet with field values variable from 0-4 kG. Initially it was attempted to have an electromagnet wound with solid copper wires of circular and square cross-section. One magnet with continuous winding of 80 turns over square cage (made by PVC material) was made as shown in figure 2.2. But the main drawback of this kind of scheme was the overheating of magnets within 15 minutes at 100 A magnet coil current. To overcome this problem, it was necessary to have windings supporting active cooling. This could be achieved with windings hollow square copper tubes. There are different techniques in winding for making electromagnets with active cooling. The double-pancake windings gives very effective cooling. In this technique the number of turns of magnets can be broken to different segments such that the forced chilled water goes in parallel scheme and the current goes in series. Here a single electromagnet was designed such that it comprised of 8 segments where each

segment had 10 turns in double-pancake winding configuration. The windings were done using a diametrically elongated semicircle cross-sectional copper pipe. The inter windings were insulated from each other by employing a glass-wool based insulator jacket of size matching with the copper pipes. The whole winding has been packed together by an appropriate cage made of poly vinyl material (PVC) with required thickness.

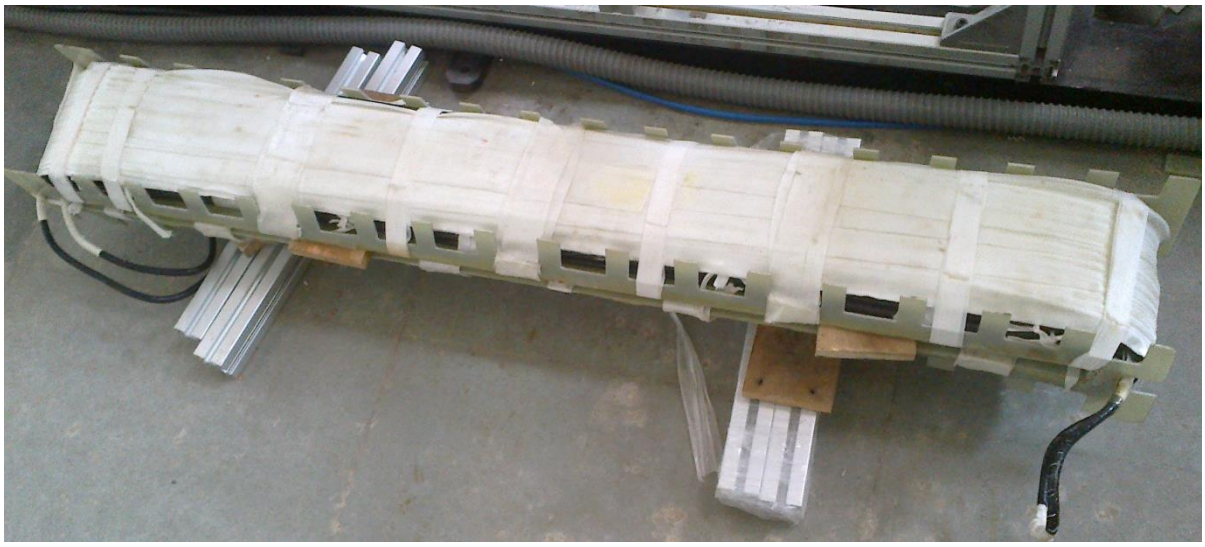

Figure 2.2. Initial magnet with solid copper rod and continuous winding (without cooling facilities).

To avoid the effect of non-uniformity in the windings along the length and also to get the net effect as using permanent magnets it was decided to use an appropriate core material. After a brief consideration vacoflux-50 was chosen as the core material. The vacoflux-50 is an alloy of iron and cobalt in the ratio 50:50. This material was selected for its high Curie temperature and high saturation flux density. Again to avoid the saturation due to sharp edges the face of core material was profiled as smooth curvature as shown in figure 2.3. The annealing of this core material is done after the shaping and machining. The physical dimensions of vacoflux-50 are 120cm, 2cm and 12 cm respectively for length, width and height respectively and is also embedded in

electromagnet as shown in figure 2.4 (a) and (b). The properties of vacoflox-50 are the following:

- Relative Permeability > 4000
- Saturation flux density >2.0 Tesla
- Curie temperature >700^{o} C
- Material (chemical composition) - Vacoflux-50 (Iron 50% and Cobalt 50% alloy)

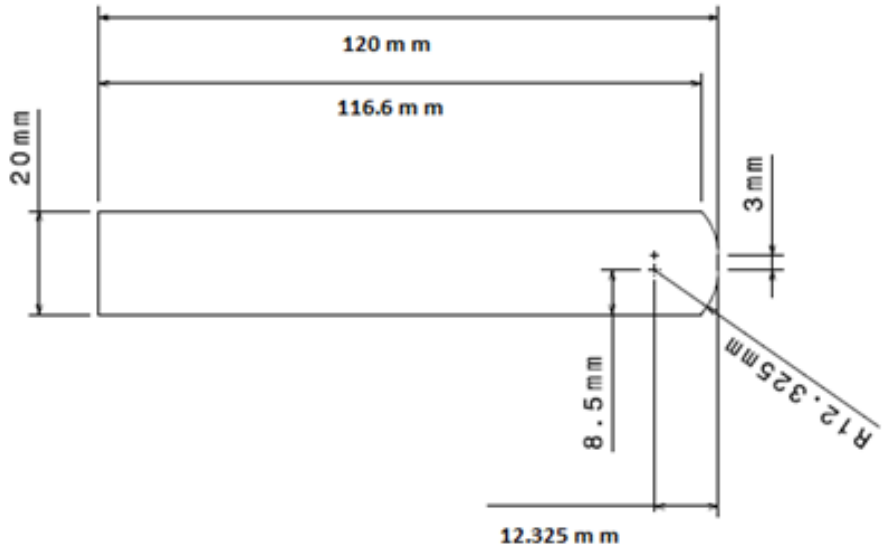

Figure 2.3. Schematic cross sectional view of vacoflux-50 showing curvature surface at one edge.

Figure 2.4 (a) shows the CATIA image of the electromagnet and its cross sectional view is shown in figure 2.4 (b). The cross sectional view shows vacoflux-50 core material is embedded in magnet. The figure 2.4 (c) shows the photo image of original electromagnet of the VMMF system. Subfigure of figure 2.4 (c) shows the series current connection and parallel water connection of 8 segments of electromagnet to improving the effective water cooling and magnet coil current. The physical dimensions of a rectangular magnet are in 132 cm, 19.5cm and 14cm for length, width and height respectively. The six replica of this electromagnet have been used for

producing the multi-pole cusp magnetic field configuration. Figure 2.5 shows the six electromagnets with embedded profiled vacoflux-50 core kept in the multi-cusp configuration at 60^{o} each over the cylindrical chamber having diameter 40cm and axial length 1.5m length.

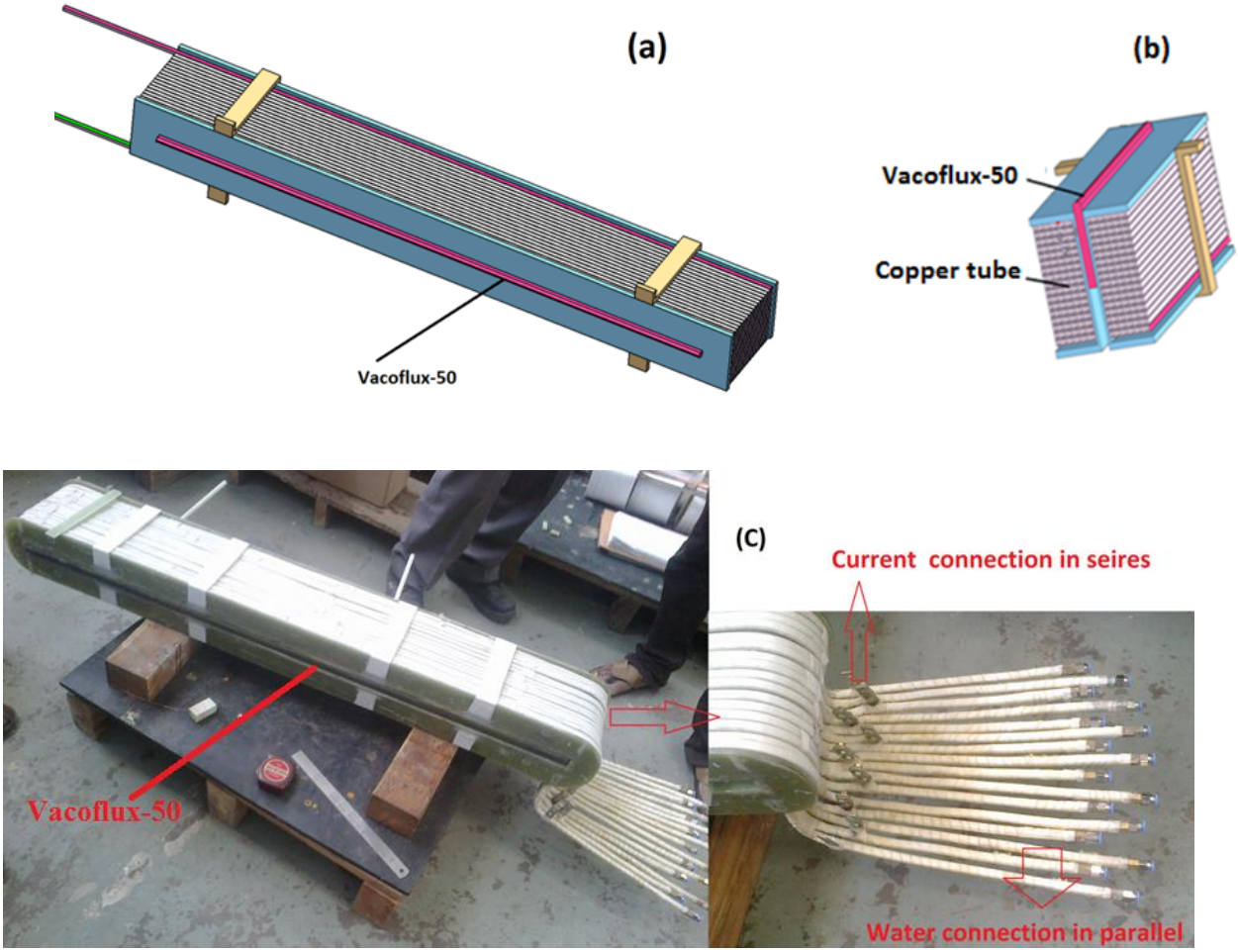

Figure 2.4. (a) Electromagnet with embedded vacoflux-50 core material constructed in CATIA software. (b) Cross sectional view of electromagnet with embedded vacoflux-50 (c) A photograph of real electromagnet.

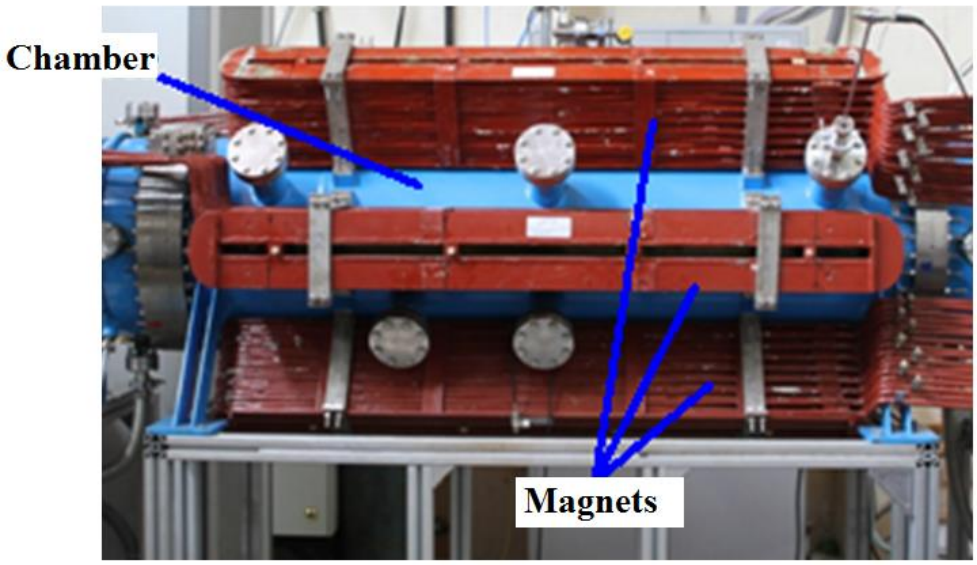

Figure 2.5. A photograph of Six-pole electromagnets over the periphery of cylindrical vacuum chamber.

2.2 Simulation and mapping of the VMMF

The model for VMMF is constructed using FEMM tool, and the simulations are performed with changing current in the magnets for vacoflux-50 core and also for air core (by simply changing the property of core material in the model). Moreover, the simulations are also performed with the changing of the edge shape of vacoflux-50 core material in the model, for observing the edge effect of core material on the magnetic field lines. The results obtained from simulations are described as follow.

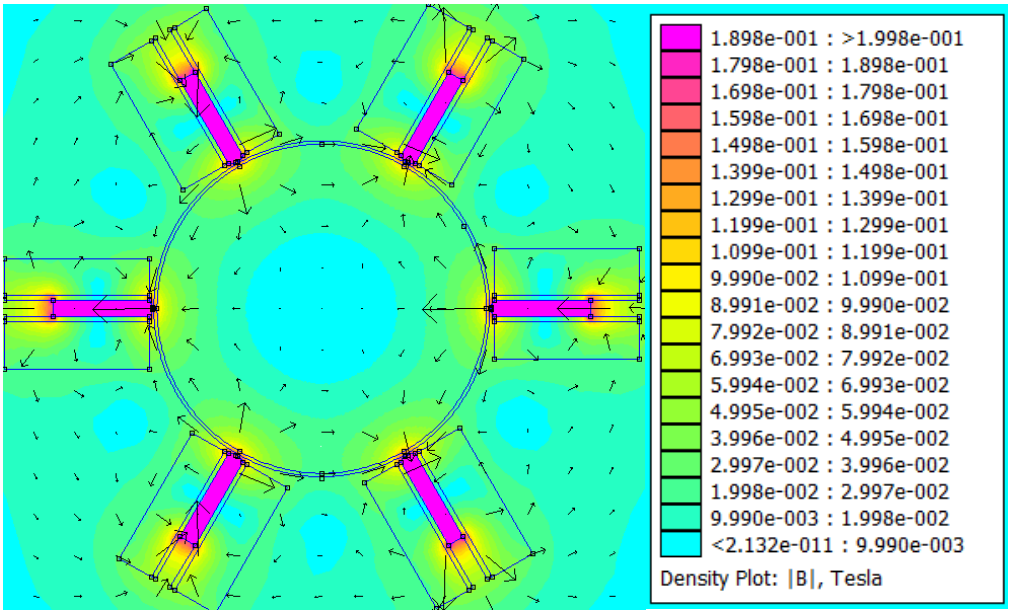

Figure 2.6. Contour plot of the vacuum field lines in (r, θ) mid plane of device from FEMM simulation when core is magnetized with 150 A, magnet coil current. Colour code for magnetic field is same for all FEMM simulation figures until and unless specified and maximum magnetic field is less than the saturation magnetic field of core.

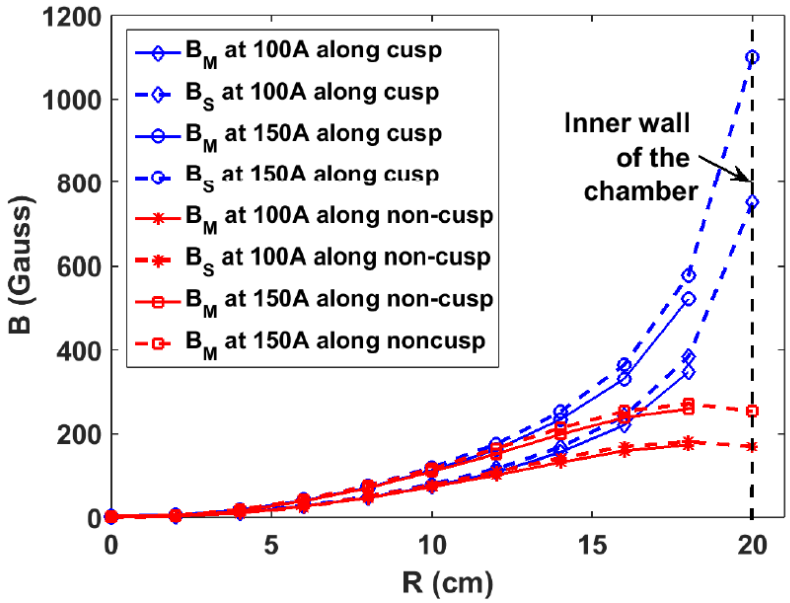

Figure 2.7. A comparison of the mean magnetic field between simulated (B_s), and measured (B_M) along the radius through the cusp and non-cusp regions when the core is magnetized with magnet coil currents 100 A, and 150 A

Figure 2.6 shows the contour plot of the vacuum field lines in the (r, θ) mid plane of the device from FEMM simulation when core material is magnetized with

150 A magnet coil current. It shows six electromagnets with embedded vacoflux-50 core, which are placed over a periphery of 40 cm diameter of the chamber. The magnetic field is measured over the different (r, θ) planes of the device using triple axis gauss probe (F. W. Bell, model Z0A99-3202) and suitable gauss meter (F. W. Bell series 9900). The radial variation of the measured magnetic field (B_m) along the cusp region (θ = 0^o) and the non-cusp region (the region exactly in between two magnets, (θ = 30^o)) are shown in figure 2.7 for two different magnet coil currents (I_{mag}, 100 A and 150 A). It shows the simulated magnetic field (B_s) is matching well with the measured value (B_m). The variation of magnetic field component B_r and B_θ are given in an appendix A.

Figure 2.8 shows contour plot of the vacuum field lines of an electromagnet with air as a core (figure 2.8 (a)) and vacoflux-50 as a core (figure 2.8 (b)). For an air core magnet, magnetic field lines pass through whole magnet. However, for the vacoflux-50, magnetic field lines pass through only the core, resulting dense magnetic field lines at the pole for vacoflux-50 core. Thus magnetic field is higher for vacoflux-50 core at the pole as compared to the air core. The edge shape of core material which affects the magnetic field lines has been also taken care. The sharp edge of core material distorts the magnetic field lines which cause the non-uniform distribution of field lines near the surface of the core. This sharp edge effect of core material on magnetic field lines is overcome by making curved edge of core material as shown in figure 2.9 (a). It shows the cross-sectional view of the vacoflux-50 material, the edge of vacoflux-50, which is profiled in curved shape with a radius of curvature of 12.32 mm. Figure 2.9 (b) shows FEMM simulation of magnetic field lines at core edge is curved and figure 2.9 (c) shows the edge of the core made sharp (rectangular). It is

clearly visible from figure 2.8 (b) that magnetic field lines are uniformly distributed over the curved edge vacoflux-50 core.

Figure 2.10 (a) shows the radial variation of magnetic field and 2.10 (b) shows its gradient along the cusp region as well as along the non-cusp region for air core and for vacoflux-50 core, when the core is magnetized with magnet coil current (I_{mag}) 150 A. It can be clearly observed from both the figures that in the nearly field free region, the gradient is weak and nearly equal for both cores. Beside near the pole (near the edge of the device), the gradient in the magnetic field increases sharply for vacoflux-50 core compared to air core along the cusp region. Figure 2.10 (c) shows the variation of pole magnetic field (B_p, near the magnet at R = 20 cm) with respect to magnet coil current for air core and vacoflux-50 core. The rate of change of pole magnetic field (B_p) with respect to magnet coil current is very high (7.53 G/A) for vacoflux-50 core compare to air core (2.15 G/A).

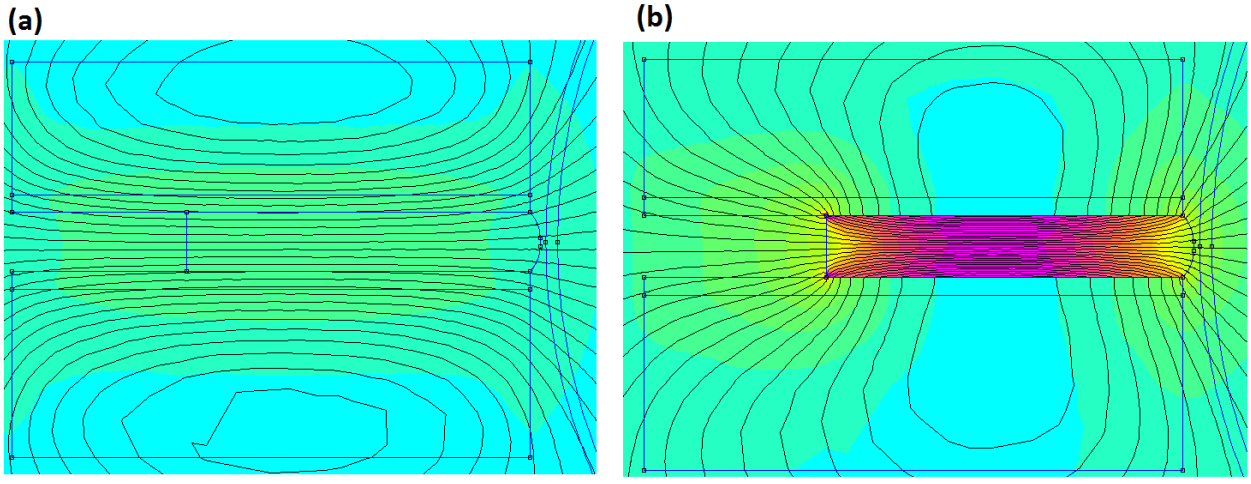

Figure 2.8. Contour plot of the vacuum field lines of electromagnet (a) for air core (b) for vacoflux-50 core when core is magnetized with magnet coil current 150 A using FEMM simulation. Colour code is same as figure 2.6, and maximum magnetic field is less than the saturation magnetic field of core.

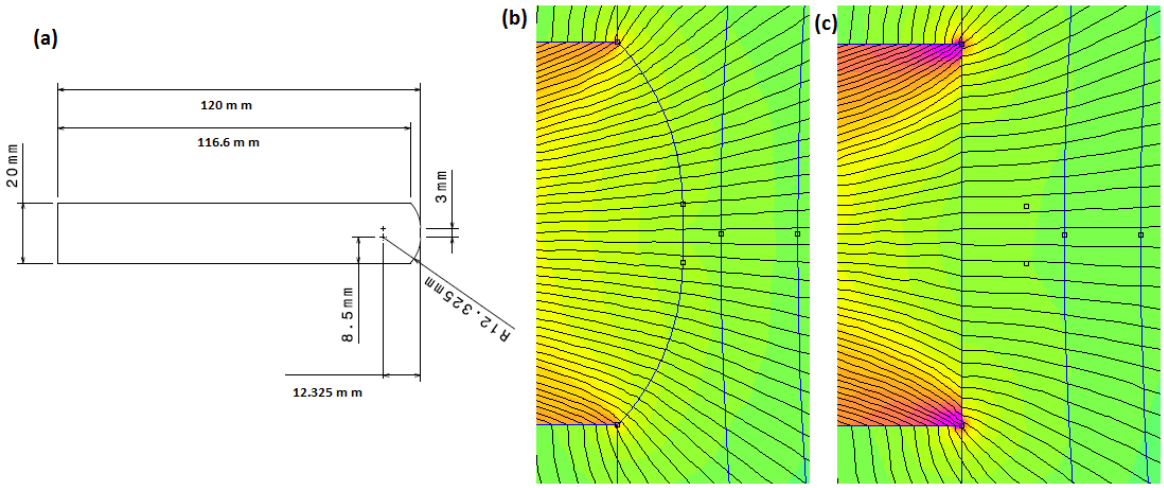

Figure 2.9. (a) Cross sectional view of vacoflux-50 showing curvature surface at one edge. Other two figure shows FEMM simulation of field lines for (b) edge of vacoflux-50 is curved and for (c) edge of vacoflux-50 is sharp (rectangular) when core is magnetized with 150 A magnet coil current (I_{mag}). Colour code is same as figure 2.6, and maximum magnetic field is less than the saturation magnetic field of core.

Figure 2.10 (d) shows the radial variation of the magnetic field in the cusp region when magnets are energized with different magnet coil currents. It can be clearly observed that the radius of nearly field free region is decreased with increasing magnet coil current. Thus, using electromagnets with the core material, field values can be varied by varying magnet coil current with the effect of using different permanent magnets and the volume of nearly field free region (null region) also changed with changing magnets coil current without changing the number of the poles.

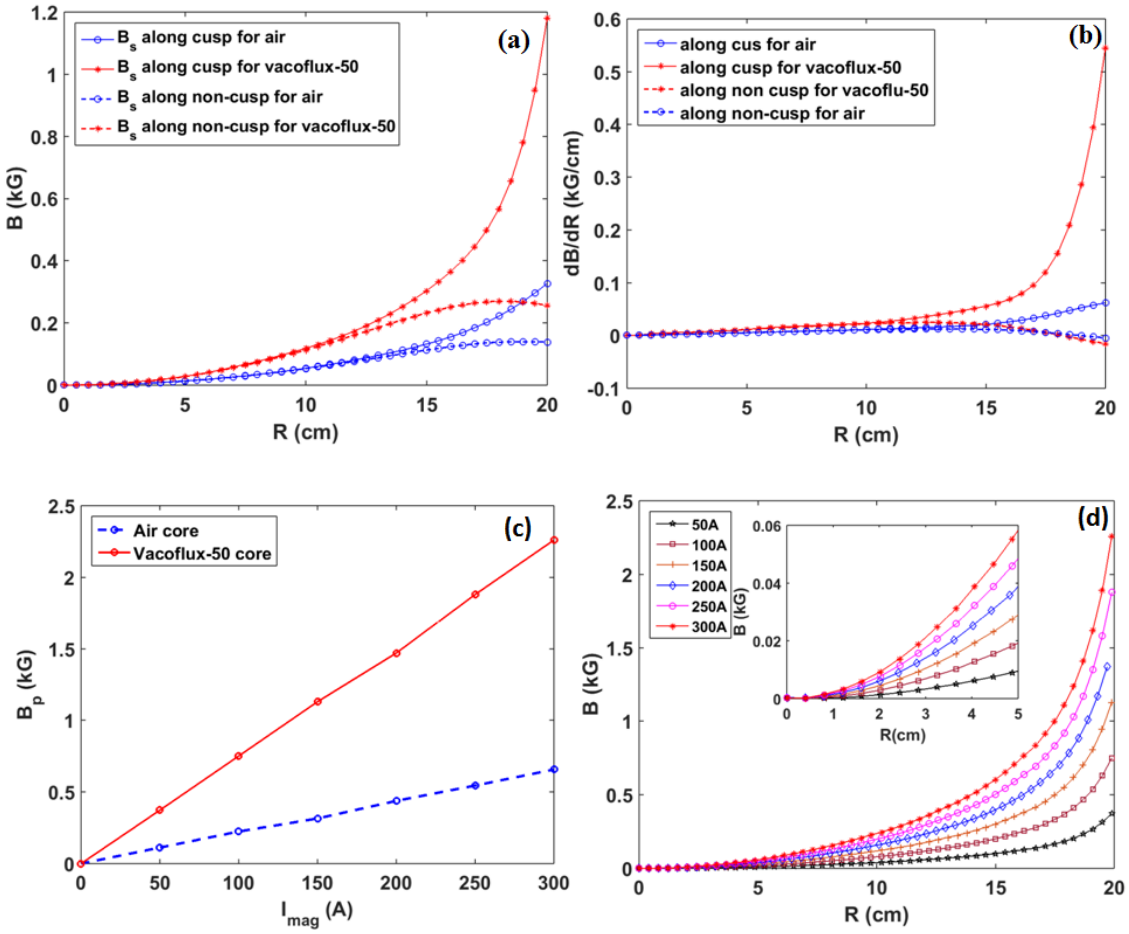

Figure 2.10. (a) Radial variation of magnetic field along cusp region and (b) its gradient with respect to radial distance for vacoflux-50 and air core and magnet coil current (I_{mag}) is 150 A. (c) Variation of pole magnetic field (B_p) (at R = 20 cm, near the pole of magnet) with magnet coil current for air Core and vacoflux-50 core. (d) The radial variation of magnetic field along the cusp region when vacoflux-50 core is magnetized with different magnet coil currents (I_{mag}).

We also compared cusp magnetic field with empirical formula for cusp magnetic field suggested by previous work in the same geometrey. With these empirical formula, all the constants are calculated for our geometries allowing the magnetic field to be calculated along the cusp region at different radial locations and to be compared with the simulation and exprimentally measured values. Figure 2.11 shows the comparison of magnetic field between measured (B_M), simulated (B_S), and calculated magnetic fields using empirical formulas from the studies of Leung *et al.*[4] and Kim *et al.*[5].

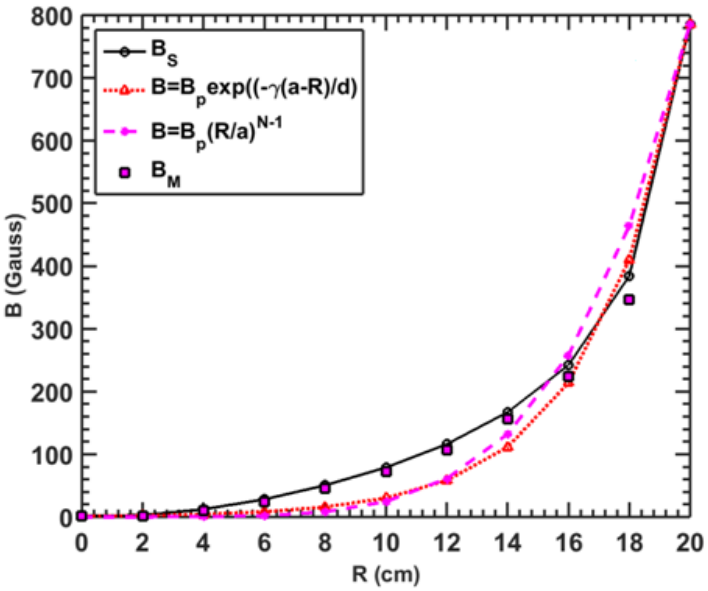

Figure 2.11. Comparison of magnetic field between simulated (B_s), measured (B_m) and calculated from empirical formula along the cusp region (θ = 0°) when I_{magnet} is 150 A. Where, $\boldsymbol{B_p}$ is pole magnetic field at R = 20 cm (near the pole), **γ** is geometrical factor of the device, ***d*** is distance between two magnets, **a** is radius of chamber, *N* is number of magnets and ***R*** is radial distance.

2.3 Adjustment of null region

These sets of magnets also provide the control over the number of null regions to be formed inside the plasma at the desired positions. While the number of null regions can be varied by energizing the required magnets, the position of the null regions can be adjusted by changing the magnet coil current in required magnets. Figures 2.12 (a) show the position of two null regions and 2.12 (b) shows the shifting of the position of the null region for a different set of currents in the magnets simulated in vacuum conditions using the FEMM software.

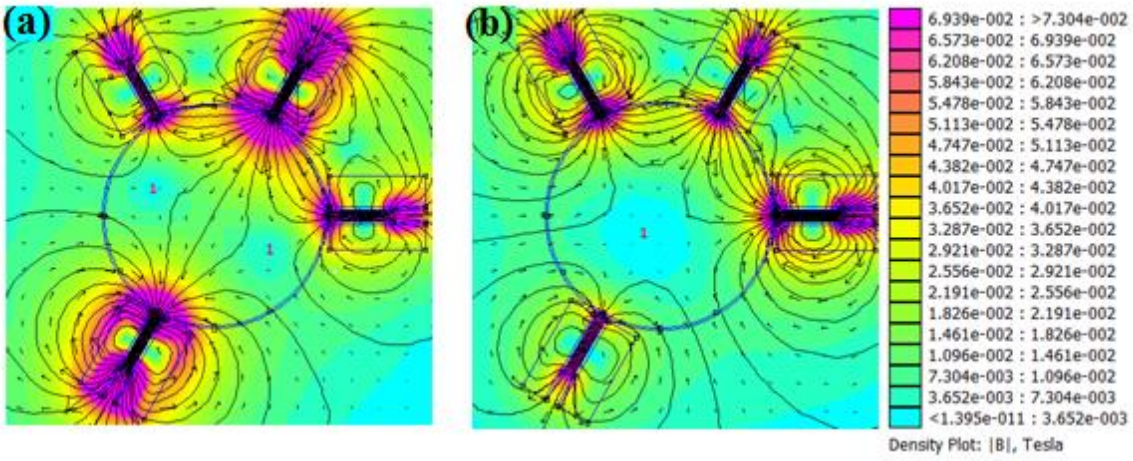

Figure 2.12. (a), and (b) shows the contour plot of the vacuum filed line in *(r,θ)* plane of device from FEMM showing two null regions and their adjustment in *(r,θ)* plane respectively. (1 - Null region)

2.4 Different cusp magnetic field configurations

These sets of magnets also provide different magnetic field configuration by appying current in the required magnets. Figure 2.13 shows the four-pole cusp magnetic field configuration and it can be produced by appying current in four cross magnets. The subfigure in figure 2.13 shows the separatix point. This configuration is widely used in magnetic reconnection experiments [6-8]. Figure 2.14 shows the mirror configuration of magnetic field and can be produced by applying current in two magnets. This configuration is also widly used in basic plasma studies like plasma diffusion in a bad curvature of magnetic field as well as different gradient forces on plasma species, loss cone instabilities etc [9-11].

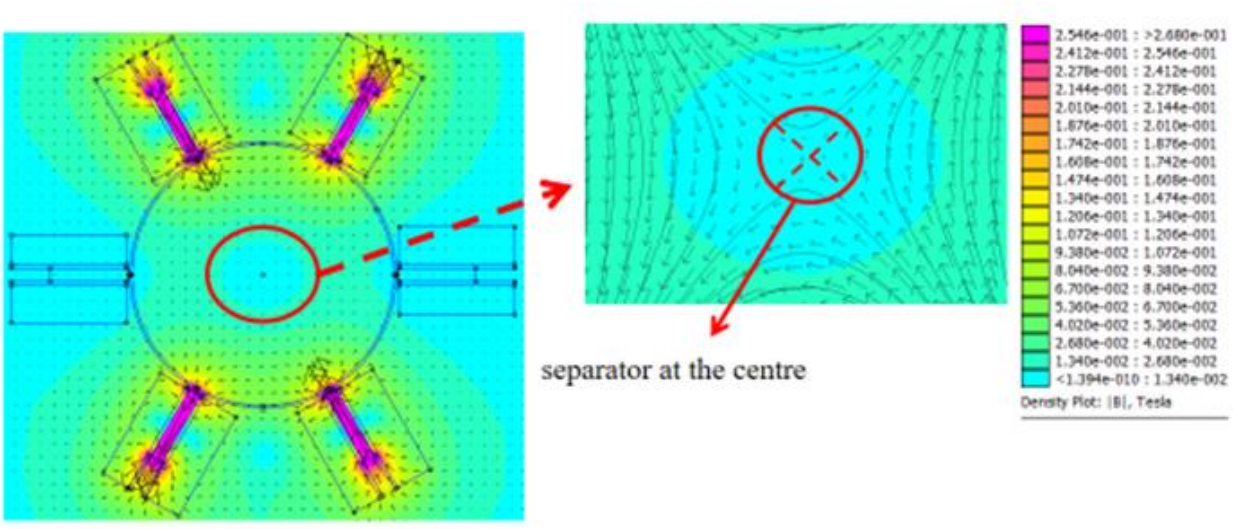

Figure 2.13. Shows the contour plot of four-pole cusp magnetic field configuration. Subfigure shows separatix point.

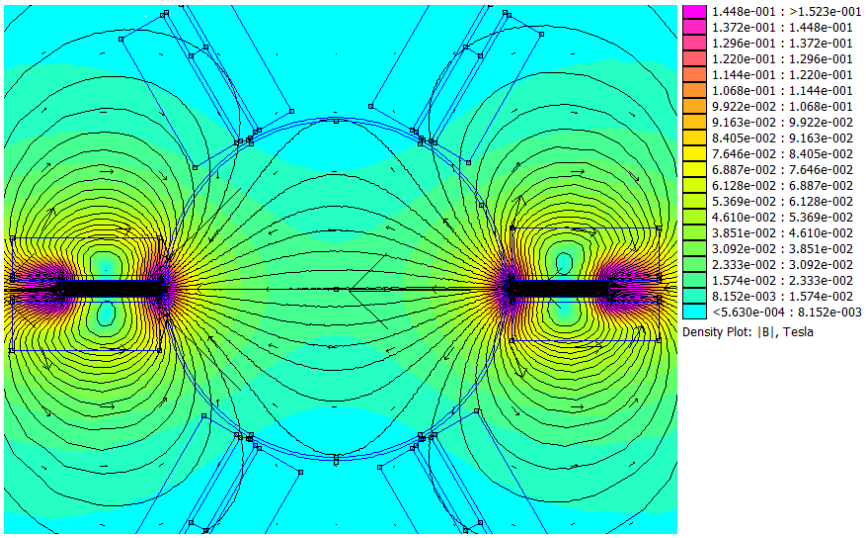

Figure 2.14. Shows the contour plot of a mirror magnetic field configuration.

References

1. R. Limpaecher, and K. R. MacKenzie, Rev. Sci. Instrum. **44**, 726 (1973).

2. K. N. Leung, T. K. Samec, and A. Lamm, Phys. Lett. A **51,** 490 (1975).

3. D. Meeker, *"Finite element method magnet"*, Version 4.2, User's Manual (2015), http://www.femm.info.

4. K. N. Leung, N. Hershkowitz, and K. R. MacKenzie, Phys. Fluids **19**, 1045 (1976).
5. J. H. Kim, Phys. Procedia **66**, 498 (2015).
6. M. N. Rosenbluth and R. F. Post, Phys. Fluids **8,** 547 (1965).
7. R. F. Post, Phys. Fluids, **9,** 720 (1966).
8. A. Makhijani, A. J. Lichtenberg, M. A. Lieberman, and B. Grant Logan, Phys. fluids **17**, 1291 (1974).
9. M. R. Brown, Phys. Plasmas **6**, 1717 (1999).
10. Masaaki Yamada, Hantao Ji, Scott Hsu, Troy Carter, Russell Kulsrud, Norton Bretz, Forrest Jobes, Yasushi Ono, and Francis Perkins, Phys. Plasmas **4**, 1936 (1997).
11. R. L. Stenzel, J. M. Urrutia, M. Griskey, and K. Strohmaier, Phys. Plasmas **9,** 1925 (2002).

Chapter 3

Plasma production and diagnostics

Usually experimental systems are built with as many options possible to do many experiments without compromising too much on the original main idea. An experimental device has been designed and fabricated for experimental studies in space plasma physics (viz. magnetic reconnection, magnetosonic wave), plasma turbulence in inhomogeneous magnetic field, and active experiment (viz. ion acoustic wave, soliton wave interaction, electron plasma wave, Landau damping, non-linear coherent structure, wave-particle trapping and un-trapping magnetosonic wave etc.) in a quiescent plasma. With these options the basic features which are considered for the planed device are as follows.

- Low plasma density to high density
- Operable at wide range of pressure to cover collision less to collisional regimes
- Having quiescence plasma allowing active experiments (viz. ion acoustic wave, soliton wave interaction, electron plasma wave, Landau damping, non-linear coherent structure, wave-particle trapping and un-trapping etc.) possible
- Control on magnetic coils to get different magnetic field configurations
- Having options of connecting various kinds of plasma sources as well as having facility to connect sources from both the ends of the chamber.

It has been tried to accommodate as much as possible in the multi-pole line cusp magnetic field plasma device (MPD).

3.1 Vacuum Vessel

The vacuum vessel of MPD is made up of non-magnetic stainless steel (SS-304L). It consists of two parts: a) conical chamber and b) main chamber. The figure 3.1 (a) shows an image of the integrated multi-pole cusp magnetic field plasma device (MPD), and 3.1 (b) shows an image of the device without magnet system. Figure 3.2 shows the sectional view of the device. The figure 3.3 shows the sectional view and isometric view of the main chamber. In both the figures all physical dimensions are in mm.

The main chamber is having length 1.5 m and 40 cm inner diameter and is made up of non-magnetic stainless steel (SS-304). It has a total 12 radial ports of DN 63 CF standard welded at various axial locations and are distributed azimuthally as shown in figure 3.3. These ports have been used for feedthroughs of electrical connections, viewing inside the chamber and for movable probe diagnostics as shown in figure 3.3. The main chamber also has slots over a periphery of main chamber to firmly support the electromagnets by non-magnetic C-clamps as shown in figure 3.1 (b). The one end of the main chamber is closed with a DN 400 CF flange and also this flange has different DN 63 CF port and DN 35 CF port for plasma viewing and for plasma diagnostics particularly for axial measurements. The other end of the main chamber connected with conical chamber through DN 400 CF joint. The conical chamber has four DN 35 CF ports distributed azimuthally 90^o apart for feedthroughs of electrical connections to the inside hot cathode source. The conical chamber is also capable to support hot cathode source and has the facility to move the source along axis in main chamber volume. The smaller end of the conical chamber is connected to a pumping system using L shaped DN 160 CF joint. The pumping system consists of a turbo molecular pump TMP

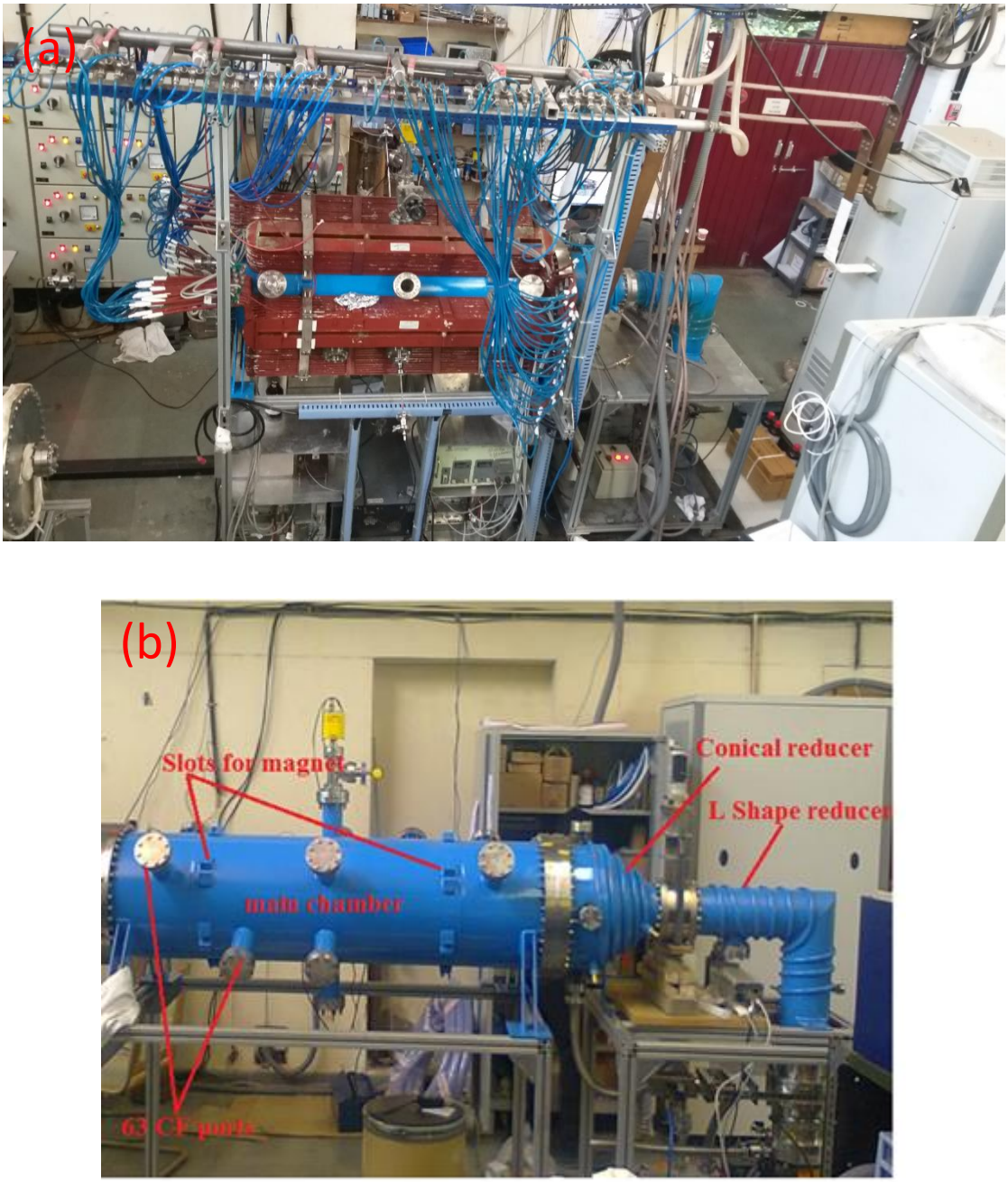

Figure 3.1. (a) Photograph of the multi-pole cusp magnetic field plasma device (MPD). (b) Photograph of the multi-pole cusp magnetic field plasma device (MPD) without magnet system.

(having speed 440 l/s and model TPH 521 PC) backed by rotary pump (having speed 3 l/s and model DUO 10 MC). This pumping system smoothly takes the system to a base pressure of 1×10^{-6} mbar within 3 hours. The conventional Pirani gauge, and a hot cathode ionization gauge (Hornet IGM-402 model) are employed to monitor the pressure of the device. All the gauges have been placed away from the magnetic field

using a suitable extension so as to reduce the effect of magnetic field on the filament. The pumping system and gauge are controlled by DCU controller. The automatic pressure controller is used for gas feed during plasma discharges. All joints and ports in vacuum system in CF standard and copper gaskets are used for vacuum seal.

The whole vacuum system is mounted on a non-magnetic stand made up of aluminium square bars. The stand containing conical chamber and pumping system can be moved axially. The L shape connector and conical chamber has been brazed with hollow copper pipe for cooling the wall.

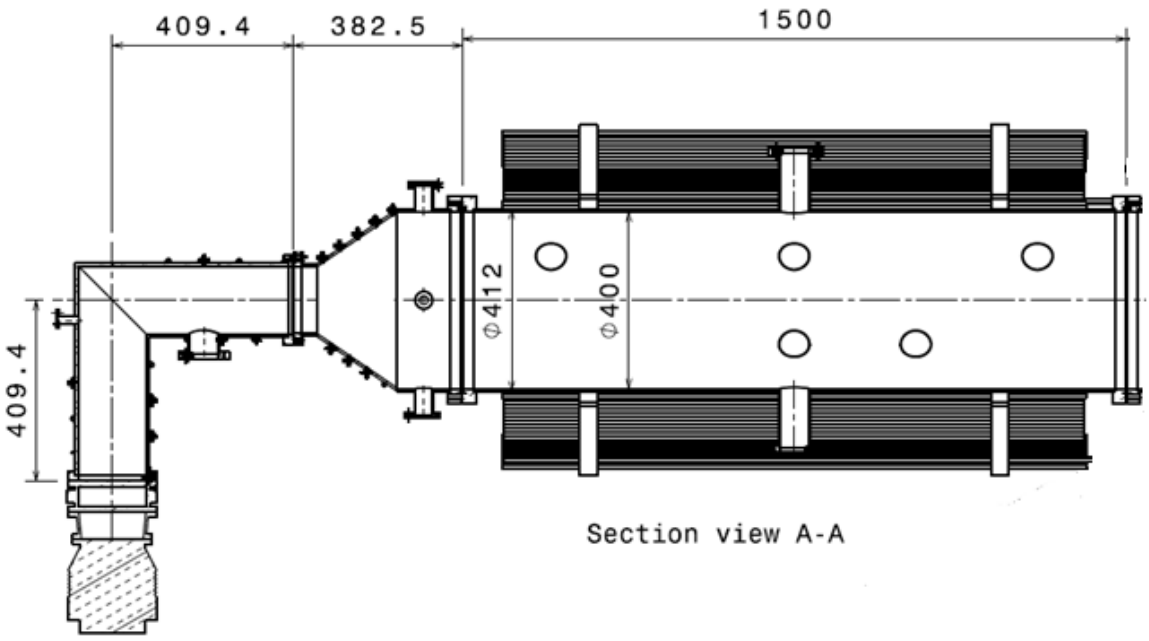

Figure 3.2. Sectional view of experimental setup. All dimensions in mm.

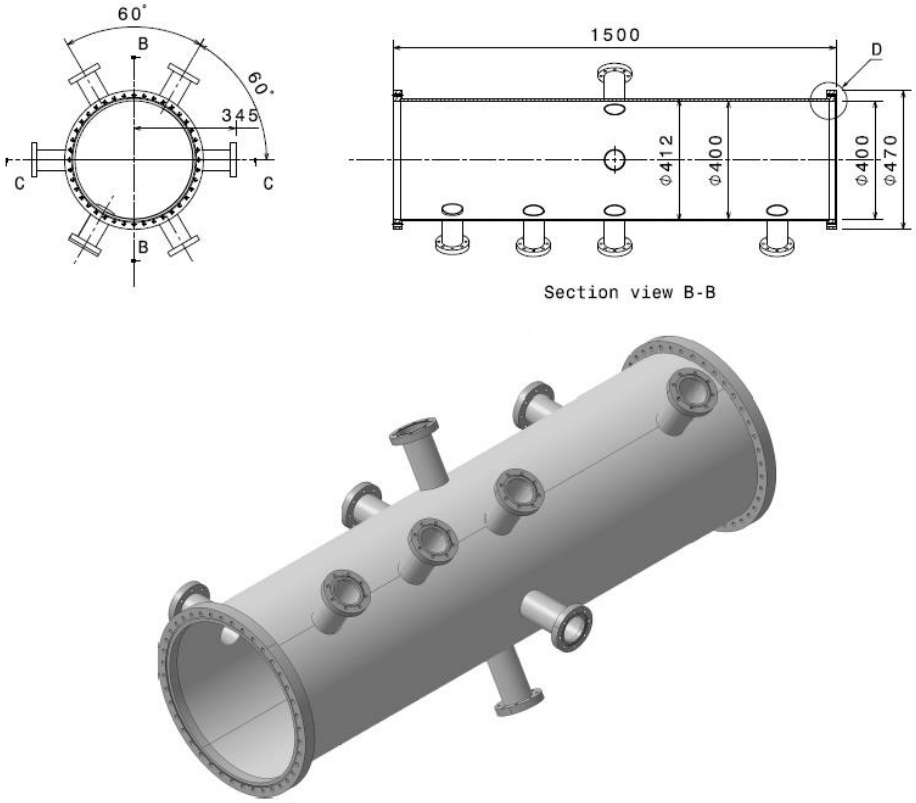

Figure 3.3. Sectional view and Isometric view of main chamber. All dimensions in mm.

3.2 Plasma source

Hot cathode plasmas which are made using tungsten filaments are generally quiescent [1]. Studying fundamental plasma phenomena such as Landau damping, non-linear coherent structure, wave-particle trapping and un-trapping etc., requires reasonably quiescent plasma of finite volume while the plasma, being in a field free region is an added advantage. It is generally observed that the ratio of m_e/m_i crucially controls the finite beta effects [2]. Hence, it is desirable to have a source which can produce plasma of gas species with different masses, especially with inert gases like Argon, Krypton and Xenon etc. With these desired considerations, a tungsten filament based source has been designed and fabricated. A two dimensional vertical array of joule heated filaments situated at the one end of the chamber and biased negatively with respect to

the grounded vacuum vessel has been used to produce plasma in MPD. This two dimensional vertical array has five filaments each having length of 8 cm made of 0.5 mm diameter tungsten wire. The filaments are arranged at 2 cm spacing, the holding system can also accommodate filaments arranged at 1 cm separation if the requirement arises. This source is fitted from the conical reducer such that the filaments are inside the main chamber itself where the magnetic field is low. Also it has been taken care to push the source well inside the main chamber to keep it away from the long edge of the magnets. The lighting photo of rectangular plasma source inside the vacuum chamber is shown in figure 3.4.

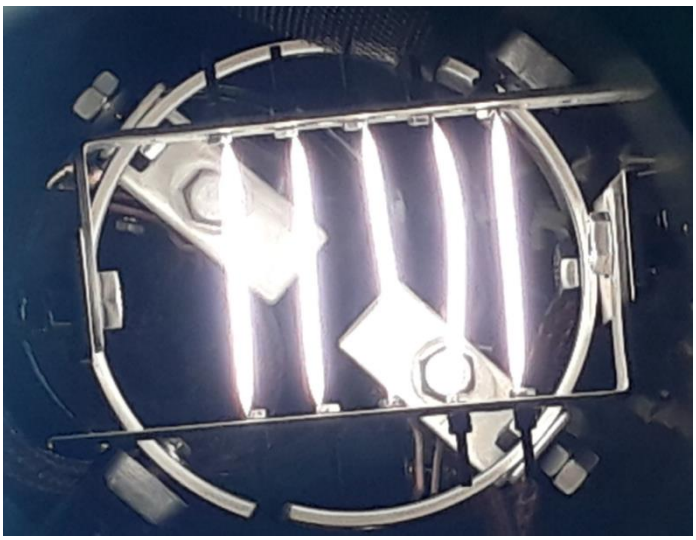

Figure 3.4. Front view of glowing rectangular hot cathode plasma source inside the vacuum chamber.

3.3 Plasma discharge mechanism

The filamentary Argon discharge plasma is struck between hot filaments based cathode source and grounded vessel wall. These filaments are powered in parallel by a 500 A, 15 V floating power supply while it is normally operated at around 16-19 A per filament. The chamber was filled with Argon gas through a needle valve many times

before plasma discharge. The filament is biased with a voltage of -76 V with respect to the grounded chamber walls using another discharge power supply. The discharge circuit diagram is shown in the schematic diagram of the device as shown in figure 3.5 (a). The primary electrons emitted from the filaments travel in the electrical field directions towards chamber wall anode, while they are confined by the cusp magnetic field lines. The confined primary electrons move back and forth between two magnets and ionized the background gas atoms. The figure 3.5 (c) shows the image of an Argon plasma confined by multi-pole cusp magnetic field at Argon gas pressure 2 x 10^{-4} mbar and 150A current in the magnets.

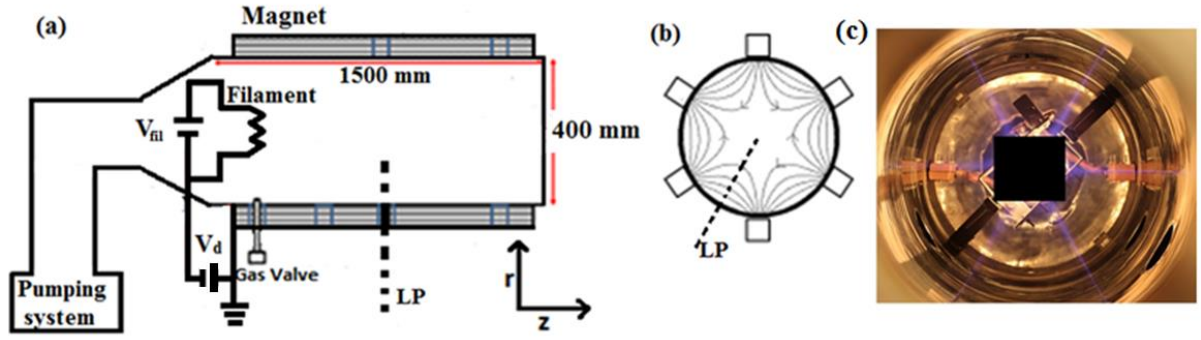

Figure 3.5. Schematic diagram of (a) Experimental setup and (b) Chamber end cross sectional view of the multi-pole line cusp magnetic field plasma device, (c) an image of the Argon plasma taken from the viewport fitted at the end of the chamber of MPD where LP-Langmuir Probe, V_{fil}-floating Power supply for filament heating, V_d-discharge power supply.

3.4 Plasma diagnostic

3.4.1 Langmuir probe

The Langmuir probe [3-7] is a conventional diagnostic for investigating plasma parameters using fundamental techniques. In its simple form it consists of a bare wire that is inserted in the plasma as shown in figure 3.5 (a). The wire is biased with respect

to a reference electrode or a grounded vessel and the current collected by the probe is corresponding to biasing voltage measured across the resistance as shown in figure 3.5 (a). The variation of the probe current with respect to the biasing voltage is termed as the I-V characteristics as shown in figure 3.5 (b). Some of the basic plasma parameters like the mean plasma densities (n), mean electron temperatures (T_e), plasma potential (V_s) and mean floating potential (V_f) are obtained from ramped (I-V) characteristic of a Langmuir probe. The following points were taken care before using the Langmuir pore is necessary,

- The effect of collisions on particles reaching to the probe is negligible
- The probe is placed in a weak / No magnetic field i.e. Larmour radius >> probe wire radius, so that the motion of ions / electrons reaching to the probe, is unaffected by the magnetic field.
- Probe wire diameter >>> Debye length of plasma
- All ions / electrons entering to the sheath are captured by the probe.
- The motion of the charged particles from the plasma reaching to the probe surface is collisionless.

3.4.1.1 Ideal probe I-V characteristic

Figure 3.6 (b), shows an ideal I-V characteristics of plasma. Conventionally, the electron current collected by the probe has been considered to be positive and the ion current to be negative. V_s is the plasma potential and V_f is the floating potential with respect to the grounded vessel wall. When the biased voltage at the probe is equal to the plasma potential, there is no electric field between the probe tip and the plasma, hence electrons and ions are collected by the probe surface with their thermal velocities. The mass of electron is much lower than the ion and temperature of electron is much higher

than the ion thus electron flux at the probe tip is much higher than the ion. As a result, the current collected by the probe tip is predominantly an electron current. If the bias voltage at the probe tip is increased above the plasma potential (V_s), a sheath is formed around the probe and thus the probe area increases with biased voltage. As a result, the probe current slowly increases on increasing the probe potential above the plasma potential as shown in the region **A** of figure 3.6. Now, decreasing the bias voltage to the probe lower than the plasma potential, the probe becomes negative with respect to the surrounding plasma thus plasma electron is reflected from the probe tip and entering in region **B,** which is known as bulk electron region. The probe current is zero when the electron current is equal to the ion current at the floating potential (V_f). Decreasing the bias voltage further, all the electrons repel and only ions are collected by the probe surface. The ion current changes very slowly with the bias voltage and this region is known as the ion saturation region (region **C**).

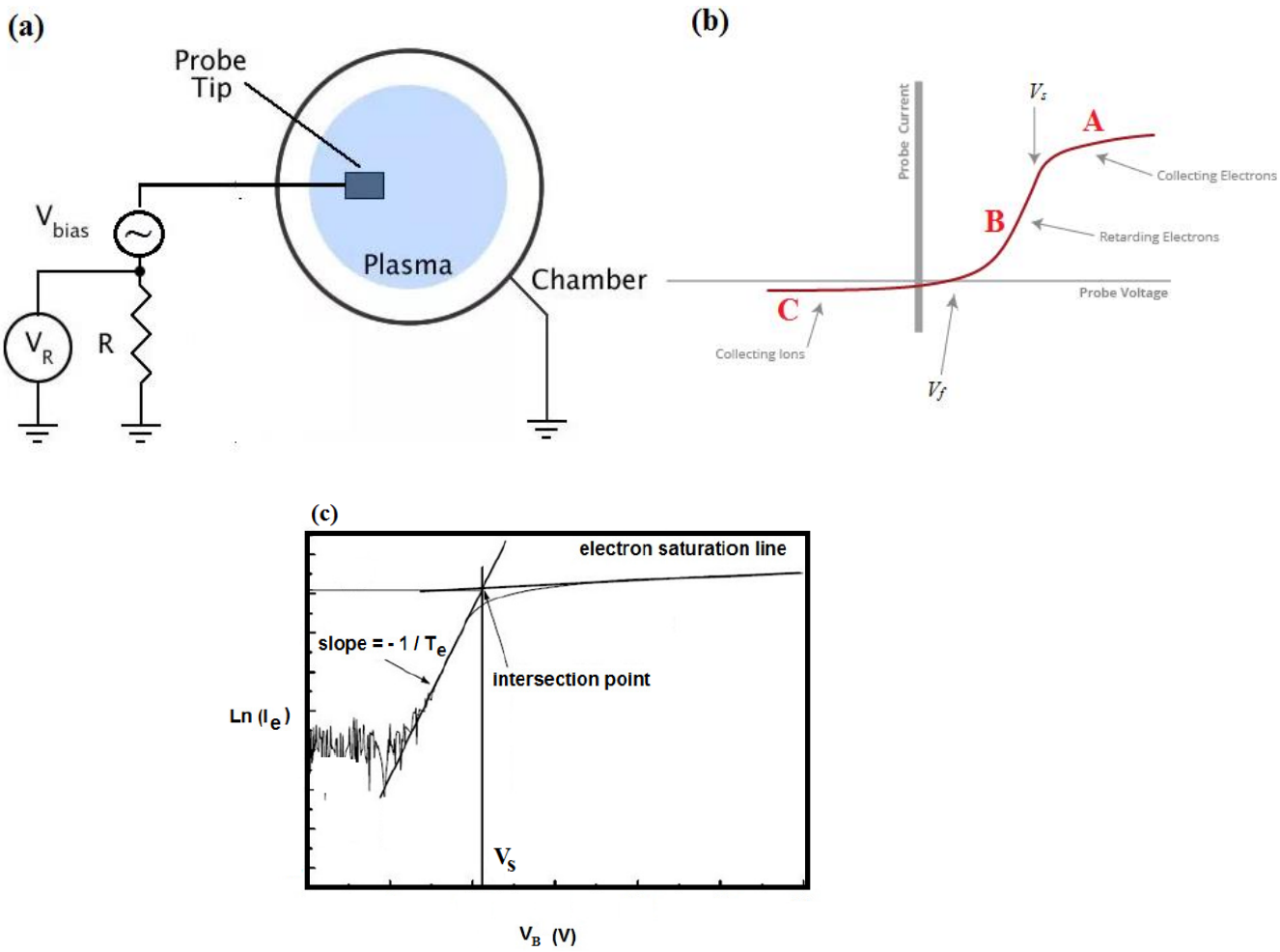

Figure 3.6. (a) A schematic of circuit diagram of Langmuir probe setup (b) An ideal I-V characteristics of plasma obtained using cylindrical Langmuir probe, (c) Logarithm variation of electron current with respect to bias voltage.

3.4.1.2 Estimation of electron temperature from ideal I-V characteristics

When the plasma is completely in thermodynamic equilibrium the electron energy distribution function will be maxwellian, and the electron temperature for maxwellian plasma is defined by,

$$T = \frac{1}{3} m_e \int_{-\infty}^{\infty} v^2 f(v) dv \quad \text{..... 3.1.}$$

Here, m_e is mass of electron, v is velocity of electron, and $f(v)$ is distribution function of electron velocity.

The complete distribution function is covered in the *V-I* characteristic of the plasma by sweeping the bias voltage of the probe. The characteristics curve thus drawn will have the information about the electron temperature. The electron current for given voltage applied is given by the equation,

$$I_e = I_{es} exp(e(V_B - V_s)/k_B T_e) \quad \text{.....3.2}$$

Here, I_{es} is the electron saturation current, k_B is Boltzmann constant, V_s is the plasma potential, and T_e is electron temperature. After little bit algebra (using equation (3.2)) the electron temperature is given by the equation,

$$k_B T_e = \frac{edV_B}{d(lnI_e)} \quad \text{.....3.3.}$$

Thus plasma temperature can be determined from the slope of the linear region of $ln(I_e)$ vs V_B plot corresponding to the exponential region of the I-V characteristics as shown in figure 3.6 (c).

For a Maxwellian distribution of electron, the plasma temperature also can be expressed by the equation,

$$V_s - V_f = \frac{1}{2}\left(\frac{k_B T_e}{e}\right) \ln\left(\frac{2}{\pi}\frac{m_i}{m_e}\right) \quad \text{.....3.4.}$$

Here, k_B is Boltzman constant, e is charge of electron, m_i is mass of ion, m_e. is mass of electron.

3.4.1.3 Estimation of electron temperarue (T_e) in the presence of energetic electrons

It has been known since long that the cusp magnetic field configuration confines energetic primary electrons emitted from the filaments by mirror effects [1]. In the presence of energetic electrons, the equation mentioned above cannot be used to determine electron temperature because of negative shifting in floating potential. Hence a correction needs to be incorporated for temperature estimation. For this experiment the correction due to energetic electrons considered is as follows [8-9].

Usually a plasma with energetic electrons can have many maxwellians representing many temperatures combined together. It is very difficult to pin down all these maxwellians. But if the given plasma is mostly thermalized, but only a small fraction of it is having energetic electrons, it can be assumed to have roughly two maxwellian, one with hot electron temperature component (T_h) and another with cold electron temperature component (T_{ec}) [8-9]. For this type of plasma, an effective temperature can be derived by assuming electron energy distribution function (EEDF) as bi-Maxwellian, $f(v) = \alpha f_h(v) + (1-\alpha) f_c(v)$, where $f_h(v)$ is the distribution function of the hot electrons and $f_c(v)$ is the distribution function of the cold electrons,α is the ratio of hot electron current to electron current at plasma potential [8-9]. For this bi-Maxwellian plasma, the effective temperature can be derived as [8-9]:

$$T_{eff} = (1-\alpha)T_{ec} + \alpha T_h \quad \ldots\ldots\ldots\ldots\ldots\ldots\ldots\ldots \quad 3.5.$$

For measuring the plasma parameters of plasma confined by multi-pole line cusp magnetic field, a sweeping circuit (as shown in the figure 3.7 (a)) of frequency 1 Hz and a voltage sweep from -80 V to +30 V has been used. The figure 3.7 (b) shows

the photograph of sweeping circuit. An analysis code has been developed in MATLAB for quick processing of the data.

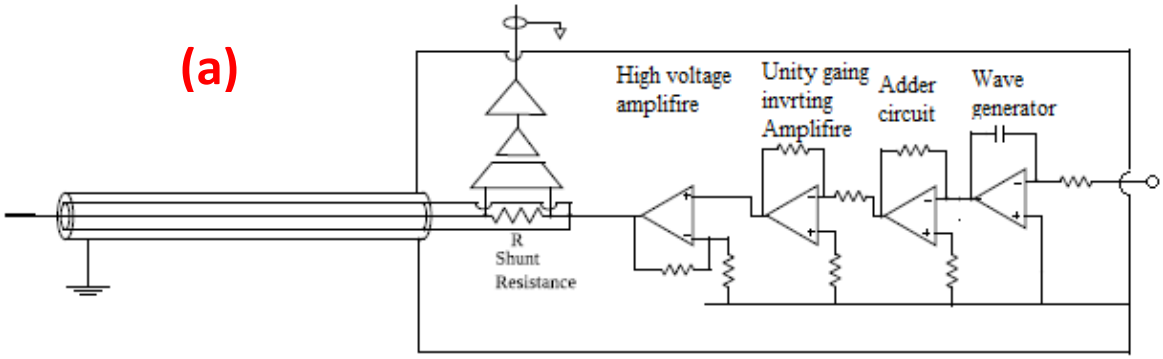

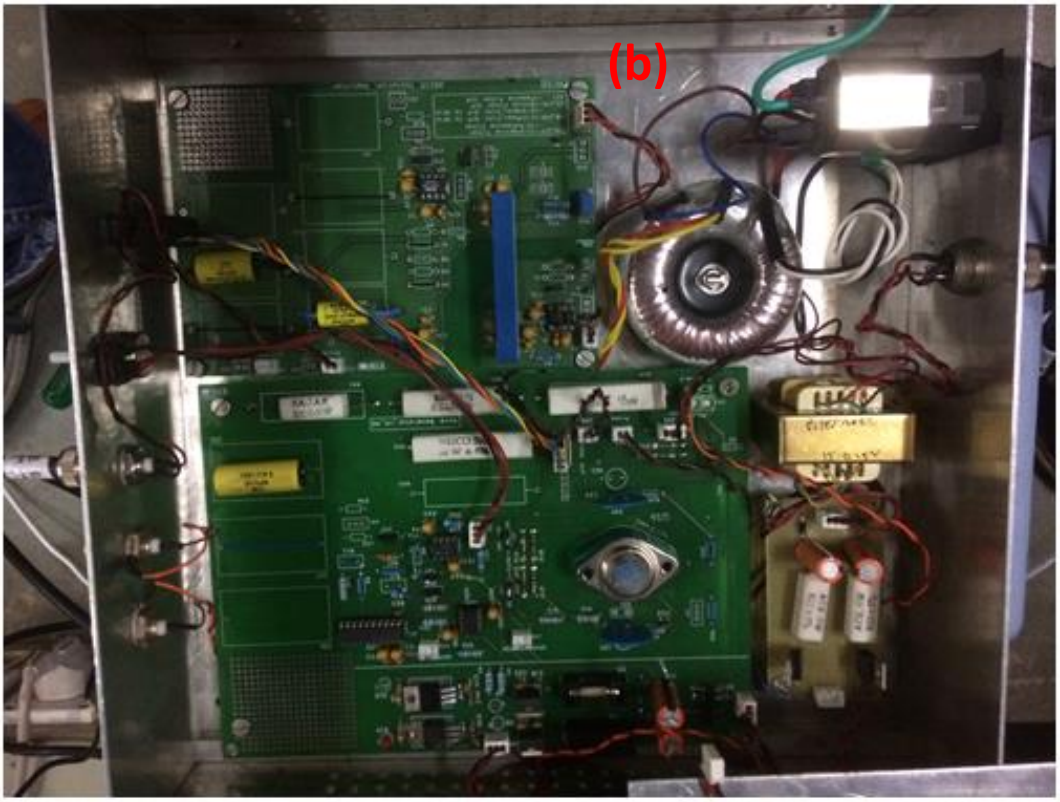

Figure 3.7. (a) Schematic of Langmuir probe circuit diagram used for acquiring *V-I* characteristics of plasma (b) A photograph of real swiping circuit.

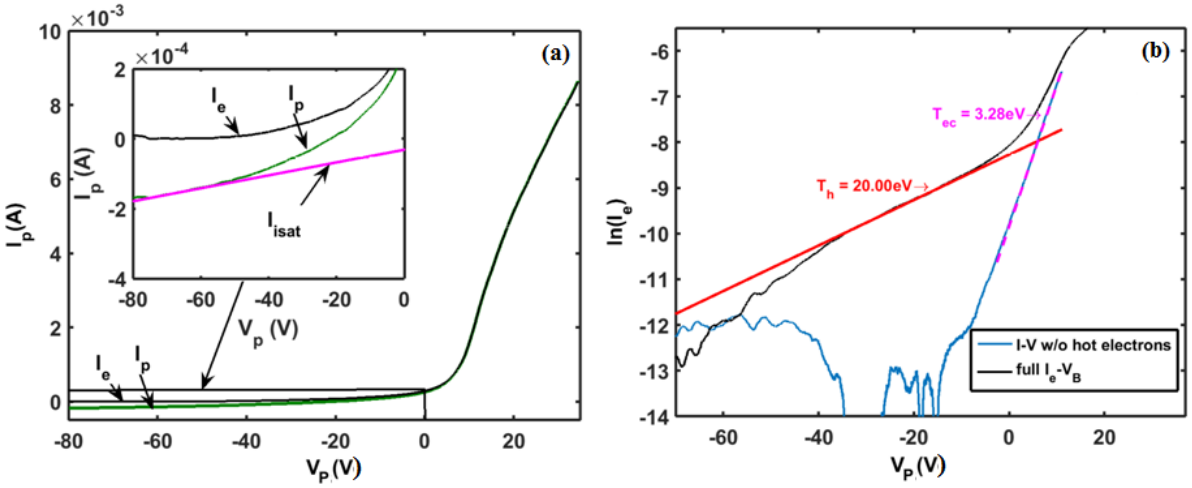

Figure 3.8. (a) Measured Langmuir probe *V-I* characteristic of plasma, fitted ion saturation current (I_{isat}) and the electron current (I_e), at R= 0 cm (centre of the device) and 2 × 10^{-4} mbar Argon gas pressure, and current in the magnets is 150 A (b) variation of $ln(I_e)$ and $ln(I_e\text{-}I_h)$ with probe potential (V_p).

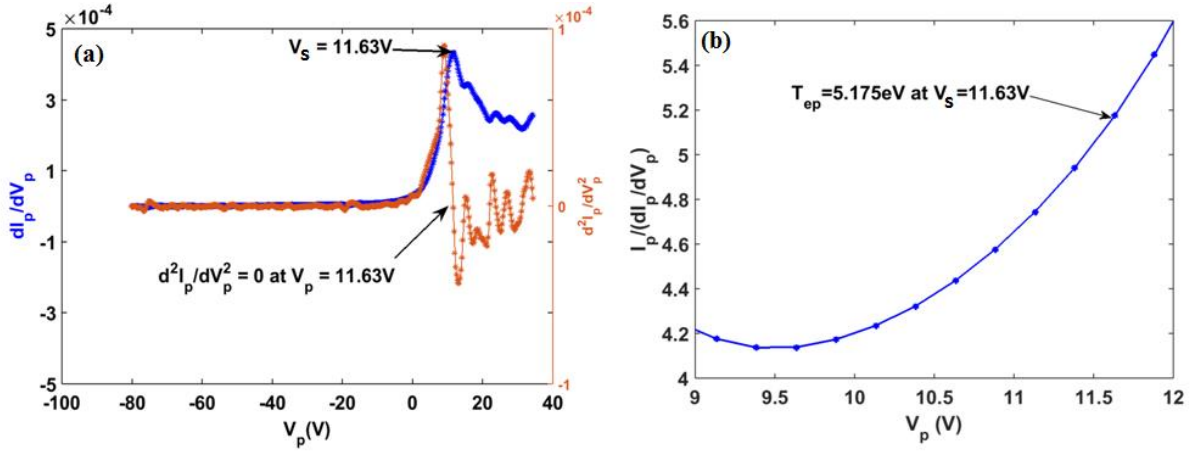

Figure 3.9. (a) Variation of first and second derivative of probe current (I_p) with probe potential (V_p), (b) variation of the ratio of probe current to first derivative of probe current with probe potential (V_p).

To estimate (T_{eff}) using Eq. (5) the technique used by Siddiqui *et al.* [9] has been followed. Firstly, the ion saturation current (I_{isat}) is obtained by removing the digital noise from the Langmuir probe characteristics. The variation of electron current (I_e) drawn by the probe with bias voltage can be obtained by subtracting the ion saturation current (I_{isat}) from probe current (I_p). In this experiment, a typical probe I-V

characteristics is shown in the figure 3.8 (a). The plasma electron current obtained by subtracting ion saturation current has also been shown in this figure. The hot electron temperature (T_h) is then estimated from the slope of the flatter line of V_p *Vs* $ln(I_e)$ curve as shown in figure 3.8 (b). The contribution of hot electron current (I_h) in the probe is estimated using this hot electron temperature (T_h). The contribution of cold electron current is then estimated by subtracting I_h from I_e. The temperature of cold electrons is then evaluated from the slope of the V_p *Vs* $ln(I_e-I_h)$ curve as shown in broken line (see Fig. 3.8 (b)). As discussed earlier, the ratio of hot electron current to cold electron current at plasma potential (V_s) gives the value of α, using the value of α, T_h and T_{ec}, T_{eff} can be estimated from Eq. (3.5).

To cross check this value of effective electron temperature, the technique used by Choi *et al*. [10] has been followed. In this technique, the electron temperature (T_{ep}) is estimated from the ratio of probe current to first derivative of probe current (I_p) with respect to probe voltage (V_p) at the plasma potential (V_s). This analysis work has been shown in figure 3.9 (b). It has been found that the electron temperature estimated from both methods matched within the experimental error. It is also to be noted that the plasma potential is measured from the inflection point of first derivative of *V-I* characteristics of Langmuir probe (as shown in fig. 3.9 (a)). To ensure that, the second derivative of *V-I* characteristics is used to check whether its value becomes zero at plasma potential 3.9 (a).

3.4.1.4 Estimation of plasma density

In a collisionless single ion species plasma the ion saturation current to the probe is given by the equation [11-13],

$$I_{isat} = 0.63e\, n\, A_P \sqrt{\frac{k_B T_e}{m_i}} \quad \text{..... 3.6.}$$

where, A_p is the probe area, n is plasma density.

The densities are calculated using Eq. (3.6). The electron temperature obtained after hot component correction has been used in the Eq. 3.6. The corresponding density value for the typical I-V characteristics as shown in figure 3.8 (a) is 5 x 10^{16} m^{-3}. Also, it has been noticed that the for error calculation in density equation, $\frac{\delta n}{n} = \sqrt{\left(\frac{\delta I_{isat}}{I_{isat}}\right)^2 + \left(\frac{1}{2}\frac{\delta T_e}{T_e}\right)^2 + \left(\frac{\delta n}{n}\right)_S}$, is considered, where $\delta I_{isat}/I_{isat}$ error in ion saturation current, $\delta T_e/T_e$ error in electron temperature measurement, $(\delta n/n)_S$ is the statistical variation in density [14]. For the rest of this thesis, the effective electron temperature (T_{eff}) and densities are estimated using only Eq. (3.5) and Eq. (3.6) respectively until and unless specified.

3.4.1.5 Fluctuations in plasma parameters

The plasma quiesence can be understood from the fluctuation levels in the various plasma parameters. The fluctuations in plasma density and floationg potential are measured using the single Langmuir probe. The fluctuations in density and potential are obtained by measuring the fluctuating components of ion saturation current ($\widetilde{I_{\imath sat}}$) and floating potential ($\widetilde{V_f}$). Figure 3.10 shows the circuit diagrams of Langmuir probe setup for plasma density fluctuation measurements and floating potential fluctuation measurements. For plasma denstiy fluctuation measuremnt the ac volage signal across the 10 kΩ resistance is measured when probe tip is biased to -100 V with respect to the grounded chamber as shown in figure 3.10 (a). The floating potential fluctuation is measured by recording the ac voltage across the 100 Ω resistance measured when the

probe is grounded through a series of 10 MΩ and 100 Ω resistances as shown in figure 3.10 (b).

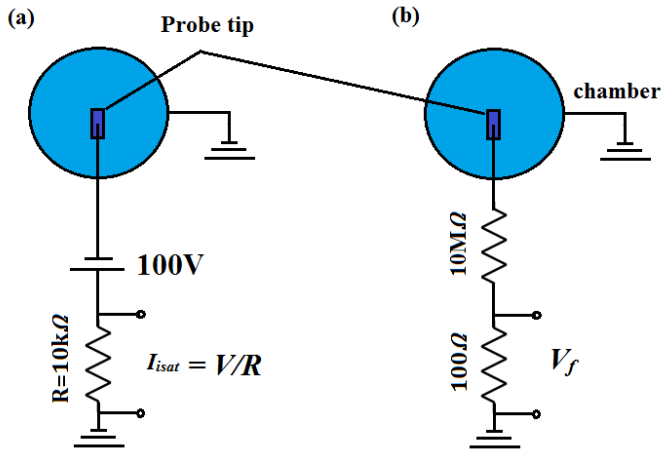

Figure 3.10. A schematic of circuit diagram of Langmuir probe setup for (a) measurement of plasma density fluctuation from ion saturation current (I_{isat}), and (b) measurement of floating potential fluctuation (V_f).

In order to identify any intrinsic instabilities, the important characteristic features such as fluctuations in plasma parameters, power spectra of fluctuations, cross correlation functions, wave number-frequency spectra are necessary [17-18]. In this regard a set of probes have been designed and made for characterising the different modes (plasma noise) present in the system. These probes are used for sampling fluctuations in ion saturation current and floating potential for examining the fluctuation spectra, cross correlation, wave number-frequency spectra etc. The data (times series) are acquired at different sampling rates and the record length. The MATLAB codes are developed for analysis of fluctuation spectra, cross correlation, wave number-frequency spectra etc. Linear spectral analysis is, however, of limited use when various spectral components interact with one another due to some nonlinear or parametric processes. In such a case, higher order spectral techniques, like the bi-spectrum (third–order spectrum) analysis, are useful for completely characterizing the fluctuating signals. Digital bi-spectral analysis technique for investigating nonlinear wave-wave interaction

in plasmas as described by Kim and Powers [19] has been used in the spectral analysis of the fluctuation data.

3.4.2 Emissive probe

Emissive probes are commonly used in plasma devices to measure the plasma potential. In 1923, the intention of emitting probe was first proposed by Langmuir [15]. Electron emission from the probe provides an opportunity for direct measurement of plasma potential. Usually the probe is heated to emit electrons and the electron emission current depends upon the potential surrounding it. Thus if the current in the emissive probe circuit is measured for a given probe temperature, one can estimate the potential around the probe locally. Emissive probe is particularly useful for the measurement of spatial gradient in plasma potential for determining electric field. The complete operation of emissive probe is as follows: When a probe is biased more positive than the local plasma potential, electrons emitted from the probe are reflected back to the probe. When the probe is biased negative with respect to the plasma potential, electrons from the emitting probe escape to the plasma and appear as an effective ion current. This process is not sensitive to plasma flow and beams because it directly depends on the plasma potential rather than electron kinetic energy.

There are three methods for determining plasma potential using emissive probe, a) floating potential method, b) Inflection point method, c) separation point method. In our experiment we have used floating potential method throughout this dissertation [16].

3.4.2.1 Floating potential method

The floating potential method is most commonly used for measuring the plasma potential. The floating potential of a sufficiently heated emissive probe is close to local plasma potential. Thus this is the most widely used method for plasma potential determination using emissive probe. Different methods are used to heat the probe viz. heated Ohmic heating using an isolated power supply, using a laser beam, or Ohmic heating through collection of electron current from the plasma itself.

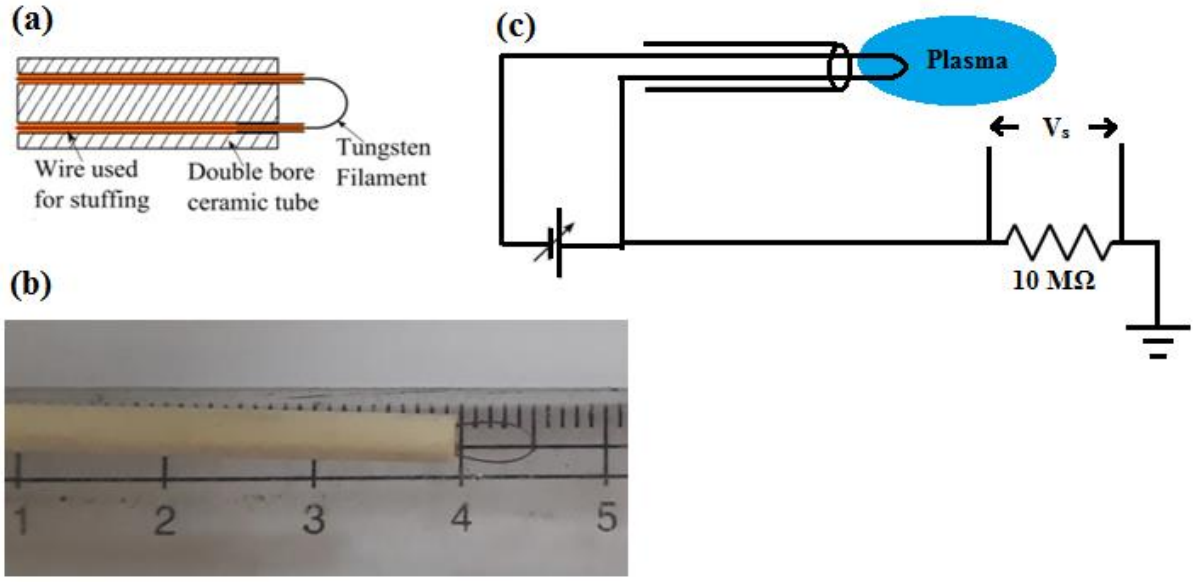

Figure 3.11. (a) Emissive probe construction, (b) Image of emissive probe, (c) Emissive probe circuit.

When an emitting probe is submerged into the plasma and sufficiently heated, the floating potential of the probe is that potential at which the incoming electron current from the plasma is balanced by the outgoing emitted current and the incoming ion current. This is due to the fact that a current of electrons emitted from the probe has the same sign as the current of positive ions flowing from the plasma to the probe. As the emission of the probe is increased lesser amount of coming ion current is necessary to balance the incoming electron current due to compensation by emitted current. Thus as

the emission increases, the floating potential of the probe is shifted toward the plasma potential until a kind of saturation is reached and further heating will be to no avail. Then this value is assumed to be a sufficiently good approximation of plasma potential (V_s).

A thin 0.125 mm tungsten wire has been used to make the emissive probe. The two ends of this half-loop are pulled through the two bores of a double-bore ceramic tube and are at the other end connected by feedthroughs to an external power supply. Thus the loop can be heated to the necessary temperature (white glow ≅ 2500 K). Contact between the leads of the wires connected to the power supply and the tungsten filament is made by squeezing the filament and the connecting wire into the bore of the ceramic tube as shown in Figure 3.11 (a). The figure 3.11 (b) shows the image of emissive probe. Plasma potential has been measured using the floating potential method. The measurement is not affected by magnetic field and large number of measurements can be carried out using this method very quickly. The filament is heated by passing current through it using a floating power supply with a very good isolation. The emissive probe circuit is shown in Figure 3.11 (c). The potential between the floating hot emissive probe and the grounded vessel is measured across 10 MΩ resistances as shown in figure 3.11 (c). The length of the emissive probe was held perpendicular to the magnetic field lines to minimize magnetic field effects on the electron emission from the probe.

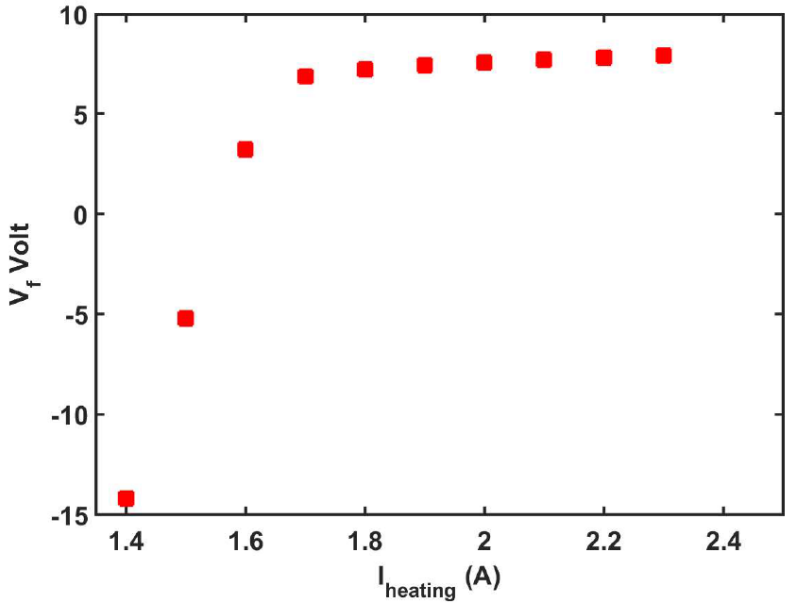

Figure 3.12. Variation of floating potential of emissive wire (probe) with increasing in heating current.

Figure 3.12 shows the variation of floating potential with increasing filament heating current. When there is no emission current in filament the probe remains at the floating potential, as we increased the heating from the no emission current, the floating potential rapidly rises at first and plateaus at the plasma potential. After this point, increasing the emission only slightly changes the floating potential due to space charge effects.

References

1. R. Limpaecher, and K. R. MacKenzie, Rev. Sci. Instrum. **44**, 726 (1973).
2. Jan Weiland, *"Collective modes in inhomogeneous plasma: kinetic and advanced fluid theory"* IOP Publishing Ltd., Bristol, (2000).
3. R. C. Davidson, Methods in nonlinear plasma theory, New York: Academic Press, 1972.
4. L. D. Landau, J. of Phys. **10**, 25 (1946).
5. Y. P. Raizer, Gas Discharge Physics, Springer-Verlag Berlin Heidelberg.
6. T. Pierre, G. Leclert, and F. Braun, Rev. Sci. Instrum. **58**, 6 (1987).
7. I. G. Brown, A. B. Compher, and W. B. Kunkel, Phys. Fluids **14**, 1377 (1971).
8. J. P. Sheehan, Y. Raitses, N. Hershkowitz, I. Kaganovich, and N. J. Fisch, Phys. Plasmas **18,** 073501 (2011).
9. M. Umair Siddiqui, and Noah Hershkowitz, Phys. Plasma **21**, 020707 (2014).
10. Ikjin Choi, Chin Wook Chung, and Se Youn Moon, Phys. Plasmas **20**, 083508 (2013).
11. F. F. Chen, Plasma Sources Sci. Technol. **18,** 035012 (2009).
12. Sayak Bose, Manjit Kaur, P. K. Chattopadyay, J. Ghosh, Y. C. Saxena, and R. Pal, J. Plasma Phys. **83,** 615830201 (2017).
13. Isaac D. Sudit, and R. Claude Woods, J. Appl. Phys. **76**, 4488 (1994).
14. Umesh Kumar, Shekar G Thatipamula, R. Ganesh, Y. C. Saxena, and D. Raju, Phys. Plasmas **23**, 102301 (2016).
15. I. Langmuir, "The pressure effect and other phenomena in gaseous discharges," Journal of the Franklin Institute, **196**, 751 (1923).
16. J. P. Sheehan and N. Hershkowitz, Plasma Sources Sci. Technol. **20,** 063001 (2011).

17. Y. C. Kim and E. J. Powers, “Digital Bispectral Analysis and its applications to Nonlinear Wave Interactions,” IEEE Transactions on Plasma Science **7**, 120 (1979).
18. J. M. Beall, Y. C. Kim, and E. J. Powers, J. Appl. Phys. **53**, 3933 (1982).

Chapter 4

Characteristics of plasma confined in a versatile multi-pole line cusp magnetic field VMMF

The **M**ulti-pole line cusp magnetic field linear **P**lasma **D**evice (MPD) designed and fabricated for the controlled study of Basic plasma physics in a quiescent plasma. Before embarking in the proposed experiments it is required to characterize the plasma in this magnetic field geometry. In this chapter, the results of the basic plasma characterization with different magnetic field values have been described along with plasma confinement. The profile of the plasma parameters (plasma density, floating potential, electron temperature) and particle confinement times have been presented. The variations of these plasma parameters profiles with different magnetic field values have also been given.

Figure 4.1, (a) shows a schematic diagram of experimental setup and figure 4.1 (b) shows end cross sectional view of experimental set up of the MPD. All experimental measurements, as well as the radial profile of plasma parameters, are measured along the non-cusp region and are carried out at mid (r, θ) plane of the device which is z = 65 cm away from the filaments.

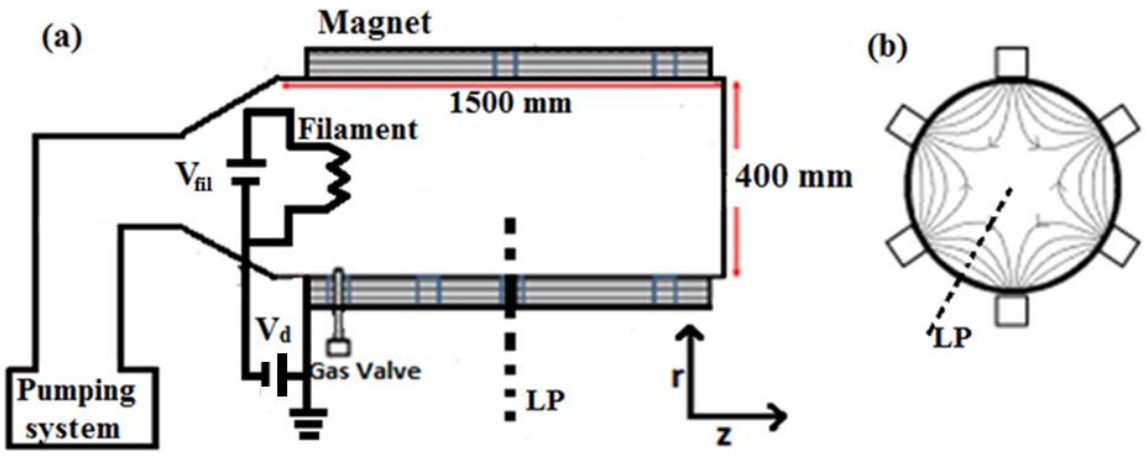

Figure 4.1. Schematic diagram of (a) Experimental setup and (b) Chamber end cross sectional view of the multi-pole line cusp magnetic field plasma device, where LP-Langmuir Probe, V_{fil}-floating Power supply for filament heating, V_d- discharge power supply.

The variation of plasma parameters with the different control parameters is studied with Langmuir probe. A cylindrical probe with radius 0.5 mm and length 5 mm has been used to measure the plasma parameters. The base pressure of the system is 1 × 10^{-6} mbar, and the system is filled with Argon gas a number of times before striking the discharge. Steady state Argon plasmas were produced in MPD and its characteristics are presented in this chapter. In the present experimental results, the six multi-pole cusp magnetic field configuration has been used as well as the pressure of Argon gas fixed at the 2 × 10^{-4} mbar.

4.1 Plasma confinement

In this section, the variation of plasma parameters at the centre of the device (null region of magnetic field) with changing current in the magnet coils has been presented. Figure 4.2 shows the variation of plasma density with respect to the change in the confining magnetic field. As expected the density is increasing with the magnetic

field. But at r = 0 cm the field is almost zero irrespective of the pole field value in the cusp region. For a Argon plasma, the plasma potential and the corresponding floating potential are related to the temperature by the equation $(V_s\text{-}V_f) = 5.4\ k_BT_e$ [1,2]. Since the cusp magnetic field configuration is expected to confine more primary electrons when the field is increased, it is expected that the temperature will increase with the field. But it is found that the case is not so. So it is tried to plot factor $(V_s\text{-}V_f)/\ k_BT_e$ with respect to magnetic field to confirm the validity of the above equation. Instead it is found the factor is increasing with respect to magnetic field as shown in figure 4.3. Since the plasma potential is not changing much with the magnetic field, it is concluded that the floating potential is increasing with magnetic field. Figure 4.3 shows the variation of plasma density and factor $(V_p\text{-}V_f)/\ k_BT_e$ with changing current in the magnets at the centre of the device R = 0 cm respectively. Hence it is found that the plasma density and factor $(V_s\text{-}V_f)/\ k_BT_e$ are increasing at the centre of the device with increasing field value at the pole even though there is no change in the magnetic field values at R = 0 cm. One needs to revisit the basic confinement mechanism in cusp configurations. When there is no magnetic field, the plasma flux will hit the surface walls along the confining chamber. But in cusp configuration the plasma flux will leak to the wall only in the cusp region and the amount of leaking flux will depend on the width of each cone in the cusp region as shown in figure 4.4. Previously [3-7], many different experiments have been performed to quantify the leak width. Bosh *et al.* define the leak width (*d*) of the quasi-neutral plasma flowing out of a cusp, with the cross-field diffusion is dominated by Bohm diffusion, as given by [3,4]

$$d = \left(\frac{D_\perp L}{C_s}\right) \quad \ldots\ldots\ldots\ldots\ldots\ldots\ldots \quad (4.1)$$

where, $D_{\perp}$is diffusion coefficient across the magnetic field near the pole of the magnet, L is the scale length of the magnetic field (B) and c_s is the ion acoustic speed.

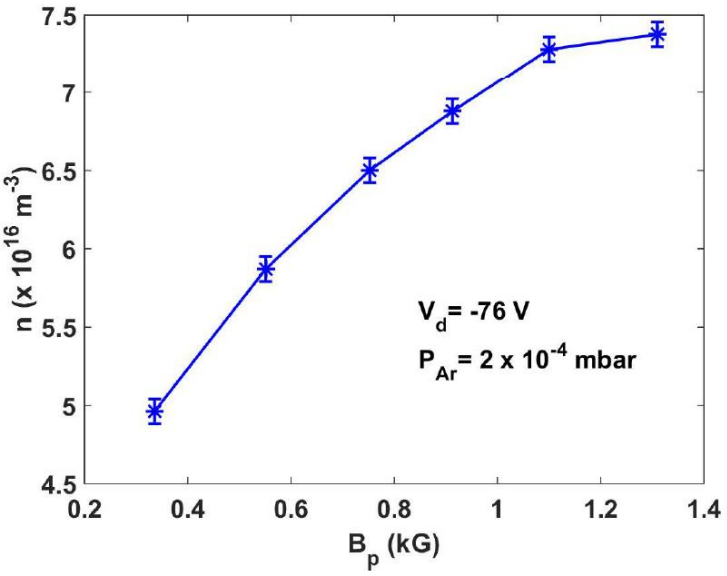

Figure 4.2. Variation of the plasma density with pole magnetic field (B_p) by varying currents in the magnets at the centre of the device (R = 0 cm) and 2 × 10^{-4} mbar Argon gas pressure.

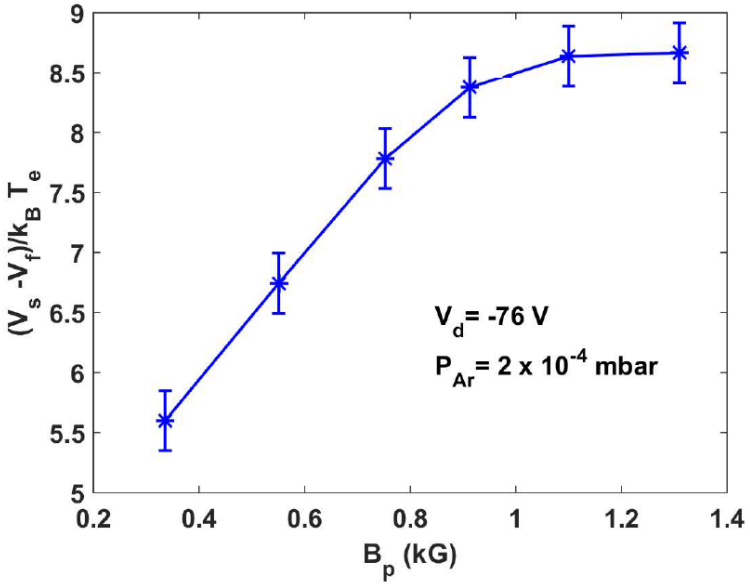

Figure 4.3. Variation of factor $(V_s\text{-}V_f)/T_e$ with pole magnetic field (B_p) by changing current in the magnets at the centre of the device (R = 0 cm) and 2 × 10^{-4} mbar Argon gas pressure. The value of factor $(V_s\text{-}V_f)/k_BT_e$ is 5.4 for maxwellian Argon plasma for reference.

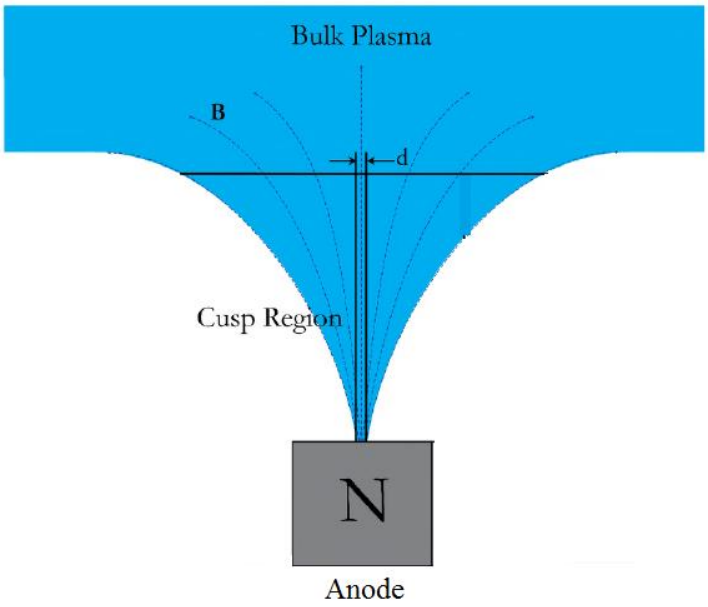

Figure 4.4. Schematic representation of leak width at the cusp region.

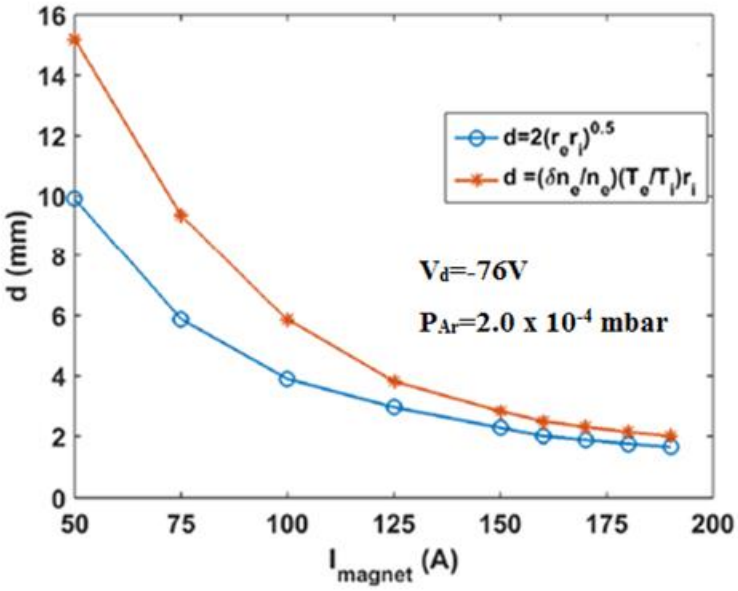

Figure 4.5. Comparison of leak width calculated from two different formulas at R = 16 cm in cusp region as a function of the current through magnet coils.

At low background gas pressure, R. Jones related the leak width (*d*) to plasma turbulence. Micro-instabilities, which are unstable in a cusp sheath (e.g. drift wave, ion cyclotron waves) give rise to Bohm-like diffusion [5, 6]. The relationship between the

relative electron density fluctuation level $^{dn_e}/_{n_e}$ and the leak width (d) for turbulent line cusp [3, 4],

$$d \geq \frac{\delta n_e}{n_e}\frac{T_e}{T_i} r_i \qquad \ldots\ldots\ldots\ldots\ldots\ldots \quad (4.2)$$

where n_e is the electron density, r_i is the ion larmor radius, T_e and T_i are electron and ion temperature respectively. Hershkowitz *et al.* [8], studied experimentally the leak width for plasmas produced using different gases and proved that the leak width varies with hybridgyro-radius of electron and ion larmor radius,

$$d = 2\sqrt{r_i r_e} \qquad \ldots\ldots\ldots\ldots\ldots\ldots \quad (4.3)$$

where r_i and r_e are ion and electron Larmor radius respectively.

For the estimation of leak width for this device using equations (4.2) and (4.3), basic plasma parameters have been measured at R = 16 cm close to the pole in the cusp region along with density fluctuations. In equation 4.2, $\frac{\delta n_e}{n_e} \approx \frac{\delta I_{esat}}{I_{esat}}$ has been considered for the density fluctuation, where I_{esat}, the electron saturation current is measured in the cusp region at R =16 cm and the ion temperature (T_i) is assumed to be approximately 10 times lesser than the electron temperature (T_e). The electron temperature (T_e) and electron saturation current (I_{esat}) are measured from same single Langmuir probe at R=16 cm near the pole of the magnet. The leak widths (d) from equation (4.2) at different pole field values are calculated and plotted as shown in figure 4.5. For comparison, the leak widths calculated from hybrid gyro-radii $d = 2(r_i r_e)^{0.5}$ [8] are also plotted in the same figure 4.5. The leak width of plasma decreases with the increase of current in the magnets and hence decreasing the loss rate of bulk plasma through the cusp. As a result, plasma density at the centre of the device is increased

with the increasing field values at the pole. The leak widths from both expressions are found to be matching well at high magnetic field values but the values are found to be different for low magnetic field values.

Figure 4.6 shows the variation of floating potential of plasma with changing of current in the magnets. The floating potential is negative and it becomes more and more negative with increasing pole field values of the cusps as higher field values allow more primary electrons to be confined [9-10]. This can also be verified by measuring the primary electron density and tracing the ion saturation current profile in the afterglow plasma. Leung *et al.* [9], had defined the primary electron density by the equation,

$$n_p = -\left(\frac{2m_e v_p}{e^2 A_p}\right) {dI}/{dV} \qquad \text{.....(4.4).}$$

where m_e is electron mass, $v_p = \sqrt{{2eV_d}/{m_e}}$ is primary electron velocity, A_p is probe area and ${dI}/{dV}$ is slope of I-V characteristics as shown in figure 4.7. Figure 4.8 shows the variation of typical I-V characteristic of plasma after subtracting the ion saturation current at the centre of device with different current in the magnets. It is observed from the figure 4.8 that the slope ${dI}/{dV}$ increases with the increasing pole magnetic field values. This shows that the primary electron density increases with the increasing magnetic field values.

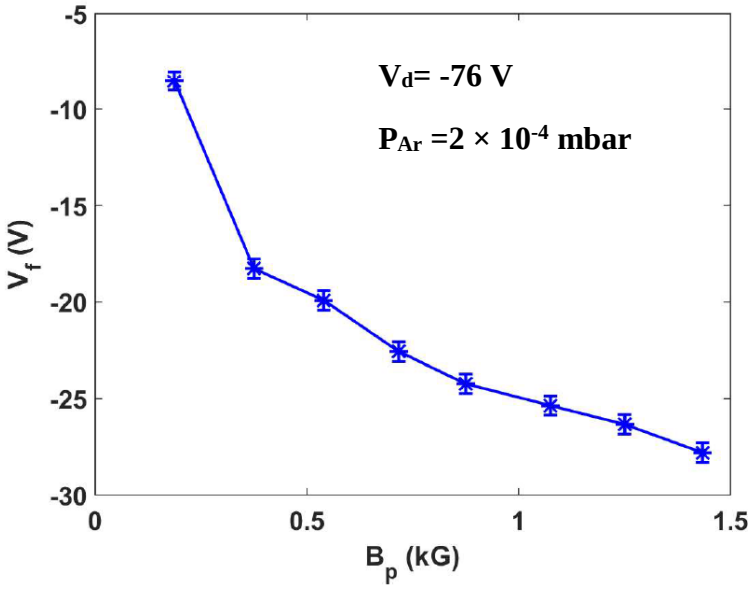

Figure 4.6. Variation of floating potential (V_f) at the centre of the device (R = 0 cm) with pole magnetic field (B_p) by changing current in the magnets and 2 × 10^{-4} mbar Argon gas pressure.

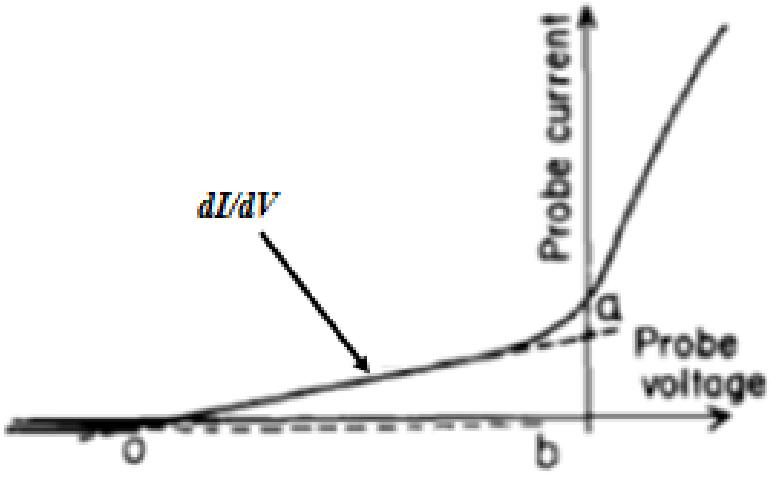

Figure 4.7. Langmuir probe I-V characteristics after subtracting the ion saturation current [9].

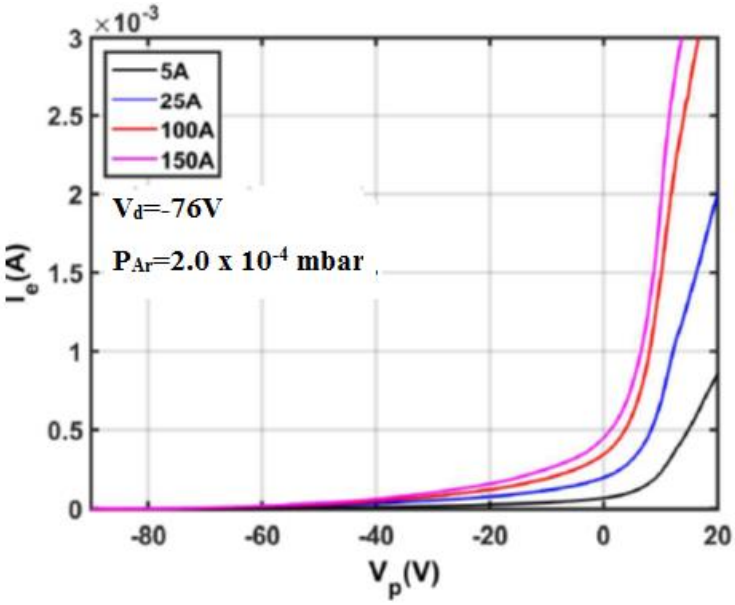

Figure 4.8. Variation of I-V characteristics of plasma after subtracting ion saturation current for currents in the magnets at the centre of the device (R = 0 cm) and 2 × 10^{-4} mbar Argon gas pressure.

The particle confinement time of the plasma needed to be studied different field values. The particle confinement time can be estimated from the temporal evaluation of the profile of ion saturation current in an afterglow plasma. The afterglow plasma is usually created and studied by switching off the filament discharge power. Repetitive afterglow plasmas can be created by using a possible switching ON/OFF mechanism in discharge circuit. The schematic of switching circuit is shown in figure 4.9. The discharge power supply is switched OFF and ON for 500 ms and the dc ion saturation current across the 10 kΩ resistance is recorded simultaneously using the same circuit as shown in figure 3.10 (a). Figure 4.10 shows the typical time evolution of normalized ion saturation current (I_{isat}) in an afterglow plasma, when probe is located at R = 0 cm and pole magnetic field is 1.1 kG. The time taken by ion saturation current to decrease by 1/e of its initial value is defined here as the particle confinement time. From figure 4.10, it can be observed that the time evolution of ion saturation current has two exponential regions representing the plasma to be associated with two particle confinement times [11]. As the cusp magnetic field confines the primary electrons, after

switching off the discharge power supply, the confined energetic (primary) electron move back and forth along the field lines and ionize the background gas. First rapid exponential decay is due to plasma bulk electron and second exponential is due to the energetic trapped electrons in cusp magnetic field [10]. Figure 4.11 shows the variation of particle confinement time with changing current in the magnets. Since the leak width of plasma is decreased with the increasing magnet current (or magnetic field), because of that plasma density at the confined region is increased and a leak rate of plasma is decreased, thus particle confinement time increases with magnet current (or magnetic field) as shown in figure 4.11.

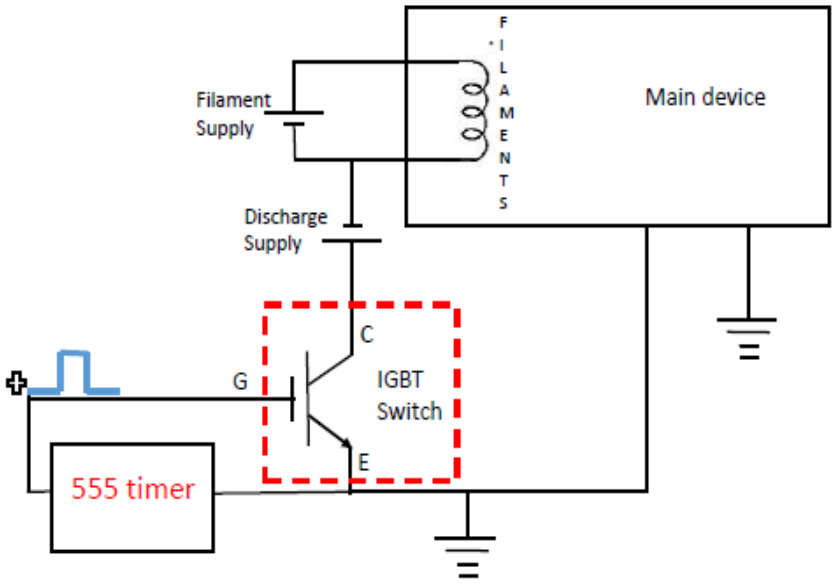

Figure 4.9. Switching circuit for discharge power supply is switched OFF and ON.

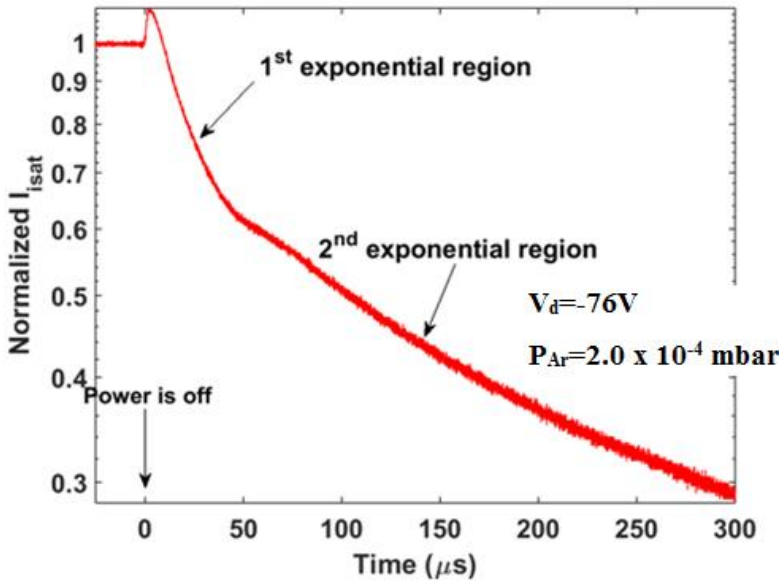

Figure 4.10. Temporal evolution of the normalized ion saturation current in the afterglow plasma at the centre of the device when current in the magnets (I_{mag}) is 150A, and 2 × 10^{-4} mbar Argon gas pressure.

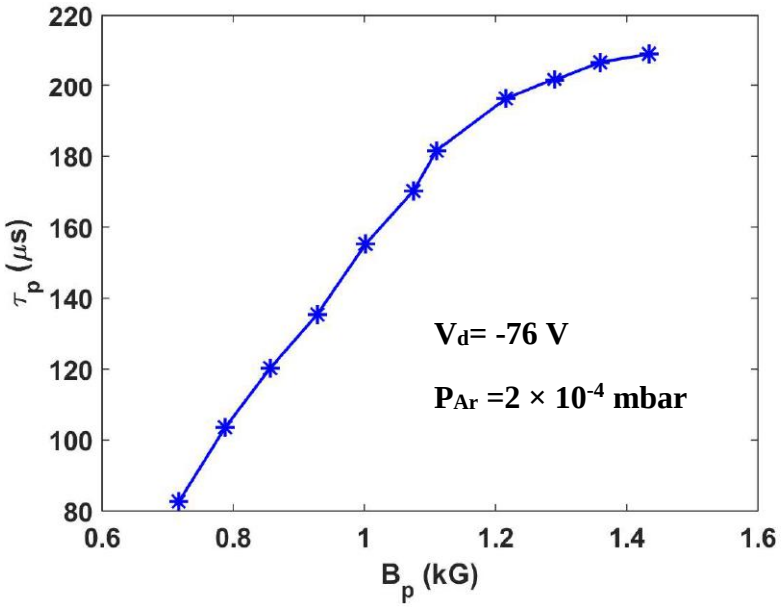

Figure 4.11. Variation of particle confinement time with pole magnetic field (B_p) by changing current in the magnets and 2 × 10^{-4} mbar Argon gas pressure.

4.2 Radial variation of plasma parameters with magnetic fields.

The confined bulk plasma in cusp magnetic field diffuses across the magnetic field lines and also streams out along the magnetic field lines. Because of its diffusion, gradients are formed in steady state of plasma parameters. In the device, the field value on the electromagnet pole can be changed by changing the magnet current, and because of that associated equilibrium profiles of plasma parameters are also changing accordingly. In the present study the relevant plasma parameters, with different magnet current values (50 A, 100 A and 150 A) are considered. The corresponding magnetic field values at the pole face of cusp (near the magnet, R = 20 cm) are 0.45 kG, 0.75 kG and 1.1 kG respectively. The radial variation of plasma parameters and their fluctuations (plasma densities, electron temperature, and floating potential) for these field values are measured along the non-cusp region and at the mid (r, θ) plane of device (the plane from z = 65 cm from the filament) as shown in figure 4.12. The Argon gas background pressure is also fixed at 2.0×10^{-4} mbar throughout this measurement.

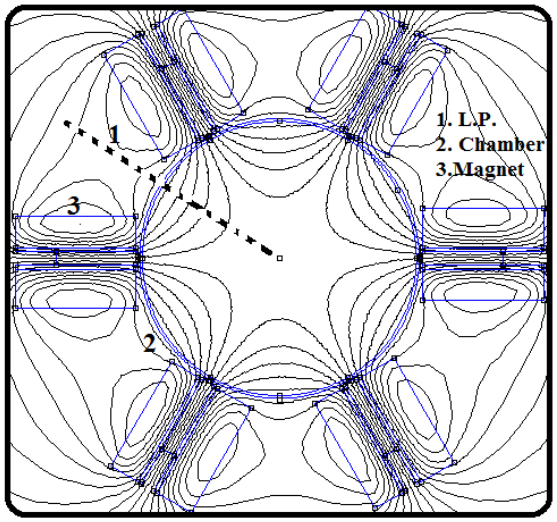

Figure 4.12. Shows the location of the Langmuir probe along the non-cusp region for measurement of radial profile of plasma parameters.

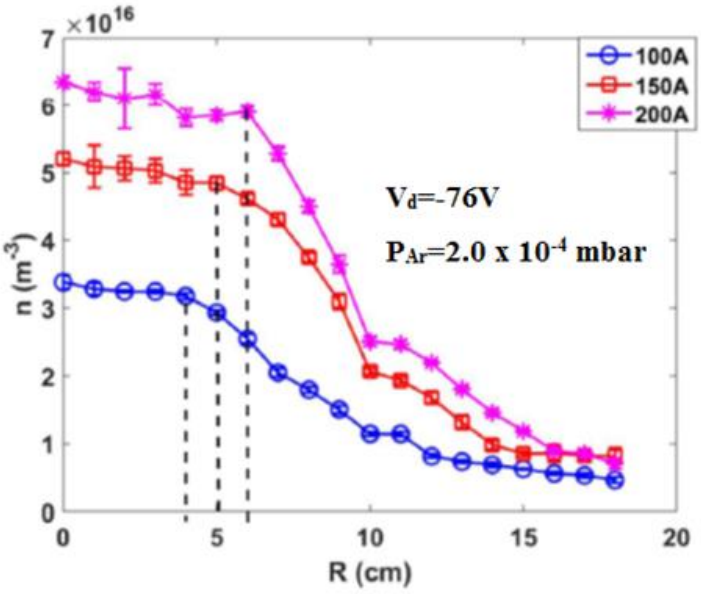

Figure 4.13. Radial variation of plasma density measured along the non-cusp region when current in the magnets are 100, 150, and 200 A and Argon gas pressure is 2×10^{-4} mbar.

The radial profiles of plasma density and electron temperature are shown in figure 4.13 and 4.14 at different magnetic field values along the non-cusp region. The nearly flat density and temperature up to a radial distance of 5 cm implies the presence of uniform plasma along a cylindrical region of about 10 cm diameter in the centre. From the radial electron temperature profile, it is also observed that the field free region is hotter up to 5cm and after that temperature decreases radially outwards. This is due to the primary electrons along the axis which rush axially to the other edge with very less collisions because of very low magnetic field. But with a small increase in radius, the field increases, though slightly, the electrons get magnetized and start following the magnetic field and hence heating all the neutral and ions on the way. Beyond 5 cm, the number of collisions becomes higher and hence the temperature starts decreasing. Moreover, it is also noticed that, the radial constant plasma density domain of plasma density across the magnetic field along the non-cusp region is increasing with the

magnetic field: 4 cm, 5 cm and 6 cm for 100 A, 150 A and 200 A magnet current respectively as shown in figure 4.13. As we increase the magnetic field the leak width of plasma decreases thus parallel diffusion lose rate decreased. Therefore, plasma density increases with decreasing leak width, thus plasma species make more collisions with each other. As a result, perpendicular diffusion coefficient increases and hence radial plasma density uniformity is increasing with the increasing magnetic field (magnet current) values. The axial variation of plasma density is given in an Appendix B.

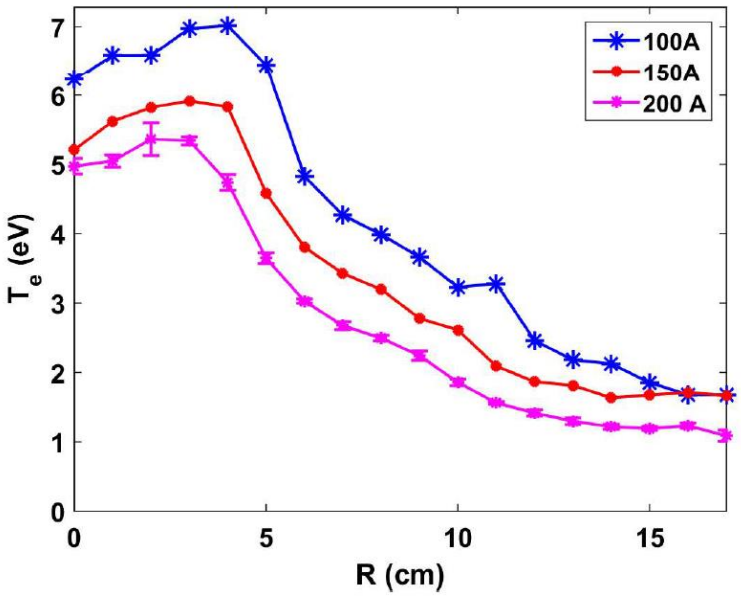

Figure 4.14. Radial variation of electron temperature measured along the non-cusp region when current in magnets are 100, 150, and 200A and Argon gas pressure is 2×10^{-4} mbar.

Figure 4.15 shows the radial variation of floating potential across the magnetic field along the non-cusp region. The cusp magnetic field confines the primary electrons in the null region and scavenges these electrons across the magnetic field thus floating potential is highly negative at confined region and decreases radially outwards across the magnetic field. The floating potential of the confined region also becomes more and more negative with the increasing magnet current because confinement of primary

electrons is increased with the increasing magnet current. The scavenging radial length across the magnetic field (i.e. floating potential becomes nearly -5 V at radial distance 7 cm, 6 cm, and 5 cm for 100 A, 150 A, and 200 A magnet current respectively) decreases with increasing magnet current. Thus VMMF scavenges the primary electrons across the magnetic field and acts as a filter, and it has control over filtering strength (scavenging length). The confined primary electron at confined region move back and forth between two poles and make collisions with background gas atoms, these collisions may ionize or excite the Argon gas atom. In figure 4.16, the violet to pale lavender blue colour is first excitation energy of Argon atom and it takes place only when the temperature of the electron is more than 3 eV thus violet to pale lavender blue colour shows the path of primary electrons, moving towards.

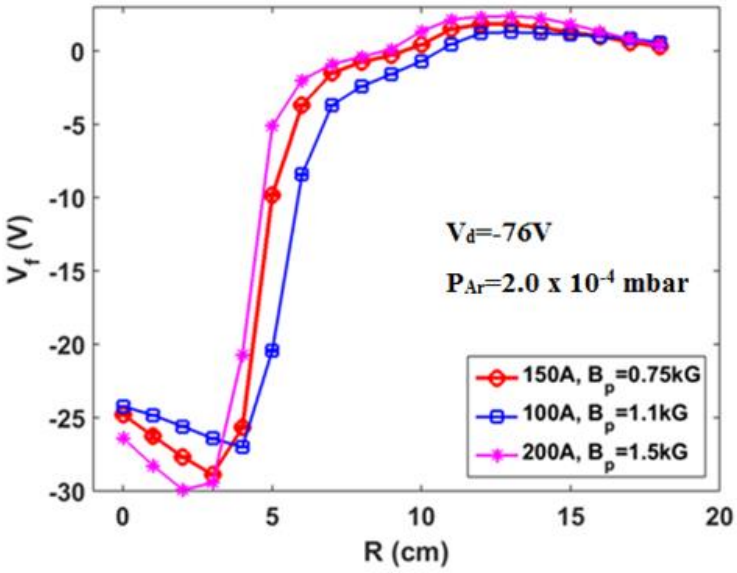

Figure 4.15. Radial variation of floating potential measured along the non-cusp region when current in the magnets are 100, 150, and 200 A and Argon gas pressure is 2×10^{-4} mbar.

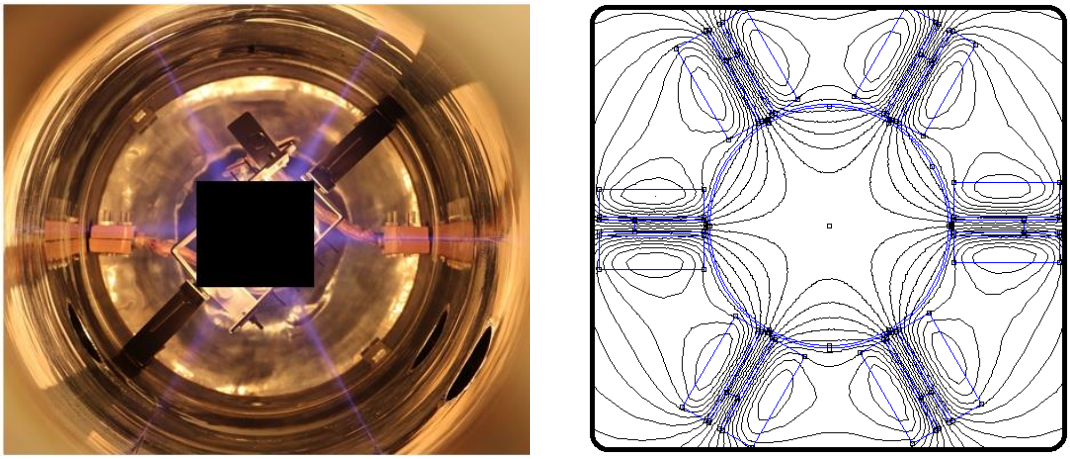

Figure 4.16. An image of the Argon plasma taken from the viewport fitted at the end of the chamber of MPD with magnet current at 150 A, and Argon gas pressure is 2×10^{-4} mbar. Side figure for reference of MMF.

References

1. R. L. Merlino, Amer. J. Phys. **75**, 1078 (2007)**.**
2. I.M. Hutchinson. Principles of plasma diagnostics. (Cambridge University Press, Cambridge, 1987).
3. R. A. Bosch, and R. L. Merlino, Phys. Fluids **29(6)** 1998 (1986).
4. R. A. Bosch, and R. M. Gilgenbach, Phys. Lett. A **128 (8)** 437 (1988).
5. R. Jones, Plasma Phys. **21** 505 (1979).
6. R. Jones, Plasma Phys. **23** 381 (1981).
7. A. A. Hubble *et. al*., Plasma Sources Sci. Technol. **23**(2014) 022001.
8. N. Hershkowitz *et. al*., Phys. Rev. Lett. **35** 277 (1975).
9. K. N. Leung *et. al.*, Phys. Fluids **19** 1045 (1976)).
10. R. Limpaecher, and K. R. Mackenzie, Rev. Sci. Instrum. **4** (1973) 726.
11. S. Aihara, M. Fujiwara, M. Hosokawa, and H. Ikegami, Nucl. Fusion **12** 45 (1972).

Chapter 5

Plasma fluctuations at different plasma regions of the device

In general, plasma diffusion across inhomogeneous magnetic fields has been a matter of great concern, both in laboratory and space plasma experiments, as it plays an important role in the efficiency of plasma devices [1-3]. Hence, the study of such plasma diffusion has received a great deal of attention in basic plasma experiments. It has been recorded that the plasma diffusion usually gets enhanced by many different instability mechanisms in different field configurations, thus resulting in anomalous transport. Drift wave turbulence is thought to be one of the dominant source of anomalous transport in the aforementioned devices [4-11]. Thus drift wave instabilities are considered as "universal instabilities" observed usually in magnetically confined plasma devices. These instabilities have relatively longer wave length and they affect the transport of particles and energy across the magnetic field.

In the **M**ulti-pole line cusp **P**lasma **D**evice (MPD) [12] there lies an opportunity to study the fluctuations as mentioned before. The device has been also constructed in such a configuration that the volume of edge region (low-β) is comparable to the volume of central region (high-β).

5.1 Quiescence level of plasma

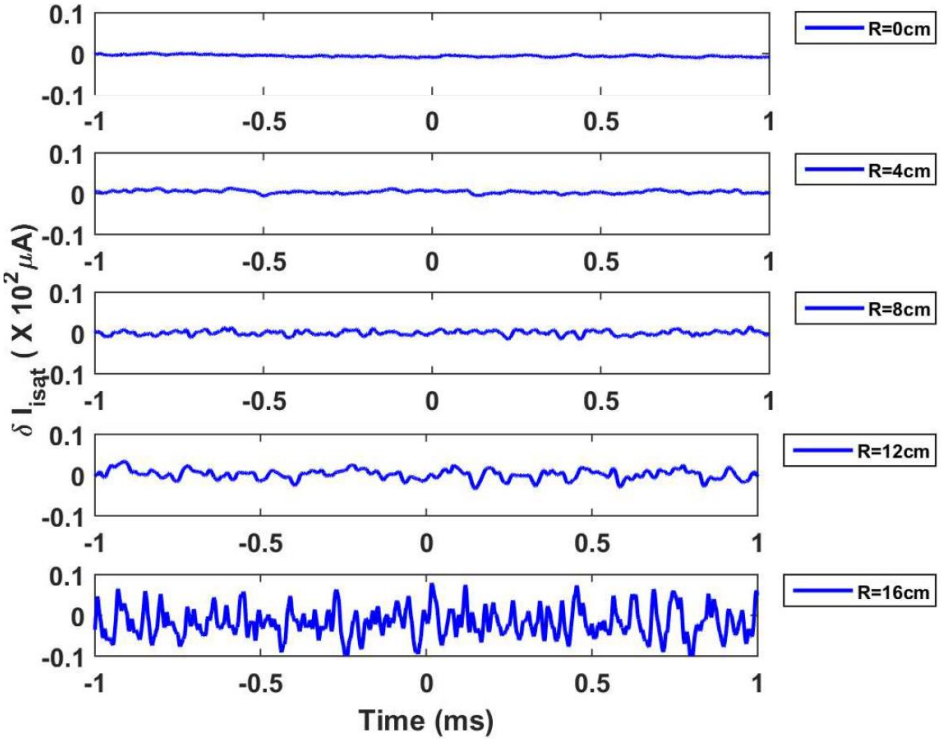

Figure 5.1. Temporal evolution of ion saturation current fluctuation (representing density fluctuation) at different radial location along the non-cusp region at current in magnets is 150A and Argon gas background pressure is 2×10^{-4} mbar.

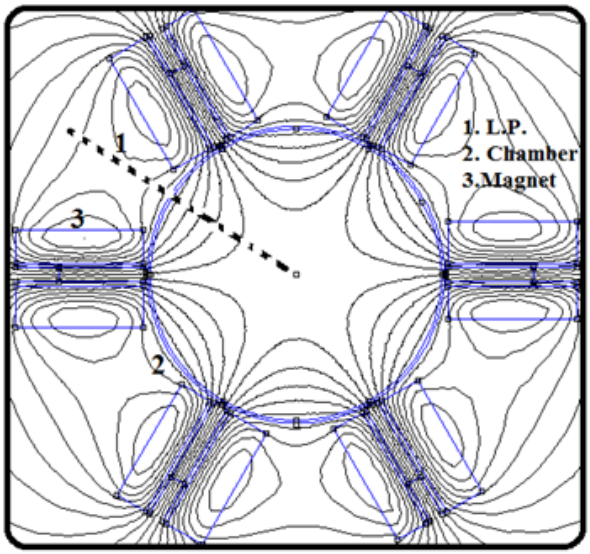

Figure 5.2. The schematic of mid (r, θ) plane of the device showing location of Langmuir probe along the radial direction.

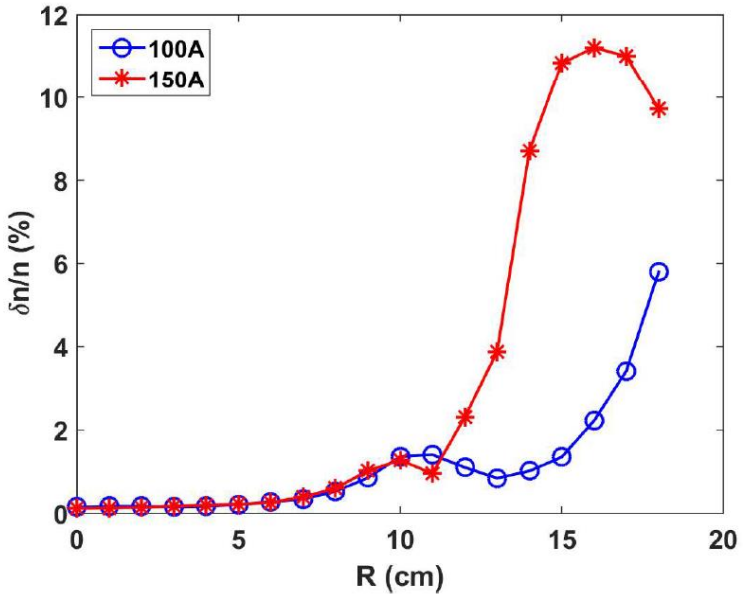

Figure 5.3. Variation of fluctuation level of density radially along the non cusp region with changing current in the magnets are 100 A, and 150 A, and Argon gas background pressure is 2×10^{-4} mbar.

Figure 5.1 shows the typical fluctuations of ion saturation current at different radial locations along the non-cusp region and at the mid (r, θ)plane of device (the plane from z = 65 cm from the filament) as shown in figure 5.2. The dotted line in figure 5.2 shows the location of Langmuir probe along the non-cusp region. These fluctuations are measured across a 10 kΩ resistance, when probe is biased at -100V as shown in figure 3.10 (a). It can be observed that the fluctuations are increasing radially outward. Figure 5.3 shows the radial variation of level of fluctuation along the non-cusp region. It can be observed that the ion saturation fluctuations are $(\delta n/n) < 1\%$ up to a distance of R = 6 cm. It is to be noticed that the fluctuation levels are very low in spite of the presence of small gradient in temperature in that low magnetic field region (up to R = 6 cm as shown in figure 4.14) though the temperature measurement may need more refinements. This cylindrical region of about 10 cm diameter in the centre has been identified to have uniform plasma density (as shown in figure 4.13) and the plasma is in a quiescent state. The plasma confined in this central cylindrical region can be utilized to study different fundamental plasma phenomena. Figure 5.4 shows the variation of time profile of ion

saturation current fluctuation at the centre of the device for different magnetic field values. It can be observed that the fluctuation in plasma density is decreasing with increasing magnetic field which shows that the quiescence of plasma is also controllable. The decreased in fluctuation of plasma density indicates that the stability of plasma increased. Thus it can be concluded that the plasma in the axial region, up to R ≤ 6 cm, is having very low fluctuations and they can still be reduced by increasing magnetic field in the cusp regions.

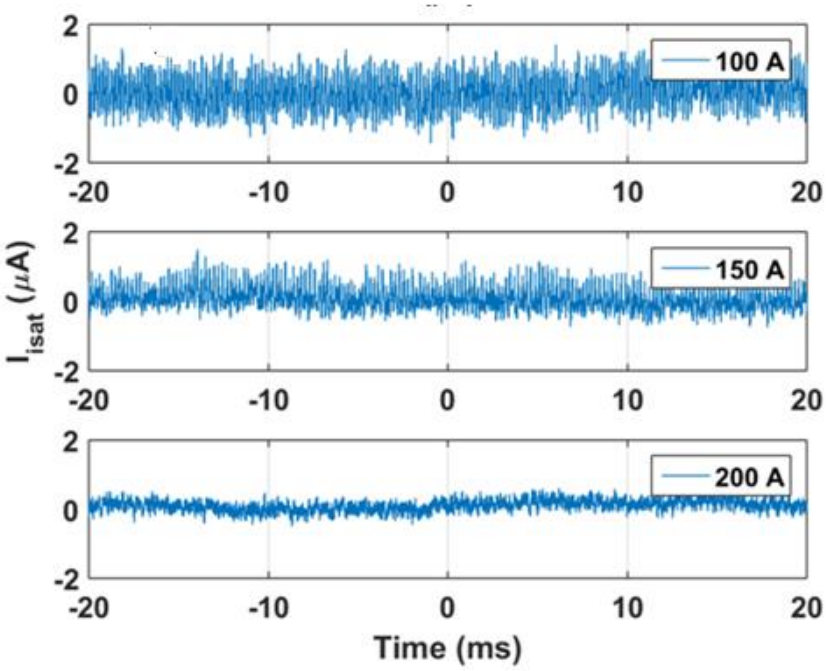

Figure 5.4. Variation of temporal evolution of ion saturation current fluctuation (representing density fluctuation) at the centre of the device with changing current in the magnets (I_{mag}) and 2×10^{-4} mbar Argon gas pressure.

From the figure 5.3, it can be observed that, in the region beyond R = 6 cm, the fluctuation level increases slowly while there is a sharp jump around R = 10 cm and it reached almost 11% at R = 15 cm for magnet field values of 1.1 kG at the pole. To identify the source of these fluctuations the following studies have been done in detail.

5.2 Equilibrium Profiles

The confined plasma in the cusp magnetic field diffuses across the magnetic field lines and streams out along the magnetic field lines. Because of their diffusion, gradients get formed in equilibrium profiles of plasma parameters. It is thought that these gradients help to generate free energy sources and these energies are transported through fluctuations. To identify these fluctuations, it is necessary to record and study the relevant plasma parameters. The radial variations of plasma density and electron temperature are measured along the non-cusp region using single conventional Langmuir probe for different pole magnetic field values.

In the present study the relevant plasma parameters and their fluctuations, with only two different magnet current values (100 A and 150 A) have been considered in which very dramatic variation of fluctuations have been identified. The corresponding magnetic field values at the pole face of cusp (near the magnet, R = 20 cm) are 0.75 kG and 1.1 kG respectively. The radial variation of plasma parameters (plasma densities, electron temperature, and floating potential) and the relevant fluctuations for these two field values have been measured radially along the non-cusp region and at the mid (r, θ) plane of device (the plane from z = 65 cm from the filament) as shown in figure 5.2. The Argon gas background pressure is 2.0×10^{-4} mbar, discharge current (I_d) and discharge voltage (V_d) have been kept at 5 A and -76 V throughout this experimental study.

The figure 5.5 and 5.6 show the radial variation of electron temperature (T_e) and plasma density (n_e) along the non-cusp region. The central region of plasma is hot (electron temperature is high), uniformly dense and confining mostly primary electrons up to 5 cm. The central bulk plasma diffuses along as well as across the magnetic field.

Because of this diffusion, gradients in plasma density and electron temperature are formed as shown in figure 5.5 and 5.6. The presence of gradients in plasma parameter profiles (like n and T_e) usually gives the hints about the sources of fluctuations in the respective regions. But to identify the sources, one needs to study the gradient length scales carefully along with correlations between the respective parameters. It will also be necessary to identify the frequencies involved and then which species is responsive to these frequencies need. For this purpose initially the gradient scale length of density and temperature are identified, then spectral studies along with correlation studies have been done. Figure 5.7 shows radial variation of theoretical plasma beta (β_e, *the ratio of plasma pressure to magnetic field pressure* [1]) along the non-cusp region. In the region away from the centre it has been observed that β_e is less than $\sqrt{m_e/m_i}$, thus it has been identified that the instabilities in these regions will be mostly electrostatic in nature.

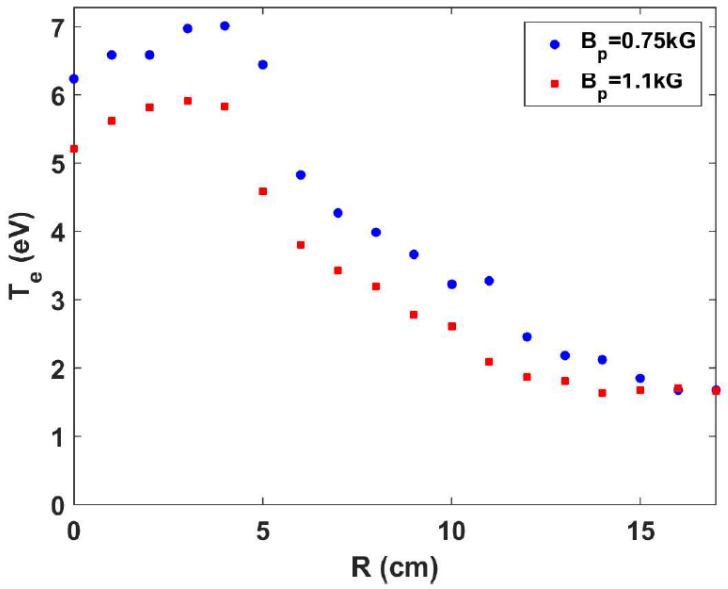

Figure 5.5. Radial variation of mean of electron temperature (T_e) along the non-cusp region at two different pole magnetic fields B_p= 0.75 kG and B_p= 1.1 kG, when magnets are energized with magnet currents 100 A, and 150 A respectively and 2×10^{-4} mbar Argon gas pressure.

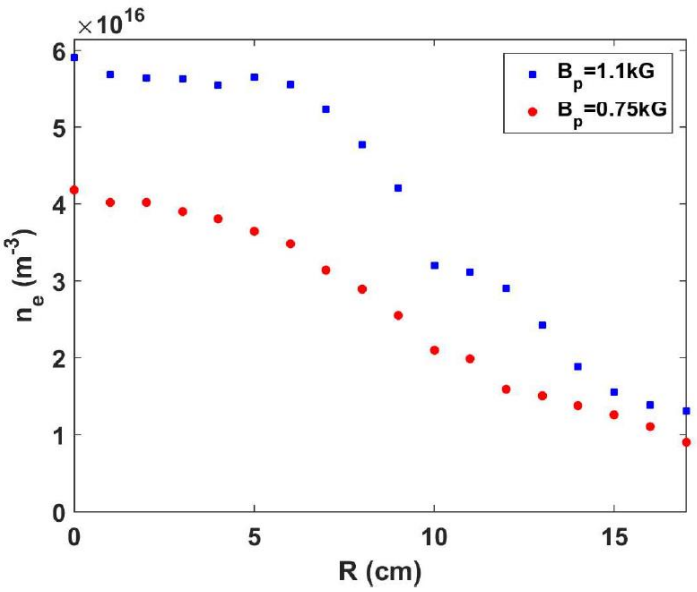

Figure 5.6. Radial variation of mean of plasma density (n_e) along the non-cusp region at two different pole magnetic fields B_p= 0.75 kG and B_p= 1.1 kG, when magnets are energized with magnet currents 100 A, and 150 A respectively and 2×10^{-4} mbar Argon gas pressure.

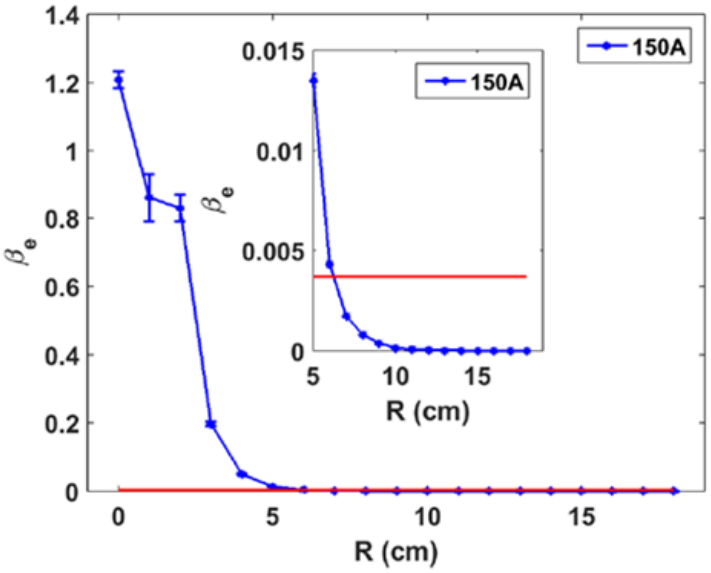

Figure 5.7. Radial variation of plasma beta (β_e) along non-cusp region when magnets are energized with current (I_{mag}) of 150 A and Argon gas pressure 2×10^{-4} mbar. The horizontal line shows the value of plasma beta line $y = \sqrt{m_e/m_i}$ for reference.

5.3 Comparison of gradient scale length of plasma parameters

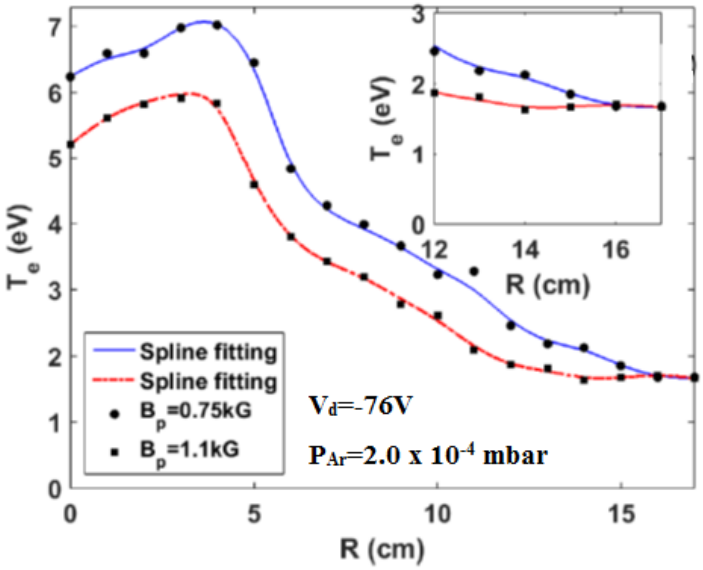

Figure 5.8. Radial variation of mean of electron temperature (T_e) with spline fitting along the non-cusp region at two different pole magnetic fields B_p = 0.75 kG and B_p = 1.1 kG.

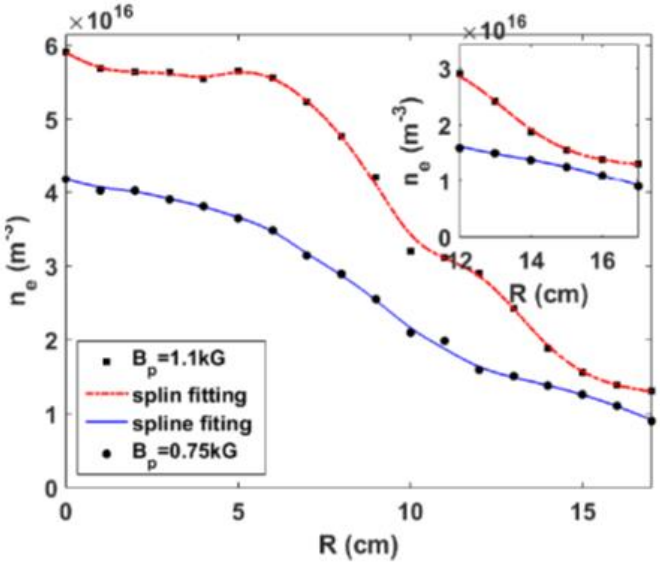

Figure 5.9. Radial variation of mean of plasma density (n_e) with spline fitting along the non-cusp region at two different pole magnetic fields B_p = 0.75 kG and B_p = 1.1 kG.

To calculate the gradient length scales from the discrete data points, appropriate curve fittings need to be done. The smoothing Spline fitting has been used on the radial profile of density (n) and electron temperature (T_e) as shown in figure 5.8 and 5.9.Then

using them the density scale length (L_n) and temperature scale length (L_{Te}) estimated. Here the scale length is defined by the equation; $L_x = |x/(dx/dR)|$, and suffix x is n and T_e. Considering these plasma parameters scale lengths, plasma of the device has been divided into three regions. First region, from radial distance R = 0 to 6 cm the plasma density and electron temperature is uniform and plasma is nearly quiescent. In the second region, from 6 to 10 cm, $L_n > L_{Te}$ (L_n = 50 cm, and L_{Te} = 6 cm at R = 7 cm for pole magnetic field B_p= 0.75 kG case), the temperature gradient is steeper compared to density gradient. In the third region from 12 to 17cm $L_{Te}>L_n$ the density gradient is sharp as compared to temperature gradient. In third region at R = 14 cm L_n and L_{Te} are 12 cm, 50 cm for pole magnetic field B_p = 0.75 kG respectively and L_n and L_{Te} are 4.27 cm, 60 cm for pole magnetic field B_p = 1.1 kG respectively. The inequality in scale length, $L_{Te}> L_n$ supports the drift wave instability in third region [13], and the inequality in scale length, $L_n> L_{Te}$ supports the temperature gradient driven instability in second region [14-16]. Figure 5.10 shows the schematic representation for comparison between plasma density scale length (L_n) and electron temperature scale length (L_{Te}) at the different region of the device along the non-cusp region.

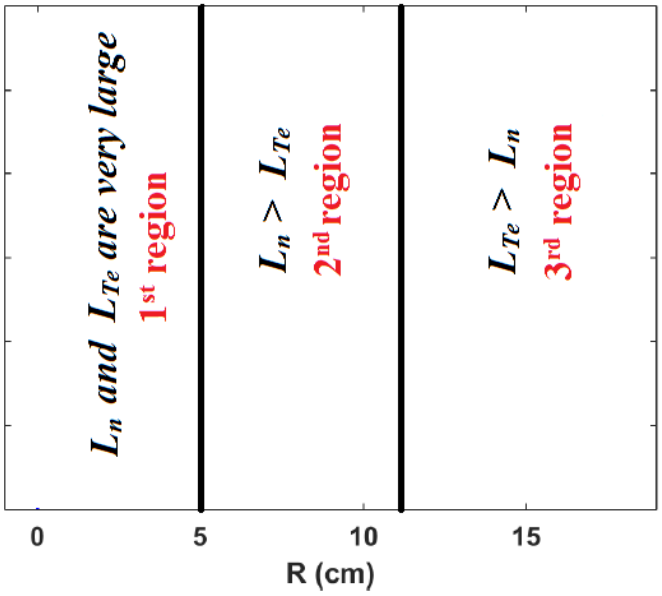

Figure 5.10. The schematic representation of plasma density scale length (L_n) and electron temperature scale length (L_{Te}) at the different region of the device along the non-cusp region.

5.4 Drift wave turbulence in the third plasma region of the device

In linear machines studied before [10, 17-19], with axial magnetic field produced by solenoid coils surrounding the cylindrical chamber there could be radial density and/or temperature gradients, (pressure gradient ∇P) because of finite boundary. These gradients may be unstable under certain conditions. Let us consider the direction of the uniform magnetic field (B_z) is taken in the z-direction. In a fluid picture these ∇P can produced diamagnetic drift velocity $(\nabla P \times B)/qnB^2$ in the azimuthal direction. If the pressure gradient is dominated by density gradients the diamagnetic drift will become same as the E x B drift where perturbed E field is due to the density gradient. Due to this perturbing radial electric field and axial magnetic field the plasma species get diamagnetic drift velocity (V_d) in θ direction as shown in figure 5.11 which can be trigger an instability /turbulence. These phenomena have been studied before

extensively [17-19]. But in a device like the multi-pole cusp magnetic field plasma device the magnetic field is directed in the $\mp\theta$ direction along the non-cusp region and density gradient is in radial direction. Hence E × B in $\mp$z direction as shown in figure 5.12. In this geometry the direction of magnetic field also changes in alternate non-cup region so the direction of drift velocity also changes as shown in the figure 5.12. This diamagnetic drift instabilities have certain properties listed as follow:

- Gradient lengths need to be appreciably small, while $L_{Te} > L_n$
- $e\delta V_f/T_e \approx \delta n/n$, as expected from Boltzmann relationship.
- δn leads δV_f, as expected from linear theory (the phase angle between them less than л/4).
- Fluctuation in density and potential measurements and the variation of fluctuations follow the gradient variations.
- Direction of perpendicular wave-number depend on the direction of the gradient and magnetic field.

In the third region of plasma of this device, conditions are favouring a density gradient driven drift wave instability; to confirm that more specific studies have been done in this geometry.

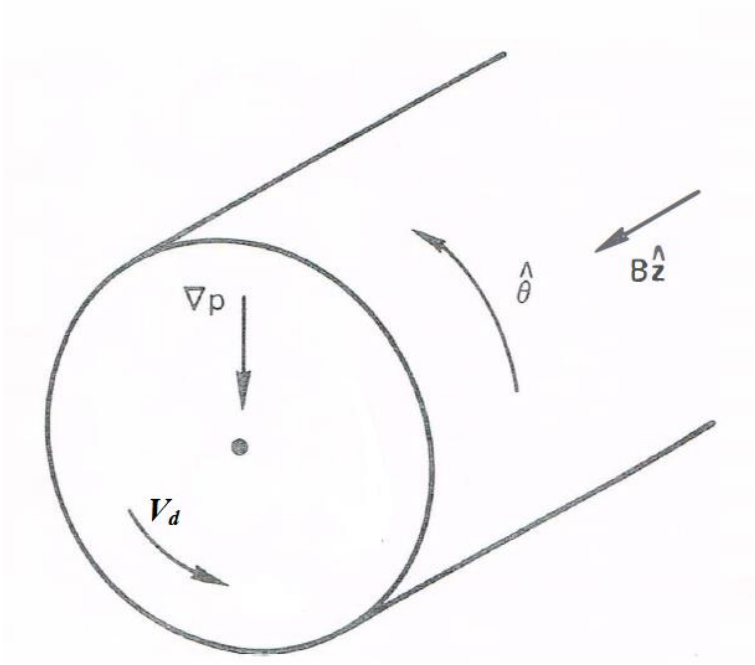

Figure 5.11. Schematic of diamagnetic drift in a cylindrical plasma having axial magnetic field [11].

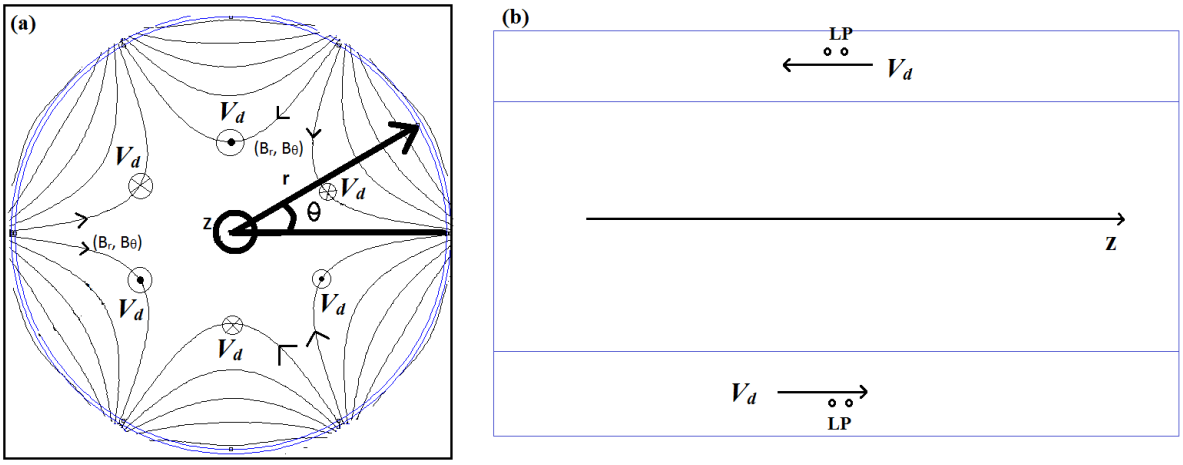

Figure 5.12. Schematic diagram of drift velocity (V_d) along the z-axis (a) in (r, θ) plane and (b) in (r, z) plane of the MPD device.

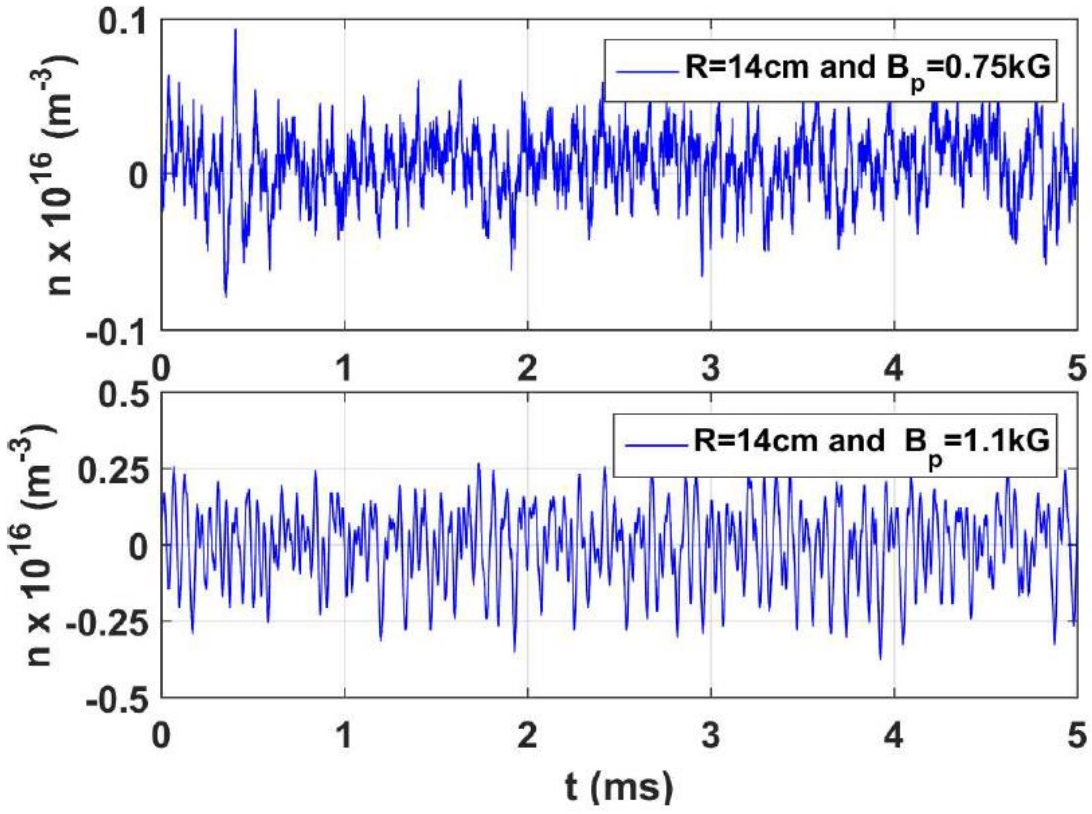

Figure 5.13. Temporal evolution of density fluctuations measured through ion saturation current, at R = 14 cm for two different pole cusp magnetic fields B_p= 0.75 kG and B_p= 1.1 kG, when current in the magnets is 100 A, and 150 A respectively. The Argon pressure is 2×10^{-4} mbar.

The figure 5.13 shows time profile of plasma density fluctuations at radial location R = 14cm and for different pole cusp magnetic fields B_p = 0.75 kG and B_p = 1.1 kG case along the non-cusp region. The figure 5.13 clearly shows the increase in fluctuation for higher pole magnetic field values (1.1kG). The density fluctuation is deduced from the fluctuation in ion saturation current. A single Langmuir probe has been used to measure ion saturation current fluctuation across the 10 kΩ resistance with sampling rate 2.5 MSa/sec and record length 500K point using KEYSIGHT DSOX2024A (200 MHz band width and 2 GS s^{-1} sampling rate) CRO.

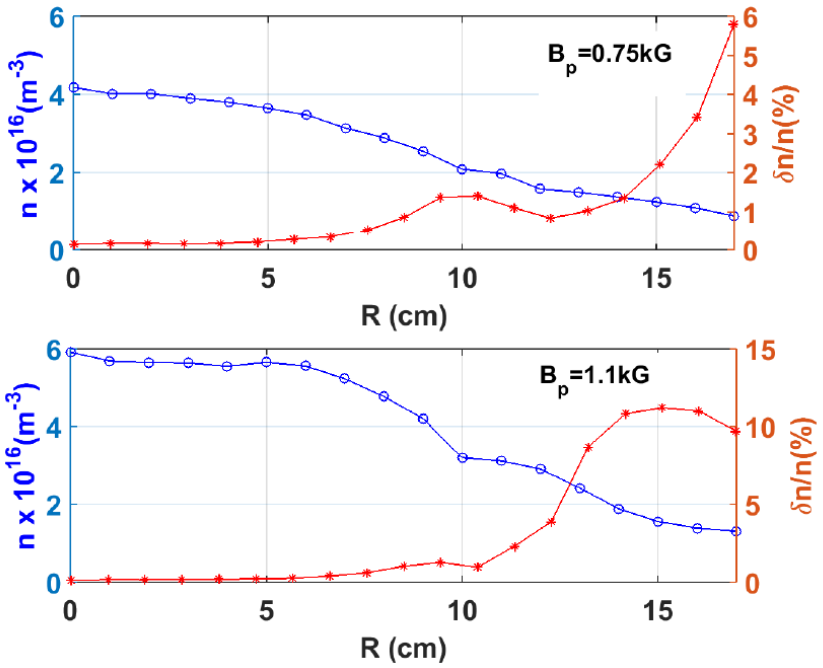

Figure 5.14. Radial profile of normalized density fluctuation level for two different pole cusp magnetic fields B_p= 0.75 kG and B_p= 1.1 kG, when current in the magnets is 100 A, and 150 A respectively. The Argon gas background pressure is 2×10^{-4} mbar.

Figure 5.14 shows the radial variation of normalised plasma density fluctuation level at two different pole cusp magnetic fields B_p= 0.75 kG, and B_p= 1.1 kG case. It is clearly observed from figure 5.14 that radial variation of normalized density fluctuation level follows the mean plasma density profile for both cases. The maximum normalized density fluctuation level are 6% and 11 % for pole cusp magnetic fields B_p= 0.75 kG, and B_p= 1.1 kG case respectively. The normalized density fluctuation level is high for pole cusp magnetic fields B_p= 1.1 kG because of the gradient in density is high for the same. These observation support the presence of density gradient driven drift wave instability [18].

5.4.1 Spectral analysis

The other important characteristic features such as power spectra of fluctuations, cross correlation function, wave number-frequency spectrum are necessary to identify the instability. Figure 5.15 shows the auto power spectrum of density fluctuations for

two pole magnetic field values (0.75 kG and 1.1 kG). It is observed that power spectra has mean frequency peak at 3 kHz for pole cusp magnetic fields B_p= 0.75 kG case and the power spectra become broad band with significant power while the central frequency is at 15 kHz for pole cusp magnetic fields B_p= 1.1 kG case. The frequency shift from 3 kHz to 15 kHz can be attributed to the increase in density gradient. The density fluctuation power spectra also follows a power law ~$1/f^{5.5}$ for f ≤ 20 kH to 90 kHz as shown in figure 5.16 as per drift wave turbulence [10, 20].

Figure 5.17 and 5.18 show the time evaluation of normalized density fluctuation and floating potential fluctuation at R =14 cm for the pole magnetic field values 0.75kG and 1.1kG. These measurements are carried out using two simple Langmuir probes of dimension 5 mm length and 0.5 mm diameter tungsten tip and distance between the two Langmuir probe is 5 mm. From both figures it can be clearly seen that density fluctuations follow the potential fluctuations. To find the correlation between them, the cross correlation function has been measured. The cross correlation function between the normalized values of density fluctuation ($\delta n/n$) with floating potential (eV_f/ k_BT_e) is found to be strongly correlated for both cases of magnetic field, as shown in figure 5.19. This helps to confirm that we are in presence of the density gradient driven drift wave instability. The correlation coefficients obtained is $c(\tau)$ ~ 0.8. There may be a slight spatial de-correlation as the probes used are not located on the same radial location. Also the phase angle between density and floating potential fluctuation is less than 45^0 [21-22] which also confirms drift wave instability.

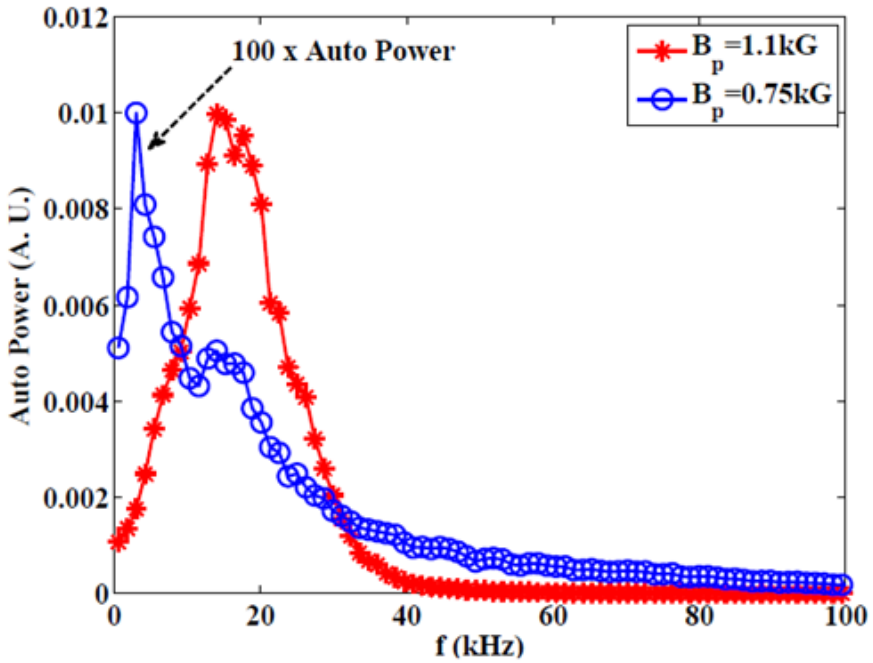

Figure 5.15. Auto-power spectrum of density at R = 14 cm and two different pole cusp magnetic fields B_p= 0.75 kG and B_p= 1.1 kG when magnets are energies with magnet currents 100 A, and 150 A respectively.

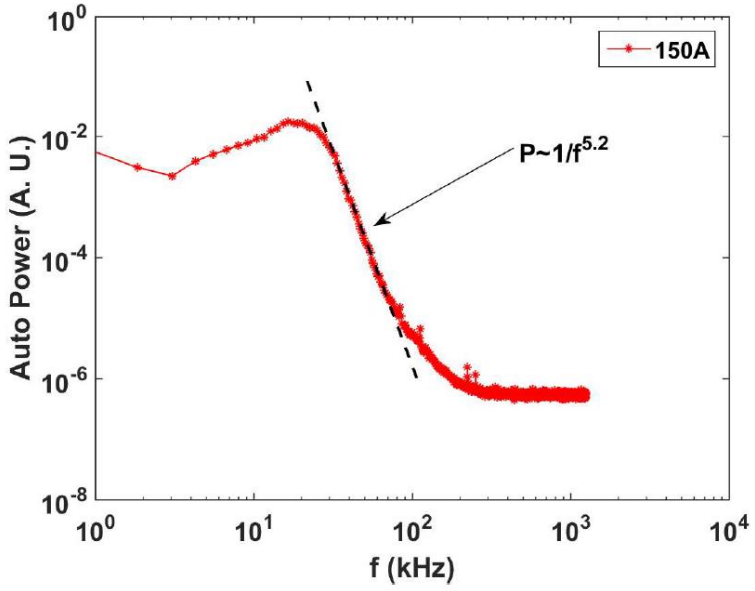

Figure 5.16. Log-log scale variation for Auto-power spectrum of plasma density fluctuation at R=14cm and 150A magnet current.

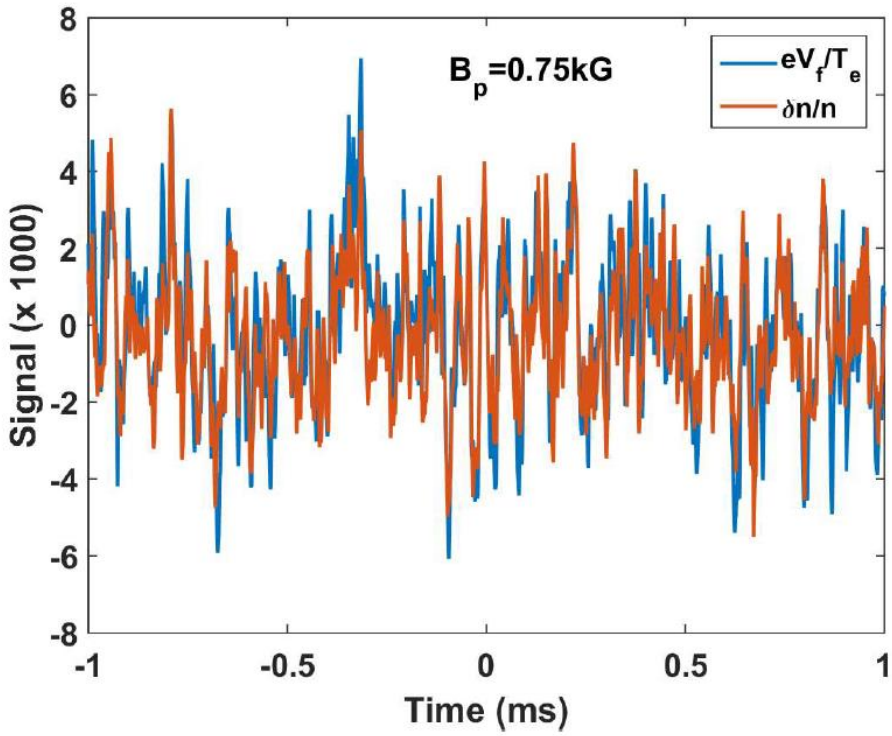

Figure 5.17. Temporal evolution of normalized density fluctuation and floating potential fluctuation at R=14cm when current (I_{mag}) in the magnets is 100 A and 2×10^{-4}mbar Argon gas pressure.

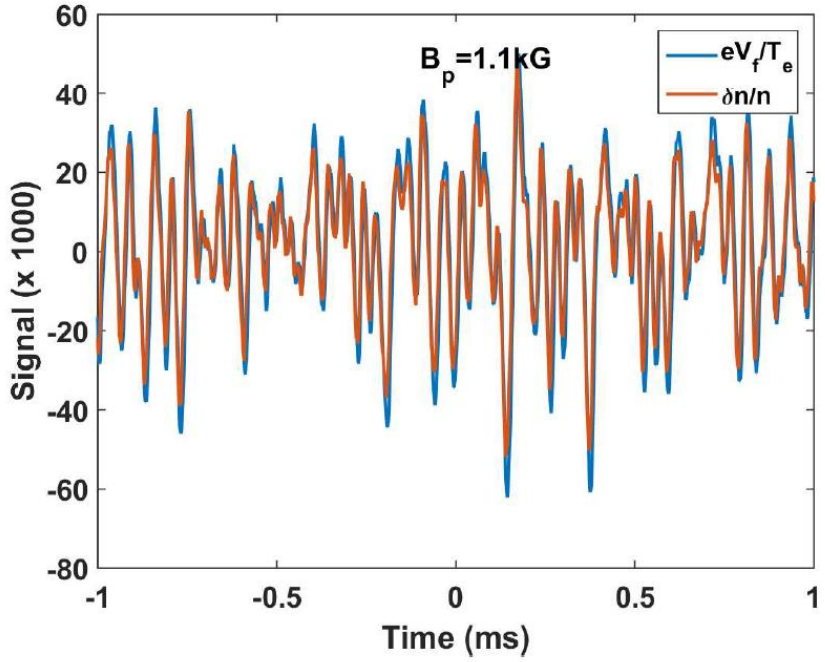

Figure 5.18. Temporal evolution of normalized density fluctuation and floating potential fluctuation at R = 14 cm when current (I_{mag}) in the magnets is 150 A and 2×10^{-4} mbar Argon gas pressure.

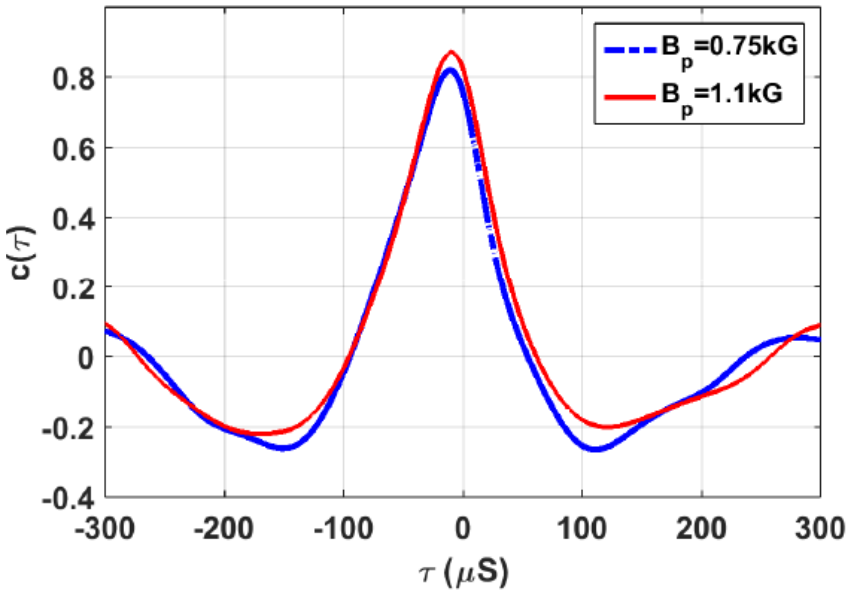

Figure 5.19. The cross correlation function c (τ) between normalized time series of density and floating potential fluctuation at R = 14 cm and two different pole cusp magnetic fields B_p= 0.75 kG, and B_p= 1.1 kG when magnets are energized with magnet currents 100 A, and 150 A respectively.

5.4.2 Wavenumber-frequency spectral analysis

Since the cusp magnetic field configuration will have different magnetic field direction at alternate non-cusp regions, the drift velocity is expected to change the direction in those alternate non-cusp regions as shown in figure 5.12. This can be established from the wave number-frequency spectrum $S\ (k_z, \omega)$. In figure 5.20 the contour plots of wave number-frequency spectrum $S\ (k_z, \omega)$ clearly captures this phenomenon. These figures have been plotted using density fluctuations, measured from two simple Langmuir probes separated by 1cm along the z-axis at radial location R = 14 cm for two different pole cusp magnetic fields B_p= 0.75 kG [5.20.(a) & 5.20.(b) for alternate non-cusp region] & B_p= 1.1 kG [5.20.(c) & 5.20.(d) for alternate non-cusp region]. These data were recorded with sampling rate 2.5 MSa s^{-1}, and record length 500K point using a same CRO. Then the drift velocity (V_d) is calculated by noting the

associated wave number (k_z) at the peak frequency (ω) from the wave number-frequency spectrum $S(k_z, \omega)$ and compared with the calculated drift velocity (V_d) from density scale length formula [17, 22-23], $V_d = \frac{\omega}{k_z} = k_B T_e / eBL_n$, where, k_B is Boltzmann constant.

For B_p= 0.75 kG, the spectrum $S(k_z, \omega)$ shows peak at frequency 3 kHz as shown in figure 5.20 (a) and its associated wave number (k_z) and wavelength (λ) of this mode are 0.11565 cm^{-1} and 54 cm respectively. The drift velocity obtained from $S(k_z, \omega)$ spectrum is 1.15 × 10^5 cm/s which matches the theoretically calculated value 1.0 × 10^5 cm/s , obtained from the density scale length formula at radial location R = 14 cm. From figure 5.20 (a) and (b) it has been observed that at the alternate non-cusp region, the direction of the drift velocity changes its sign which leads to negative wave number. Similarly, for B_p= 1.1 kG the spectrum $S(k_z, \omega)$ broadens at central frequency 15 kHz, as shown in figure 5.20 (c), and the associated wave number (k_z) & wavelength (λ) of this mode become 0.3665 cm^{-1}& 17 cm respectively. The drift velocity is obtained from the slope of line fitted at broadband frequency of $S(k_z, \omega)$ [as shown in figure 5.20 (c)]. In this case the drift velocities from $S(k_z, \omega)$ spectrum and calculated from the density scale length at radial location R = 14 cm are 2.9 × 10^5 cm/s and 2.55 × 10^5 cm/s respectively. Figure 5.20 (d) shows the wave-number frequency spectra $S(k_z, \omega)$ opposite non-cusp region. The drift velocity observed at peak frequency from spectrum $S(k_z, \omega)$ is nearly matching the one with calculated from density scale length for m = 1 for B_p = 0.75 kG and m = 2 for B_p= 1.1 kG drift wave mode and the wavelength of mode (λ) is also very large compared to ion gyro radius (ρ_i) for both cases. The mode number is calculated using the equation $v_d = (fL_z/m)$ where L_z is plasma size (75 cm) of the system.

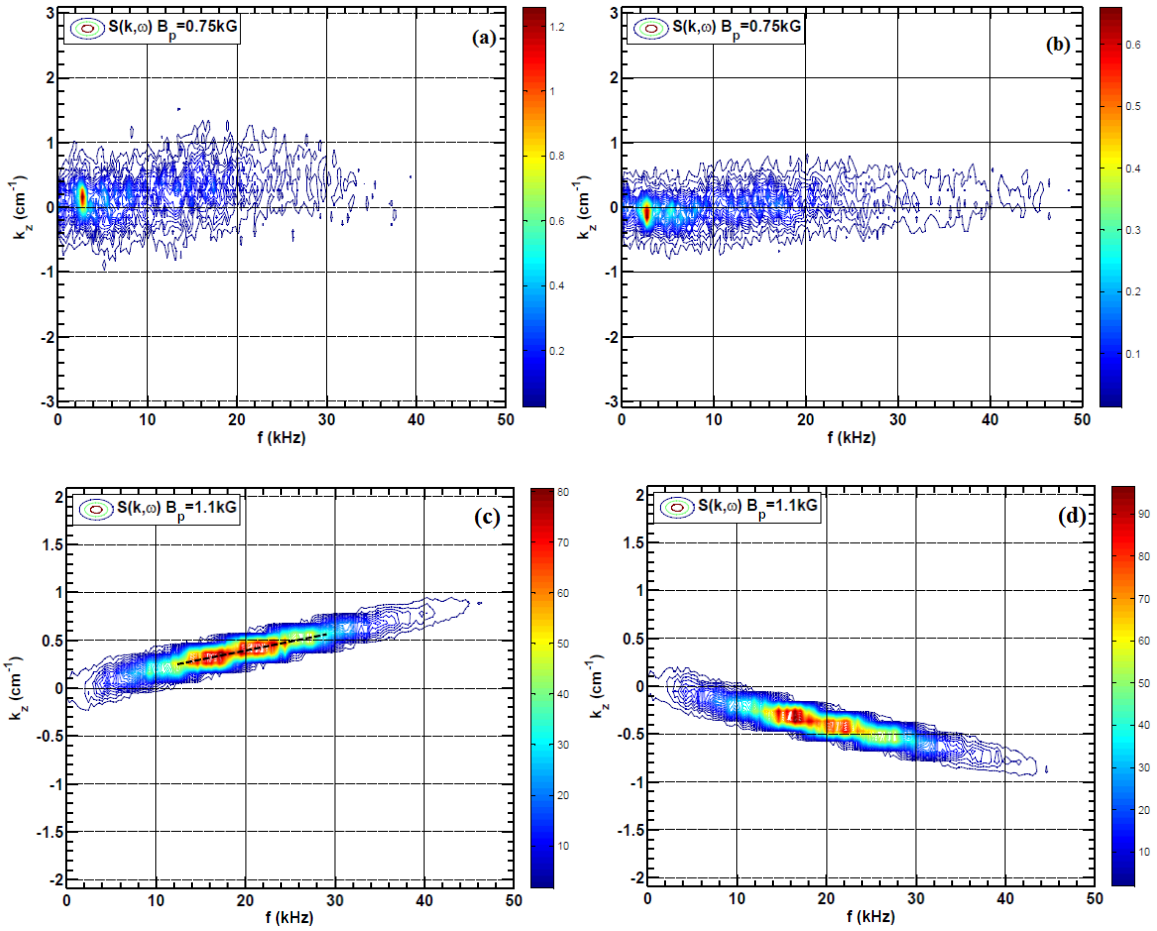

Figure 5.20. The contour plot of joint wave number and frequency specturm at R = 14 cm; (a) and (b) at pole cusp magnetic fields B_p=0.75 kG, (c) and (d) at pole cusp magnetic field B_p= 1.1 kG in non-cusp region. Here (b) and (d) are contour plots in alternate non-cusp region.

5.5 Electron temperature gradient (ETG) turbulence in the second plasma region of the device

In the second plasma region of the device, from 6 to 9 cm, $L_n > L_{Te}$ (L_n = 60 cm, and L_{Te} = 6 cm at R = 7 cm for pole magnetic field B_p= 1.1 kG case), the temperature gradient is large compared to the density gradient. The inequality in scale length, $L_n > L_{Te}$

supports the temperature gradient (ETG) driven instability in second region [14]. This ETG instability have certain properties listed as follow;

- Comparison in scale length, $L_n > L_{Te}$ support the condition for ETG instability.
- The linear calculation for ETG shows the value of $\eta_e >> 2/3$, where $\eta_e = L_n/L_{Te}$.
- The mode frequency fall in the lower hybrid range $\Omega_i < 2\pi f << \Omega_e$.
- $\frac{e\delta V_f}{T_e} \approx -\delta n/n$, density fluctuation are negatively correlated with floating potential.
- The phase angle between δn and δV_f is close л.
- The frequency power spectra follow the power law, $p \sim f^{-3.0}$.

In second plasma region of this device a conditions are favouring an ETG instability to confirm that more specific studies have been done in this geometries.

The linear calculation for ETG shows the value of η_e ($\eta_e = L_n/L_{Te}$) is must be more than 2/3 [14-16] for ETG turbulence. Figure 5.21 shows the variation of ETG parameter η_e with radial distance. This ETG instability condition is satisfied in our case.

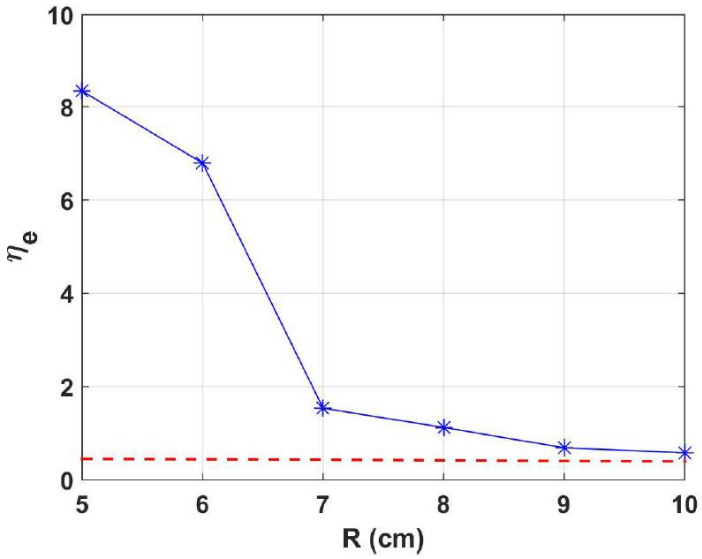

Figure 5.21. Radial variation of ETG threshold ($\eta_e = L_n/L_{Te}$) when current (I_{mag}) in the magnets is 150 A and 2 × 10^{-4} mbar Argon gas pressure. The red dashed line shows $\eta_e = 2/3$ for reference.

5.5.1 Spectral analysis

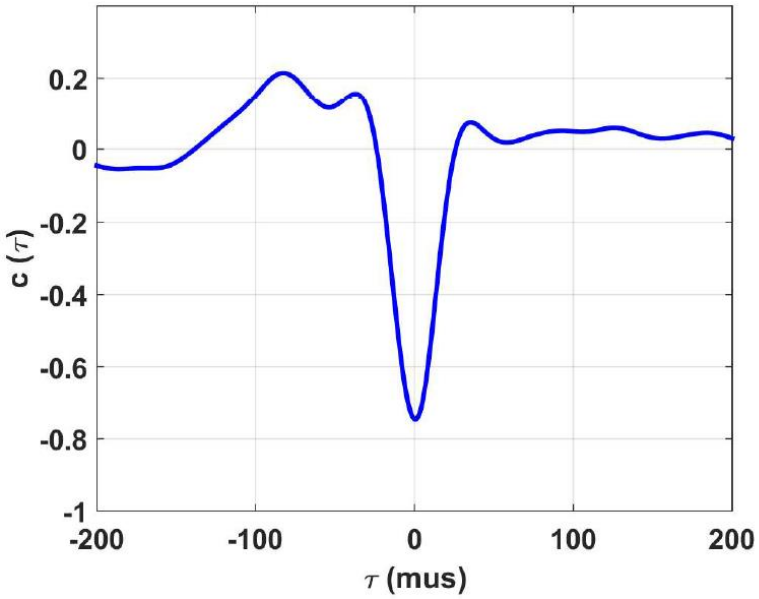

Figure 5.22. The cross correlation function c (τ) between normalized time series of density and floating potential fluctuation at R = 7 cm when current (I_{mag}) in the magnets is 150 A and 2 × 10^{-4}mbar Argon gas pressure.

The important characteristic features for identifying the temperature gradient (ETG) driven instability are obtained from the measured power spectra and cross correlation function. The measured correlation coefficients between two physical quantities are shown in figure 5.22. The cross correlation function between the normalized values of density fluctuation (δn/n) with floating potential (eV_f/k_BT_e) is found to be strongly anti-correlated. The correlation coefficients c(τ) ~ -0.8. Which is characteristics of ETG turbulence [15-16]. The phase between floating potential and density is more than 170 degree. The negative cross correlation is also captured from the simultaneous measurement of normalized time series of density and floating

potential as shown in figure 5.23 and oblate phase space distribution of density and floating potential fluctuation in figure 5.24. The observed instabilities has one peak at 5 kHz with significant power in density power spectra at R = 7 cm as shown in figure 5.25. The power spectra of density also follows power law of $1/f^{3.0}$ for $f \leq 20$ kHz to 150 kHz as per ETG turbulence [15-16]. The frequency of the mode lies in the lower hybrid range $\Omega_i < 2\pi f << \Omega_e$ [14]. All above characteristics indicate that the basic instability drive ETG turbulence. A more detailed analysis, comparing these experimental results with theoretical model calculations for this geometry, will be carried out in future.

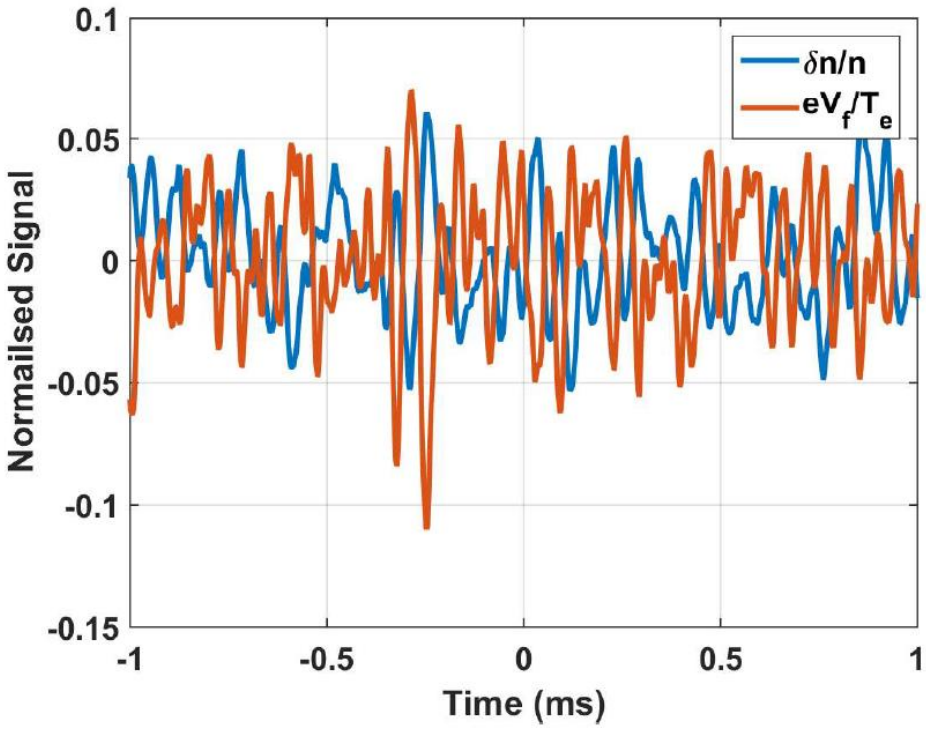

Figure 5.23. Temporal evolution of normalized density fluctuation and floating potential fluctuation at R = 7cm when current (I_{mag}) in the magnets is 150 A.

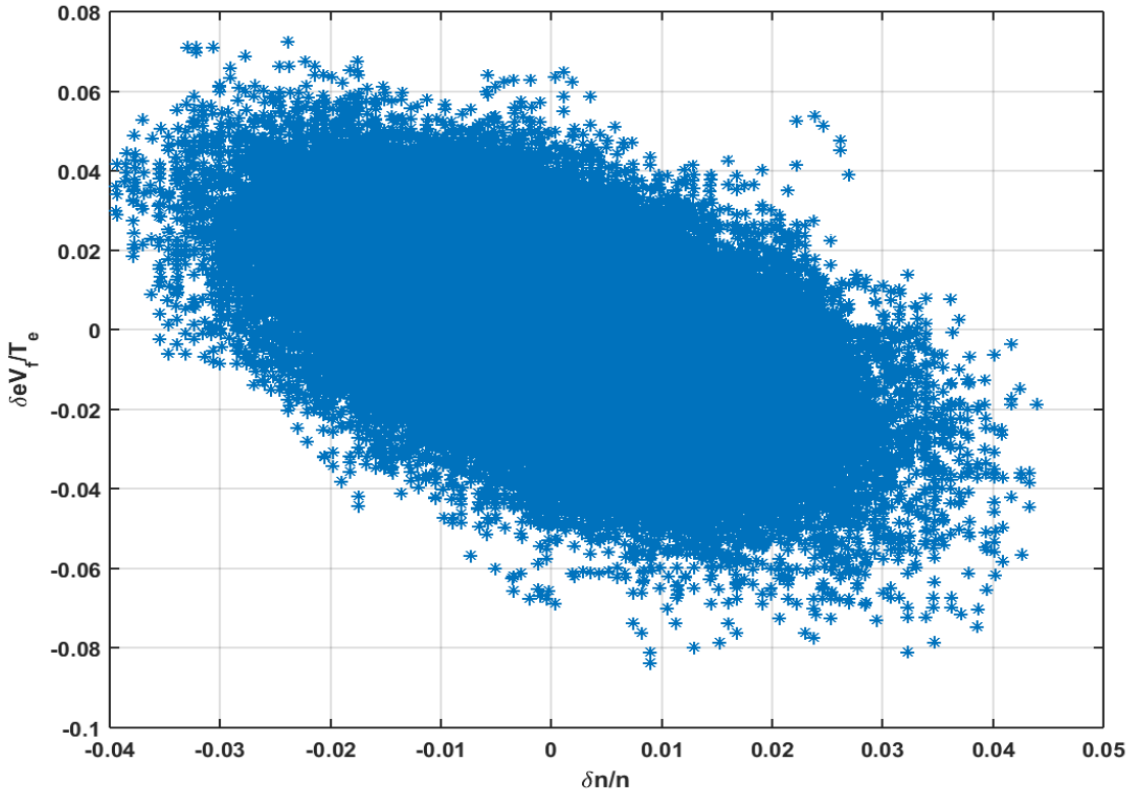

Figure 5.24. The phase space diagram of normalized density fluctuation and floating potential fluctuation at R = 7 cm.

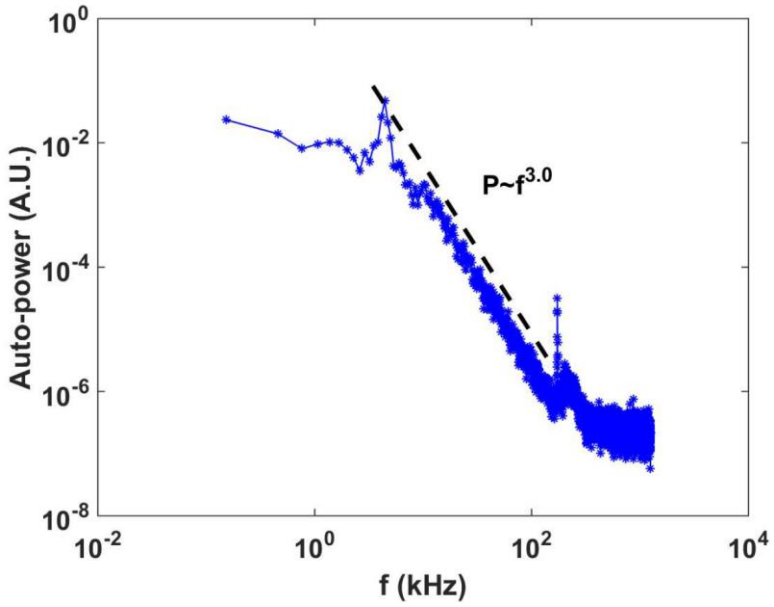

Figure 5.25. Auto-power spectrum of density fluctuation at R = 7cm when current (I_{mag}) in the magnets is 150 A and 2×10^{-4} mbar Argon gas pressure.

Reference

1. M. G. Haines, Nucl. Fusion, **17**, 811 (1977).
2. L. S. Combes, C. C. Gallagher, and M. A. Levine, Phys. Fluid, **5**, 1070, (1962).
3. C. B. Forest, K. Flanagan, M. Brookhart, M. Clark, C. M. Cooper, V. Désangles, J. Egedal, D. Endrizzi, I. V. Khalzov, H. Li, M. Miesch, J. Milhone, M. Nornberg, J. Olson, E. Peterson, F. Roesler, A. Schekochihin, O. Schmitz, R. Siller, A. Spitkovsky, A. Stemo, J. Wallace, D. Weisberg and E. Zweibe*et al*., J. Plasma Phys., **81**, 345810501 (2015).
4. K. Itoh, S-I. Itoh, and A. Fukuyama, *Transport and Structural Formation in Plasmas* (Institute of Physics), Bristol, (1999), p. 235.
5. R. J. Groebner, K. H. Burrell, and R. P. Seraydarian, Phys. Rev. Lett., **64**, 3015 (1990).
6. K. Toi, K. Kawahata, S. Morita, T. Watari, R. Kumazawa, K. Ida, A. Ando, Y. Oka, M. Sakamoto, Y. Hamada, K. Adati, R. Ando, T. Aoki, S. Hidekuma, S. Hirokura, O. Kaneko, A. Karita, T. Kawamoto, Y. Kawasumi, T. Kuroda, K. Masai, K. Narihara, Y. Ogawa, K. Ohkubo, S. Okajima, ' T. Ozaki, M. Sasao, K. N. Sato, T. Seki, F. Shimpo, H. Takahashi, S. Tanahashi, Y. Taniguchi, and T. Tsuzuki, Phys. Rev. Lett., **64**, 1895 (1990).
7. R. A. Bosch, and R. L. Merlino, J. Appl. Phys., **60**, 3056 (1986).
8. S. T. Ratliff, J. M. Dawson, and J. N. Leboeuf, Phys. Rev. Lett., **50**, 1990 (1983).
9. C. Schröder, T. Klinger, D. Block, A. Piel, G. Bonhomme, and V. Naulin, Phys. Rev. Lett., **86**, 5711 (2001).
10. F. F. Chen, Phys. Rev. Lett., **15**, 381 (1965).
11. W. Horton, Rev. Mod. Phys., **71**, 735 (1999).

12. A. D. Patel, M. Sharma, N. Ramasubramanian, R. Ganesh, and P. K. Chattopadhyay, Rev. Sci. Instrum., **44**, 726 (2018).
13. N. DÁngelo, and R.W. Motely, Phys. Fluids **6**, 422 (1963).
14. S. K. Singh, L. M. Awasthi, R. Singh, P. K. Kaw, R. Jha, and S. K. Mattoo, Phys. Plasmas **18**, 102109 (2011).
15. S. K. Mattoo et. al., Phys. Rev. Lett., **108** 255007 (2012).
16. S. K. Singh, L. M. Awasthi, S. K. Mattoo, P. K. Srivastava, R. Singh and P. K. Kaw, Plasma Phys. Control. Fusion, **54** 124015 (2012).
17. N. DÁngelo, and R.W. Motely, Phys. Fluids **6**, 422 (1963).
18. N. DÁngelo, D. Eckhartt, G. Grieger, E. Guilino, and M. Hashmi, Phys. Rev. Lett., **11**, 525 (1963).
19. T. Ohkawa, and D. W. Kerst, Phys. Rev. Lett., **7**, 41 (1961).
20. H. L. Pécseli, Ann. Geophys., **33**, 875 (2015).
21. J. C. Perez, W. Horton, K. W. Gentle, W. L. Rowan, K. Lee, and R. B. Dahlburg, Phys. Plasmas **13**, 032101 (2006)
22. W. Horton, Rev. Mod. Phys., **71**, 735 (1999).
23. H. L. Pécseli, T. Mikkelsen, and S. E. Larsen, Plasma phys., **25**, 1173 (1982).

Chapter 6

Conclusion and Future Scope

The last chapter of this dissertation is divided into two sections. The first section gives an account of brief summary of the work described in this dissertation followed by the conclusions drawn from it. In the second section, a brief discussion on the further experimental works that can be carried out is presented.

6.1 Summary

In this Thesis work an Argon plasma was produced in a multi-pole cusp magnetic field and their characteristics have been studied in detail. The device mainly consists of a vacuum chambers, plasma sources (hot cathode), pumping system, magnet system and plasma diagnostics. A multi-pole cusp magnetic field system has been designed such that a cylindrical high beta region is formed surrounded by a comparable volume of low beta region. This has been achieved by placing six electromagnets (with embedded profiled vacoflux-50 core and double pancake winding) over a large cylindrical chamber having dimension 103cm axial length and 40cm diameter. The unique feature of this VMMF is that it is profiled using a core material of the electromagnets which allows changing the field values with the effect of using different permanent magnets. This multi-pole cusp magnetic field (VMMF) system has been made to be versatile such that many different plasma confinement configurations and field values can be studied. The 2-D simulation of the VVMF has been performed using the Finite Element Method Magnetic software and has been validated by experimentally

measured values. The magnetic field simulation results show that the generated VMMF has full control over a nearly field free region (null region) without changing poles of magnets and the that rate of change of pole magnetic field with respect to magnet current is very high for vacoflux-50 core compared to simple air core. The sets of magnets system of this device can also provide different magnetic field configuration viz. quadrupole cusp magnetic filed configuration and mirror magnetic field configuration by applying the current in the required magnets.

The whole chamber is pumped down to a pressure 10^{-6} mbar using a Turbo Molecular Pump (TMP) backed by a rotary pump, while a combination of the Ionization and Pirani gauges are used for pressure measurement. The Argon gas is filled to a pressure of the order 10^{-4} mbar for plasma production. The plasma discharge has been struck between two dimensional vertical array of tungsten filament based cathode source and grounded chamber wall. The cathode source is fitted well inside the main chamber and inside the field free region of magnetic field to avoid the edge effects of the magnets. These filaments are powered by a 500 A, 15 V floating power supply (V_{fil}) while it is normally operated at around 16 - 19 A per filament. The source is biased with a voltage of - 76 V with respect to the grounded chamber walls using discharge power supply (V_d). The primary electrons emitted from the filaments travel in the electrical field directions, while they are confined by the cusp magnetic field lines. Because of mirror effects due to cusp configuration, electrons move back and forth between the poles and they ionize the background gas atoms and thus an Argon plasma is produced. A number of diagnostics have been developed for characterizing the plasma viz. simple Langmuir probe for plasma parameters (electron temperature, plasma density, and floating potential) measurement, an emissive probe for plasma potential measurements. A MATLAB script has been written for quickly processing the single Langmuir probe

I-V characteristics for determining the plasma parameters. A set of rack probes for simultaneous measurement of density and potential fluctuations in the plasma has been developed. The MATLAB scripts for frequency power spectra, cross-correlation function, and wave-number frequency spectra are written to analyse the fluctuations data obtained from these rack probes for detailed experimental study of instabilities in MPD. Thus in last it can be concluded that the MPD in a DC plasma state is ready for controlled study of space plasma physics as well as basic plasma.

The Argon plasma thus produced and confined by multi-pole line cusp magnetic field is found to be have different characteristics at different regions. The central high beta plasma volume is found to be quiescent ($\delta n/n < 1\%$) and uniform and also it is found that to be controllable in size and plasma characteristics by changing the magnet current. This volume would be beneficial for basic plasma studies (viz. ion acoustic wave, soliton wave interaction, electron plasma wave, Landau damping, nonlinear coherent structure, wave-particle trapping and un-trapping etc.). While the edge regions surrounding the central high beta region is found to have many interesting phenomena, which are studied in detail. The plasma characteristics, radially along the non-cusp region, were recorded for different magnetic field values at the poles using Langmuir probes. The profiles of electron density, temperature, floating potentials with different magnetic field values at the poles helped to complete the plasma characterization. One of the key parameters involved in the plasma confinement in the cusp magnetic field is the effective leak width of plasma (the width of the profile of plasma escaping through the cusp). The estimated leak width has been compared with model calculations from previously published different scaling and is found to be matching well. The experimental results show that the leak width of plasma decreases with increasing of current in the magnets. Thus the plasma loss rate at the anode (at the leak width) where

plasma meets vessel chamber wall decreases with increasing current in the magnets, hence the confinement of primary electron at the null region of magnetic field increases. These confined primary electrons move back and forth between two poles of cusp magnetic field and also collide with background Argon gas. As a result, the plasma density at the null region of magnetic field increases with the decreasing of leak width of plasma. All the plasma parameters are increasing with the decrease of the plasma leak width thus stability of plasma also increases, which can be clearly observed from the decrease of the density fluctuation. All the above functional flexibility and wide range of operation regimes make this device an instrument of choice for carrying out studies of fundamental plasma phenomena.

The bulk plasma at the central region is uniform and dense (null region). This plasma diffuses across the magnetic field and streams out along the magnetic field lines toward the cusp, as a result, gradients in plasma parameters (plasma density, electron temperature, and floating potential) are formed. The radial variation of plasma parameters measured along the non-cusp region (across the magnetic field) and scale length of plasma parameters are measured. Using the different measured scale lengths of plasma parameters, the whole plasma can be divided into three regions. The central plasma region is uniform and quiescent where density and electron temperature scale length are very high. In the mid profile region of the plasma, the temperature gradient is dominating compared to the density gradient. Finally in edge region, the density gradient is dominating compared to temperature gradient. These gradients are also controllable by changing magnetic field values. The fluctuations and hence instabilities due to the gradients in the density and temperature have been studied to identify the sources of free energy. The role of the magnetic field in these fluctuations has also been studied for 100 A, and 150 A of magnet current. It has been observed that the frequency

of the instability changes explicitly with the density gradient. Moreover, the scale length of the plasma parameters, frequency spectrum, cross-correlation function, and fluctuation level of plasma densities has been measured in order to identify the instability. In this chapter we have reported the experimental observations of density gradient driven drift wave turbulence in low-β plasma confined by an inhomogeneous cusp magnetic field. The generated instability has been identified by explicitly studying the following properties:

- Comparison of scale lengths of plasma parameters, as for example inequality in scale length, $L_{Te} > L_n$ support the condition for drift wave instability.
- In time evolution of density profile, fluctuations have been observed when the density gradient present, whereas these fluctuations are suppressed in uniform plasma confined region. This radial variation of normalized density fluctuation level follows the density profile which excites drift wave instability.
- The density fluctuation frequency power spectra has power index 5.5.
- The strongly correlated cross correlation function between normalized floating potential fluctuations and density fluctuations hold the relation $(\delta n/n) \approx (eV_f/k_BT_e)$ with a phase angle difference of nearly to л/4 between them both are proving that the density fluctuations lead floating potentials fluctuation for density gradient driven drift wave turbulence.
- Lastly, the cross field drift velocity due to the fluctuations in plasma parameters have been measured from the wave number- frequency $S(k_z, \omega)$ spectra and are compared with the theoretical values, obtained from density scale length formula. Also the wavelength of the mode (λ) is very large compared to the ion gyro radius(ρ_i), which leads to "anomalous diffusion" across the inhomogeneous magnetic field.

Thus all above diagnostics confirm the instability in non-cusp region is drift wave instability due to the density gradient along the radius and across the magnetic field (B_θ). Thus the particles drift due to density fluctuation along the axial direction (z-direction). Moreover, it has been the first time observed that, the direction of the drift wave velocity changes its sign in alternate non–cusp region.

In the second plasma region of the device, from 6 to 9 cm, the temperature gradient is large compared to the density gradient. The inequality in scale length, $L_n > L_{Te}$ supports the temperature gradient (ETG) driven instability in second region. This ETG instability have been identified by the properties listed as follow;

- Comparison in scale length, $L_n > L_{Te}$ support the condition for ETG instability.
- The linear calculation for ETG shows the value of $\eta_e >> 2/3$, where $\eta_e = L_n/L_{Te}$.
- The mode frequency fall in the lower hybrid range $\Omega_i < 2\pi f << \Omega_e$.
- $\frac{e\delta V_f}{T_e} \approx -\delta n/n$, density fluctuation are negatively correlated with floating potential.
- The phase angle between δn and δV_f is close л.
- The frequency power spectra follow the power law, $p \sim f^{-3.0}$.

6.2 Future scope

The experimental studies presented in the Thesis can be extended to some numerical and experimental studies to give deeper insight in particular study. Some of these are listed follow.

The plasma confined in this magnetic field configuration is quiescent and the level of quiescence is also controllable. Thus the next plan of our experiment will be to study the magnetic reconnection, magnetosonic wave, soliton wave interaction, and ion acoustic soliton wave propagation perpendicular to the magnetic field in a quiescent plasma. Moreover, in low background gas pressure, R. Jones (1981, [1, 2]) studied the

leak width (*d*) of plasma and conclude that micro-instabilities are unstable in a cusp sheath (e.g. drift wave, ion cyclotron waves). The detailed analysis of these instabilities with changing pole magnetic field values has still not been studied yet and is accessible to the study in the future using this device.

In this multi-pole line cusp configuration of the magnetic field, plasma can be also produced by various methods depending upon requirement. These methods include RF discharge, which includes helicon discharge and both capacitively and inductively coupled discharges, microwave discharge, etc. [3-5]. The effect of magnetic field values on this type discharges will be studied in future.

The sets of magnets of this device also provide different magnetic field configuration viz. quadrupole cusp magnetic field configuration and mirror magnetic field configuration by applying the current in the required magnets. The quadrupole cusp magnetic field configuration is widely used in magnetic reconnection experiments [6-8] and the mirror magnetic field configuration is also widely used in basic plasma studies like plasma diffusion in a bad curvature of magnetic field as well as different gradient forces on plasma species, loss cone instabilities etc [9-11]. Since in this device poles of magnetic field configuration made by the electromagnets thus variable magnetic field with this configuration is an added advantage.

Many results have been published about the measurement of the width of plasma leakage at the cusp (near the pole magnet) and still an exact scaling for the amount of plasma being leaked in a given cusp configuration is yet to be ascertained. Though many scaling exists, ranging from electron gyro-radius to ion gyro-radius apart and also the so-called ‘hybrid gyro-radius’ [12-17]. The exact scaling of plasma leaking through a

cusp magnetic field still an open issue. In addition, the variation of leak width of plasma with changing pole magnetic field values has still not been studied before.

References

1. R. Jones, Nuovo Cimento **34** (1982) 157.
2. R. Jones, Plasma Phys. **21** (1979) 505.
3. T. Shibuya, S. Hashimoto, E. Yabe, and K. Takayama, Nucl. Instrum. Methods **B 55**, 364 (1991).
4. K. Yamauchi, S. Shibagaki, A. Kono, K. Takahashi, T. Shibuya, E. Yabe, and K. Takayama, Ion Implantation Technol. **92**, 683 (1993).
5. Michael A. Lieberman and Allan J. Litchtenberg, *"Principle of Plasma Discharges and Materials Processing"*, Johan Wiley and Sons, 2005.
6. M. R. Brown, Phys. Plasmas **6**, 1717 (1999).
7. Masaaki Yamada, Hantao Ji, Scott Hsu, Troy Carter, Russell Kulsrud, Norton Bretz, Forrest Jobes, Yasushi Ono, and Francis Perkins, Phys. Plasmas **4**, 1936 (1997).
8. R. L. Stenzel, J. M. Urrutia, M. Griskey, and K. Strohmaier, Phys. Plasmas **9,** 1925 (2002).
9. M. N. Rosenbluth and R. F. Post, Phys. Fluids **8,** 547 (1965).
10. R. F. Post, Phys. Fluids, **9,** 720 (1966).
11. A. Makhijani, A. J. Lichtenberg, M. A. Lieberman, and B. Grant Logan, Phys. of fluids **17**, 1291 (1974)
12. M. G. Haines, Nuclear Fusion **17** (1977) 811.
13. R. A. Bosch and R. L. Merlino, Phys. Fluids **29(6)** (1986) 1998.
14. R. A. Bosch and R. L. Merlino, Rev. Sci. Instrum. **57**(1986) 2940.
15. R. A. Bosch and R. M. Gilgenbach, Phys. Lett. A 128 **(8)** (1988) 437.

16. C. M. Cooper, D. B. Weisberg, I. Khalzov, J. Milhone, K. Flanagan, E. Peterson, C. Wahl, and C. B. Forest, Plasma Phys. **23** (2016) 102505.

17. A. A. Hubble, E. V. Barnat, B. R. Weatherford and J. E. Foster, Plasma Sources Sci. Technol. **23**(2014) 022001.

Appendix A:

A complete magnetic field mapping should have the individual directional components also. Accordingly, two plots have been added in a new appendix. They show the variation of B_r, B_θ and mean B along the cusp region (figure A) and the non-cusp region (figure B) at a coil current of 100 A in the magnets. In the both edges of the magnets, B_z components will also be present. But since the experimental interests are there in the central region where B_z is almost zero, B_z component variation has been excluded.

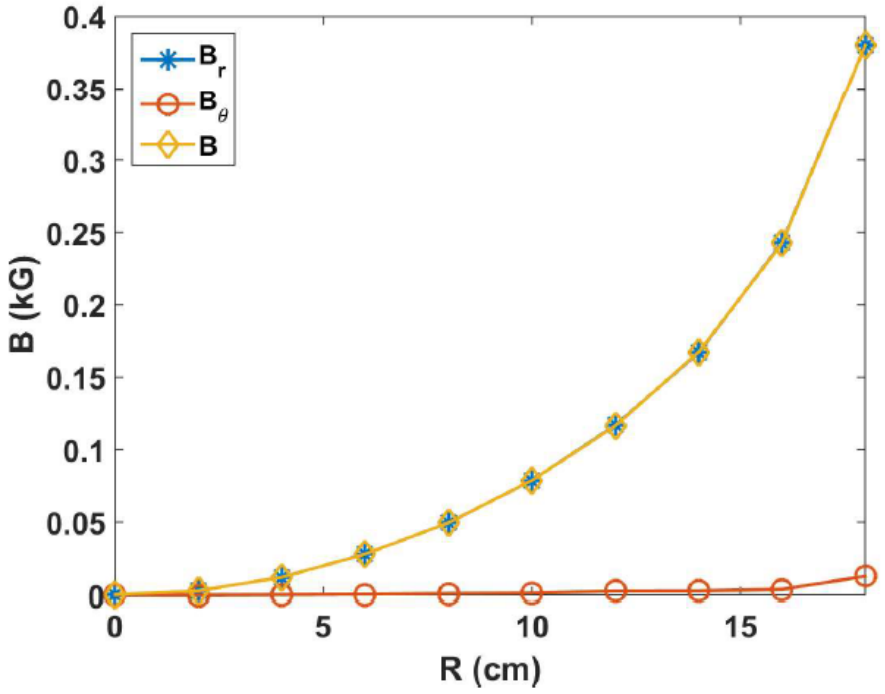

Figure A: Radial variation of B_r, B_θ and mean B along cusp region at 100A magnet coil current.

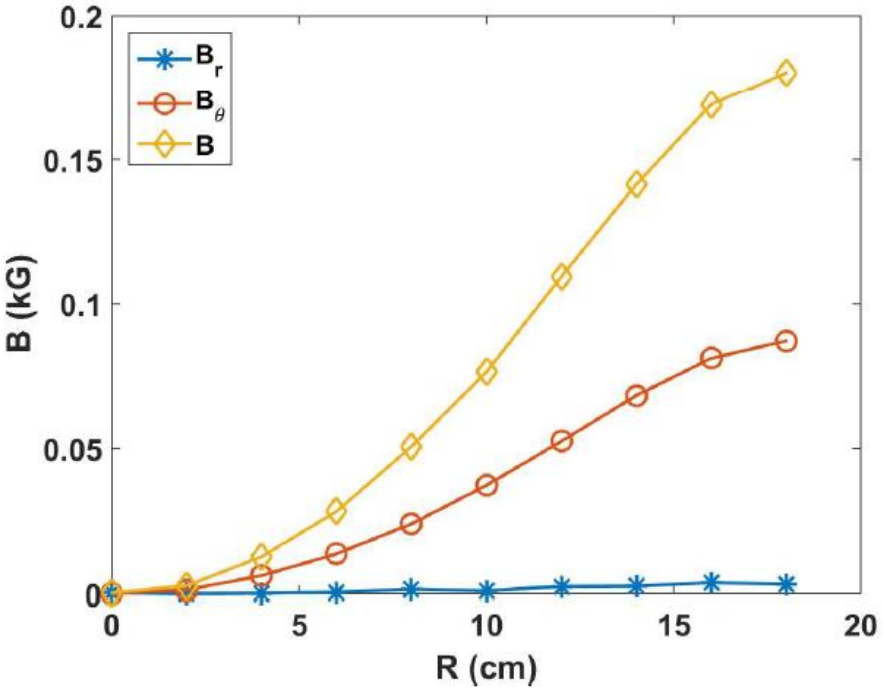

Figure B: Radial variation of B_r, B_θ and mean B along non-cusp region at 100A magnet coil current.

Appendix B:

During the machine characterization, axial variation of plasma density has been indeed measured. It was performed using a single Langmuir probe inserted from the flange at the opposite end of the machine towards the source and the mean plasma density was measured along the axis. A typical axial profile of density has been shown in the figure C. It has been observed that the density gradient scale length ($L_n^{-1} = -\frac{1}{n}\frac{dn}{dz}$) is nearly 0.6 m. It was felt that this gradient length much more for the purview of this Thesis. Also even if the cantilever effects (because of the long shaft) and / or shadowing effects, the gradients lengths are going to more than this.

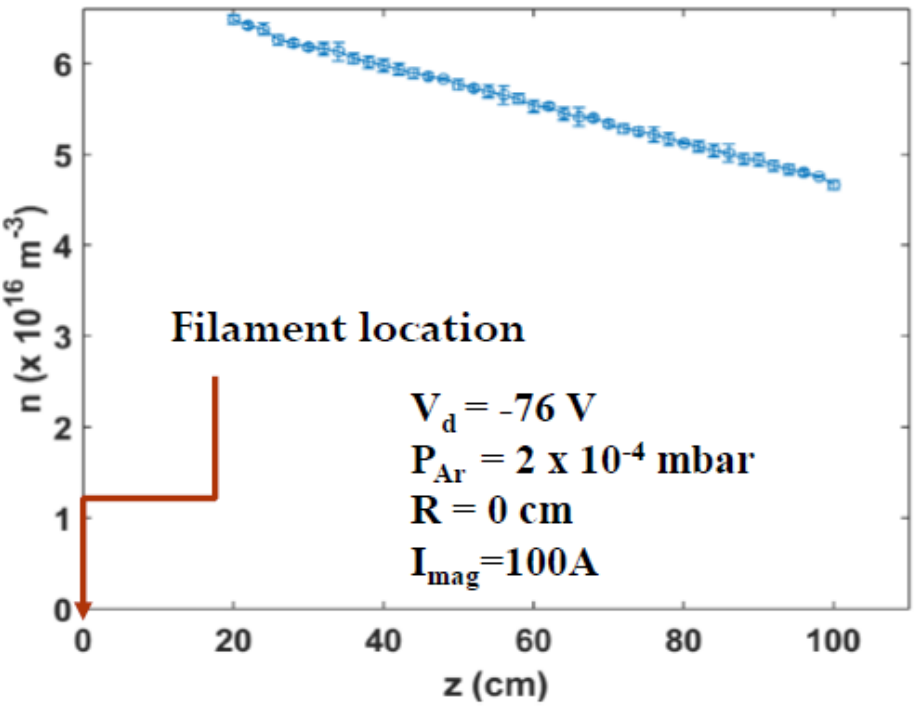

Figure C: Variation of mean plasma density along the axis of the device in field free region at 100A magnet current.